Assembly and Activation of the Plasmodial Pyridoxal 5'-Phosphate Synthase Complex

Understanding the Structural Mechanism of PLP Biosynthesis

Dissertation

by

Gabriela Liuvanova Guédez Rodríguez

2011

Dissertation

submitted to the
Combined Faculties for the Natural Sciences and for Mathematics
of the Ruperto-Carola University of Heidelberg, Germany
for the degree of
Doctor of Natural Sciences

presented by
MSc. Biochem. Gabriela Liuvanova Guédez Rodríguez
born in Miranda State, Venezuela

date of oral examination: .....

Assembly and Activation of the Plasmodial Pyridoxal 5'-Phosphate Synthase Complex

Understanding the Structural Mechanism of PLP Biosynthesis

Dissertation

by

Gabriela Liuvanova Guédez Rodríguez

Referees:
Prof. Dr. Irmgard Sinning
PD Dr. Barbara Kappes

to Zenaida, Armando and Larry

„Was ich weiß, kann jeder wissen. Mein Herz habe ich allein.“
Die Leiden des jungen Werther - Am 9. Mai 1772

Johann Wolfgang von Goethe

Acknowledegements

My special thanks go to Ivo Tews for providing me an interesting project, for the teaching times and sharing knowledge with me about x-ray crystallography, for giving me valuable advises during these years. I thank you for being a motivating team leader in the lab as well as in the Heidelbergmann Thriatlon ⌣̈. It was a very enriching experience working with you

Special thanks to Professor Irmi Sinning for giving me the opportunity to make my PhD studies in her laboratory and for all useful scientific discussions about the paper and during the group-seminars and Lab-retreat

Thanks to Barbara Kappes for the scientific suggestions and nice discussions about the interesting world of plasmodial parasites

Thanks to Bettina Böttcher and Katharina Hipp for the Electron microscopy analyses

Thanks to Klemens Wild for the discussions about symmetry in crystallography and cool trips to the summit of french mountains

Thanks to Jürgen Kopp and Claudia Siegmann for protein crystallization at the crystallization platform

Thanks to Elke Herwig for the technical assistance

Thanks to Valérie Panneels for the kind help in discussing data, for the given encouragement on the walls ⌣̈

Thanks to Wilfried Klug for the corrections of "die Zusamenfassung", for the nice friendship and being a pretty cool lab-mate ⌣̈

Thanks to all former and current members of the Sinning Group for the nice lab atmosphere, specially to my project-mate Volker Windeisen for the nice discussions about the project. Also Patrick, Domenico, Anja, Frau Adrian, Bernd, Nico, Iris, Sebastian, Astrid, Timo, Gabi, Lisa, Przemek, Goran, Gert, Gunter, Simon, Bhalchandra. Thanks to Lutz Nücker for the computer support. Thanks to Bianca Derrer from the Kappes group

Gracias a mis padres Zenaida y Armando. A Larry, por cada momento. A mis hermanos Liu Ho, Hanoi, Itxaro y Aquiles. Nada ha sido posible para mi sin ustedes conmigo.

Summary

Biosynthesis of vitamin B_6 is essential for all living cells. Most organisms use the pyridoxal 5'-phosphate (PLP) synthase complex to synthesize the cofactor form, PLP, from the three substrates ribose 5-phosphate (R5P), glyceraldehyde 3-phosphate (G3P) and ammonia. PLP synthase complex is a glutamine amidotransferase (GATase) class I, consisting of 12 Pdx1 and 12 Pdx2 subunits. Pdx1 is responsible for the PLP synthesis and Pdx2 is the glutaminase that hydrolyses glutamine to produce ammonia, which is transfered to the Pdx1 active site. In this PhD Thesis, studying Pdx1 and Pdx2 proteins from the human parasite *Plasmodium falciparum* and from the rodent parasite *Plasmodium berghei* gave important insights into the assembly, activation and substrate tunneling of the PLP synthase complex.

Electron microscopy analyses showed that association of the PLP synthase and glutaminase subunits was random, suggesting a non cooperative mechanism independent of neighboring Pdx1 binding sites to be occupied by Pdx2. Complex assembly is critical for glutamine hydrolysis by Pdx2, although the presence of an ammonia acceptor in the Pdx1 active site did neither enhance the Pdx1/Pdx2 interaction nor the catalytic rate of Pdx2 *in vitro*, as tested by biophysical and kinetic experiments. In particular, the PLP synthase complex does not show allosteric activation by R5P or glutamine binding that would result in synchronization of the glutaminase and PLP synthesis reactions. Therefore, the Pdx1/Pdx2 interaction is enough to stimulate glutamine hydrolysis.

A particular motivation of this Thesis was to crystallize the PLP synthase complex from the malaria causing parasite, *P. falciparum*, for the potential use of the 3D structure in drug design. However, the complex assembled into fibers *in vitro*, induced by the Pdx1 subunit, making the crystallization trials of this enzyme impossible. A chimeric complex formed by Pdx1 from *P. berghei* and Pdx2 from *P. falciparum* proved to be a catalytically active system, suitable for structural studies of the plasmodial complex. Crystal structure of this enzyme complex gave two major advances in the understanding how prokaryotic and eukaryotic PLP synthase complexes resemble each other or differ in protein interaction and activation. Variations at the Pdx1/Pdx2 interface occur through insertion sequences in eukaryotic systems, notably in the plasmodial PLP synthase complex by the loop 95-111 in Pdx2. Activation of the glutaminase is highly conserved in both systems. The process entails reorganization of structural regions at the Pdx1/Pdx2 interface through stabilization of αN and the oxyanion hole region. Activation of the PLP synthase requires a helical segment, named α2', for sugar binding. The helix is observed in two alternative positions in the Pdx1/Pdx2 and Pdx1-R5P structures: an open conformation to allow the entrance of the substrate and a closed conformation oriented towards R5P, sequestering the substrate in the catalytic center. The pentose substrate is bound in the P1 site to the catalytic Lys84 via a Schiff base with the ribose C1 atom.

GATases are characterized by two separate active sites for glutamine hydrolysis and enzyme-specific metabolite syntheses. Previously, ammonia transfer between two catalytic centers was proposed to occur by flexible methionine residues within a transient tunnel in Pdx1. The plasmodial proteins show an ammonia tunnel distict from bacterial orthologs as some of the residues lining the passage are exchanged. Biochemical analysis confirmed that the $(\alpha/\beta)_8$-barrel of Pdx1 passes the reactive ammonia produced in Pdx2 to Pdx1 active site, assigning function of key residues for the ammonia channeling.

The differences between eukaryotic and prokaryotic systems provide insight into PLP synthase complex regulation, which may be exploitable in drug design for the treatment of malaria.

Zusammenfassung

Die Biosynthese von Vitamin B6 ist wichtig für alle lebenden Zellen. Die meisten Organismen nutzen den Pyridoxal 5'-phosphat (PLP) Synthase Komplex um den PLP Cofaktor aus den drei Substraten Ribose-5-Phosphat (R5P), Glyceraldehyd 3-Phosphat (G3P) und Ammoniak zu bilden. Der Enzyme-Komplex ist eine Glutamin Amidotranstransferase (GATase) der Klasse I, bestehend aus 12 Pdx1 und 12 Pdx2 Untereinheiten. Pdx1 ist verantwortlich für die PLP-Synthese und Pdx2 ist eine Glutaminase, die Glutamin zu Ammoniak hydrolysiert um es auf Pdx1 zu übertragen. In dieser Doktorarbeit geht es im Wesentlichen um das Studium der Pdx1 und Pdx2 Proteine aus dem menschlichen Parasiten *Plasmodium falciparum* und dem Mausmalaria Parasiten *Plasmodium berghei*. Diese Studie gibt dabei wichtige Einblicke über Aufbau, Aktivierung und Substrat-Tunneling des PLP-Synthase-Komplex.

Elektronen mikroskopische Analysen zeigten, dass die Komplexbildung zwischen Pdx1 PLP-synthase und Pdx2 Glutaminase Untereinheiten eher zufällig abläuft, was auf einen nicht kooperativen Mechanismus hindeuted, der unabhängig davon ist, ob benachbarte Bindungsstellen am Pdx1-Ring von Pdx2 Untereinheiten besetzt sind. Die Komplexformierung ist entscheidend für die Glutamin-Hydrolyse durch Pdx2, obwohl die Anwesenheit eines Ammoniumionakzeptors im aktiven Zentrum von Pdx1 weder zu einer Zunahme der Pdx1/Pdx2 Interaktion noch der Pdx2 katalytische Rate führt, was durch biophysikalische und kinetische Experimente belegt ist. Insbesondere weist der PLP-Synthase-Komplexe keine allosterische Aktivierung durch R5P- oder Glutamin- Bindung auf, was in einer Synchronisierung der Glutaminase- und der PLP-Synthese-Reaktionen resultieren würde. Demzufolge ist die Pdx1/Pdx2 Interaktion ausreichend un die Glutamin Hydrolyse zu stimulieren.

Eine besondere Motivation dieser Doktorarbeit war die Kristallisation des PLP Synthase-Komplex aus dem Malaria-Parasiten *P. falciparum* aufgrund seines potentiellen Einsatzes im Drug-Design. Allerdings aggregiertete der Komplex zu Fasern *in vitro*, induziert durch die Pdx1 Untereinheit. Die Kristallisation der PLP Synthase war deshalb nicht erfolgreich. Ein chimärer Komplex gebildet aus Pdx1 von *P. berghei* und Pdx2 von *P. falciparum* erwies sich als katalytisch aktives System, geeignet für strukturelle Untersuchungen am *Plasmodium* Komplex. Die Kristallstruktur liefert zwei bedeutende Beiträge zum Verständnis darüber, wie sich prokaryotische und eukaryotische PLP-Synthase-Komplexe in Proteininteraktion und -aktivierung ähneln oder unterscheiden. Variationen der Pdx1/Pdx2 Interaktion treten durch die Anwesenheit von Insertionssequenzen in eukaryotischen Systemen auf. In *Plasmodium* PLP Synthase-Komplexen ist die Loop-Region 95-111 in Pdx2 an der Komplexbildung beteiligt, welche in bakteriellen Pdx2 Enzymen deletiert ist. Die Aktivierung der Glutaminase ist in beiden Systemen hoch konserviert: eine Umordnung struktureller Regionen am Pdx1/Pdx2 interface führt zu einer Stabilisierung von αN und der Oxyanion-Region. Die Aktivierung der PLP-Synthase erfordert ein helicales Segment, genannt α2', für die Bindung von Zucker molekülen, welches an zwei alternativen Positionen beobachtet wird: die offene Konformation in der Pdx1/Pdx2

Struktur erlaubt eine offene Konformation den Zugang für Substrate; dagegen wird in der Struktur des R5P Substrat Komplexes eine geschlossene Konformation beobachtet, die das Substrat im katalytischen Zentrum sequestriert. Das Pentose Substrat wird an der P1 Stelle des katalytischen Lys84 über eine Schiff-Base an das C1-Atom der Ribose gebunden.

GATases haben zwei separate aktive Zentren, eines für die Ammoniak Produktion und eines für die Synthese Aktivität. Ein Modell des Ammoniak Transfers vermittelt durch flexible Methioninaminosäuren innerhalb eines transienten Kanals in Pdx1. Hier wird gezeigt, dass bei Plasmodien Proteinen einige der Reste dieses Kanals ausgetauscht sind. Die biochemische Analyse bestätigte, dass das $(\beta/\alpha)_8$-Barrel Ammoniak von Pdx2 zu Pdx1 transferiert. Durch Mutagenese Analysen wurde den Aminosäuren eine Funktion im Ammoniak - Channeling zugewiesen.

Die Unterschiede zwischen eukaryotischen und prokaryotischen PLP-Synthase Systemen erlauben Einblicke in Enzymregulierung, welche für das Drug Design für die Behandlung von Malaria nutzbar sind.

Contents

List of Figures

List of Tables

Chapter 1

Introduction

In living cells, many biochemical reactions catalyzed by enzymes take place with the support of nonprotein components, called coenzymes or cofactors. They fulfill crucial chemical steps required for a succesful enzymatic catalysis. Cells contain different types of cofactors classified as organic molecules such as biotin, nicotinamide adenine dinucleotide, thetrahydrofolate, thiamine pyrophosphate, etc., and inorganic ions such as, Mg^{2+}, Fe^{2+}, Mn^{2+}, Zn^{+2}, etc. Cofactor biosynthesis is essential for all living organisms because many enzymes reactions depend on at least one cofactor. However, cofactors are not assembled by the ribosome, rather by biosynthetic enzymes and here I focus on Vitamin B_6 biosynthesis.

Vitamin B_6 is composed by six vitamers with a common pyridinium ring, whose members are pyridoxal (PL), pyridoxamine (PM), pyridoxine[1] (PN) and their respective phosphorylated forms: pyridoxal 5'-phosphate (PLP), pyridoxamine 5'-phosphate (PMP) and pyridoxine 5'-phosphate (PNP). Of these compounds, only PLP and PMP are the biologically active forms, while the others function as PLP precursors. Their chemical structures are shown in Figure 1.1.

Vitamin B_6 in the form of PLP has diverse functions in a large number of enzymes, the mayority of them catalyze reactions for the amino acid metabolism. PLP serves as a transient carrier of specific functional groups in different reactions at the α, β and γ carbons of amino acids. Examples of PLP-dependent reactions are decarboxylations, racemizations, α,β-elimination and transaminations. Pyridoxal 5'-phosphate is commonly bound through an aldimine (Schiff base) linkage to the ε-amino group of a lysine residue in the active site of the PLP-dependent enzyme.

As a common role of PLP in many transamination reactions, a general view of the catalytic process is depicted in Figure 1.2. The aldehyde group of PLP can accept an amine via a Schiff base with the amino acid. A highly unstable

[1] also known as pyridoxol

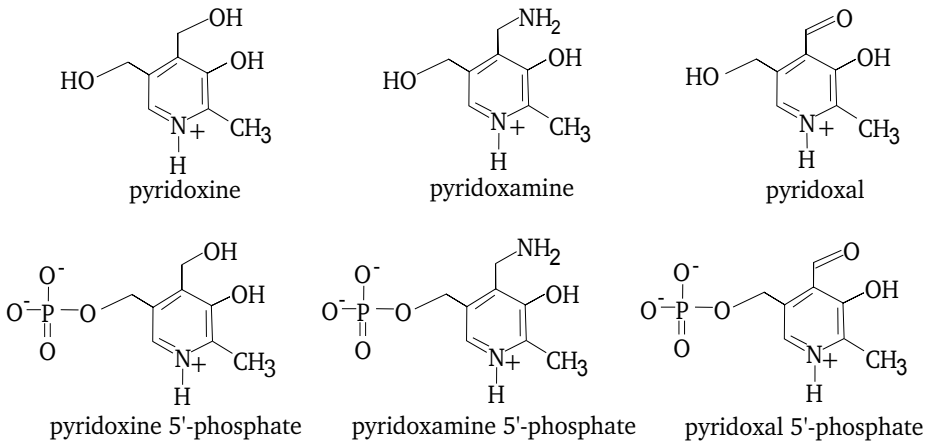

Figure 1.1: Vitamin B_6 compounds. Six alternatives of vitamin B_6: pyridoxine, pyridoxamine, pyridoxal and phosphorylated forms pyridoxine-5'phosphate, pyridoxamine-5' phosphate and pyridoxal-5'phosphate.

carbanion is avoided because the electron charge at the α-carbon is reduced by resonance stabilization in the pyridinium ring of PLP (aldimine). In all transamination, racemization and carboxylation reactions, a quinonoid intermediate is formed, where the bond between the amine α-carbon to the adjoining functional group - a side chain of an amino acid, a hydrogen, or a carboxyl - weakens and consequently breaks. The products in each of the routes, transamination, racemization, and carboxylation, are an α-ketoacid and PMP, a D-amino acid, or an amine, respectively. The reverse transformation of PMP into PLP can occur when the amino group is donated to an α-keto acid.

PLP is a very diverse functional cofactor, it also participates in reactions required for glycogen breakdown, formation of several amines functional in nervous tissue (e.g., epinephrine, serotonin or norepinephrine), hemoglobin biosynthesis and sphingolipid synthesis. Besides the important role as a cofactor, PLP has antioxidant function against reactive oxygen free radicals [1, 2].

1.1 Pyridoxal 5'-phosphate biosynthesis

Enzymes for *de novo* biosynthesis of vitamin B_6 are found in some organisms, i.e., archaebacteria, bacteria, some protists, fungi and plants [3], while other organisms like humans must obtain it from the diet. Vitamin B_6 in the form of PNP or PLP as the active form can be synthesized directly by two distinct *de novo* routes: the deoxyxylose 5'-phosphate (DXP)-dependent and ribose 5-phosphate (R5P)-dependent[2] pathways, respectively (Figure 1.3). Both routes contain highly conserved genes, but comparison of the encoded proteins shows they are different in the amino acid sequence, suggesting that the two pathways diverged during evolution. In addition to the *de novo* PLP biosynthesis, PLP

[2]also found in the literature under the name DXP-independent pathway

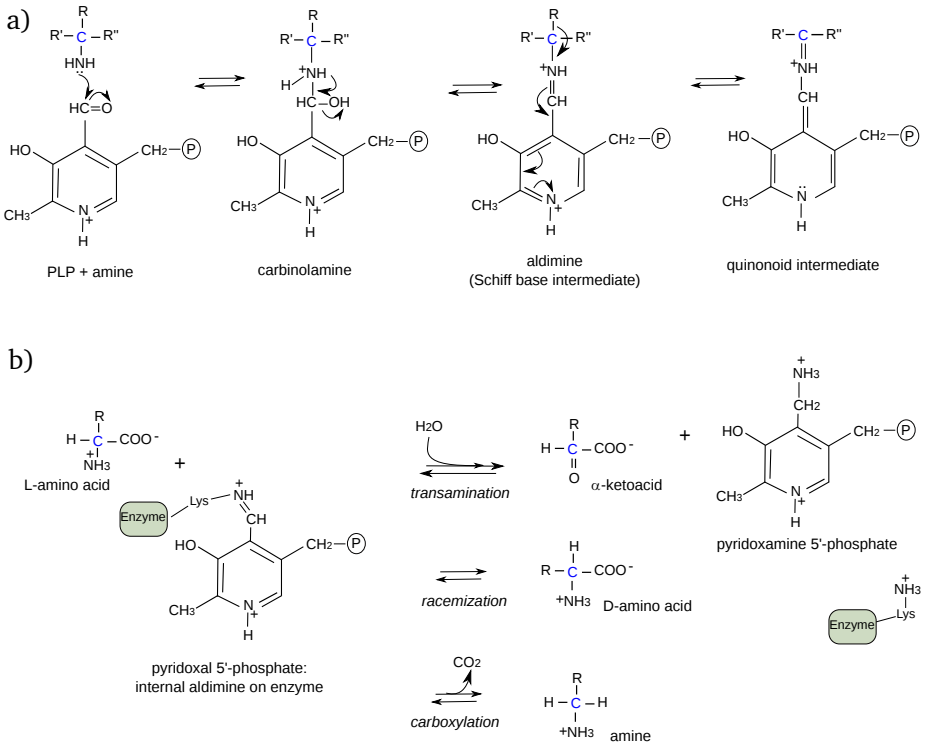

Figure 1.2: PLP reaction with a general amine. a) A general reaction catalyzed by PLP at the α-carbon (colored blue) of an amine: the Schiff base linkage between PLP and the amino acid is stabilized by resonance with the pyridine nitrogen in PLP, forming a quinonoid intermediate. b) PLP bound to a lysine through a Schiff base at the active site: an amino acid substrate enters the active site and condenses to PLP via a new Schiff base (not shown). In a aminotransamination reaction, PLP accepts the amine, forming an α-ketoacid and PMP. Conversion of PMP into PLP is reversible, by donation of the amino group to an α-keto acid. The alternative racemization and carboxylation reactions give rise to a D-amino acid and amine, respectively. R and P stem from a functional group and phosphate ion.

can be synthesized from precursors in the form of PL, PN, PM, PNP and PMP that are converted to PLP in the so-called *salvage pathway*. This pathway functions mainly as the recycling and interconvertion of the B_6 vitamers by several kinases and phosphatases present in the known proteome of living organisms, as well as, by transaminases and oxidases, Figure 1.3.

1.1.1 The DXP-dependent pathway

The DXP-dependent pathway is found in a subset of the γ-division of proteobacteria and in the well characterized gram-negative bacterium, *Escherichia coli* [4]. The mechanism is divided into two steps for the synthesis of 4-phosphohydroxy-L-threonine (4-HTP) and deoxyxylulose 5-phosphate (DXP) that converge in a last step to form PNP. Three enzymes PdxA, PdxB and PdxJ are unique for the *de novo* PNP biosynthesis. The initial step requires D-Erythrose 4-

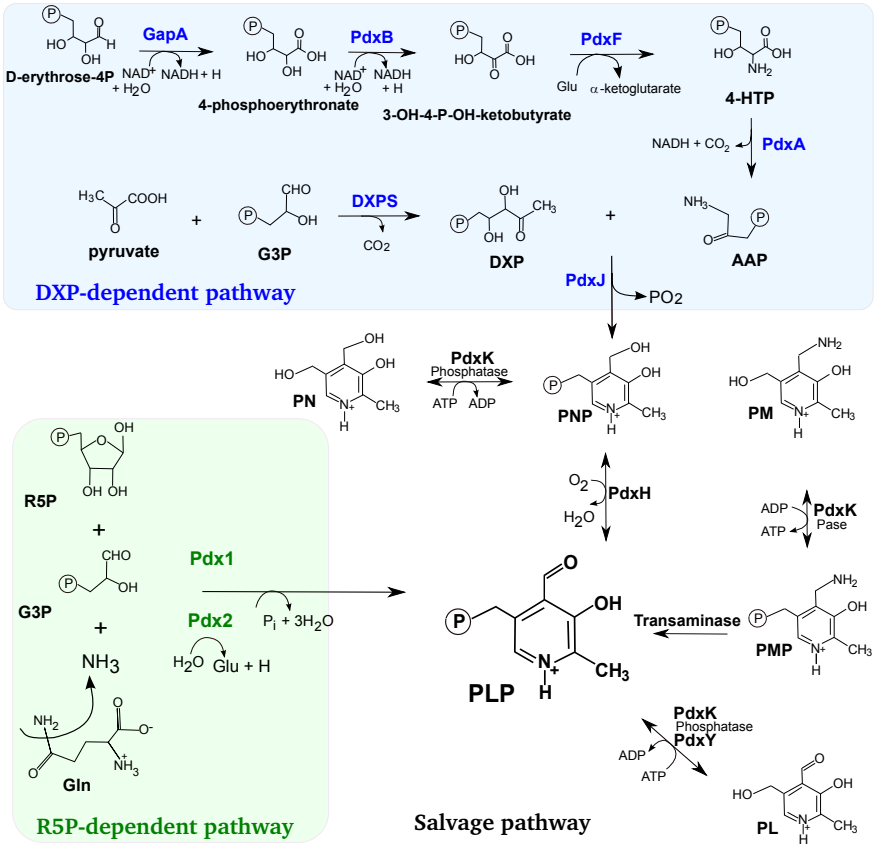

Figure 1.3: PLP biosynthesis. The three routes to synthesize PLP: two *de novo* routes DXP-dependent and R5P-dependent for the synthesis of PNP and PLP, respectively; and the salvage pathway, in which the B_6 vitamers PN, PNP, PM, PMP and PL are converted to PLP. See § 1.1 for more details.

phosphate and glutamate as substrates to produce 4-HTP in sequential steps carried out by the enzymes GapA, PdxB and PdxF. 4-HTP is decarboxylated by PdxA to form 3-hydroxy-1-aminoacetone phosphate (AAP), a very unstable intermediate. DXP is synthesized from pyruvate and G3P by the enzyme DXPS. The process is finalized by PdxJ, which catalyses the cyclization of DXP and AAP to produce PNP and P_i, Figure 1.3. PNP can be oxidised to form PLP by an enzyme of the salvage pathway, PdxH, Figure 1.3.

1.1.2 The R5P-dependent pathway

Genes encoding proteins involved in the R5P-dependent pathway were first identified in *Cercospora nicotianae* [5, 6], when investigating the resistance mechanism of the plant fungus against oxydative stress. From this study, a novel *de novo* pyridoxine biosynthesis pathway was found to be commonly distributed whithin some bacteria, archaea and many eukaryotes, including plants and fungi.

The pathway consists only of two enzymes: Pdx1 and Pdx2. The three substrates R5P, glyceraldehyde 3-phosphate (G3P) and glutamine are required for direct PLP biosynthesis[3]. The heterocyclic nitrogen of PLP is derived through hydrolysis of L-glutamine by Pdx2 [7, 8], Figure 1.3

1.2 The glutamine amidotransferase Pdx1 and Pdx2 complex

Most of the reactions in the biosynthesis of amino acids, nucleotides and coenzymes are catalyzed by enzymes which use glutamine as ammonia source, called glutamine amidotransferases (GATases). GATases have two structural domains: a glutaminase, where ammonia is produced from glutamine and a synthase domain, which binds the ammonia acceptor substrate. There are two types of GATases: class I [4] and class II [5] GATases [9]. Both class of enzymes carry out the same catalytic reaction, using a conserved cysteine residue in the glutamine binding site. The two classes of GATases differ in the way they use the nucleophilic cysteine: GATases class I use histidine and glutamate residues to activate the thiol group of cysteine; and in GATases class II the cysteine residue is positioned at the N-terminus and is activated by its α amino group [9]. The thiol group of the cysteine becomes highly nucleophilic by its interaction with the imidazol-N of the His residue and can attack the γ carbonyl of glutamine, producing ammonia and glutamate. This reaction results in the formation of a negatively charged transition state with tetrahedral geometry in the active site of the glutaminase, Figure 1.4. This transition state is stabilized by hydrogen bonds oriented to form a pocket called oxyanion hole (OXH), critical for glutamine hydrolysis. The ammonia produced in this reaction is subsequently transfered through an ammonia tunnel to the synthase domain, where it reacts with the acceptor substrate to form the aminated product. An example is the imidazole glycerol phosphate (ImGP) synthase [10], a key enzyme required to link amino acid and nucleotide biosynthesis. The PLP biosynthetic Pdx1 and Pdx2 proteins assemble into glutamine amidotransferase type I enzyme with Pdx1 as the PLP synthase and Pdx2 as the glutaminase [11, 12]. A proposed mechanism for class I GATases is depicted in Figure 1.4.

1.2.1 Pdx1/Pdx2 interaction

The x-ray crystallographic structure of the PLP synthase complex has been obtained so far from the bacteria *T. maritima* (PDB code 2ISS, [13]) and *B. subtilis* (PDB code 2NV2, [14]). The Pdx1/Pdx2 complex builds a 24-mer multienzyme, consisting of each subunit of the dodecameric Pdx1 core in independent interaction with one Pdx2 subunit. Pdx1 and Pdx2 active sites are far from each

[3] the chemical reaction is explained in more detail in § 3.5
[4] also named triad GATases
[5] also named N-terminal nucleophile (Ntn)

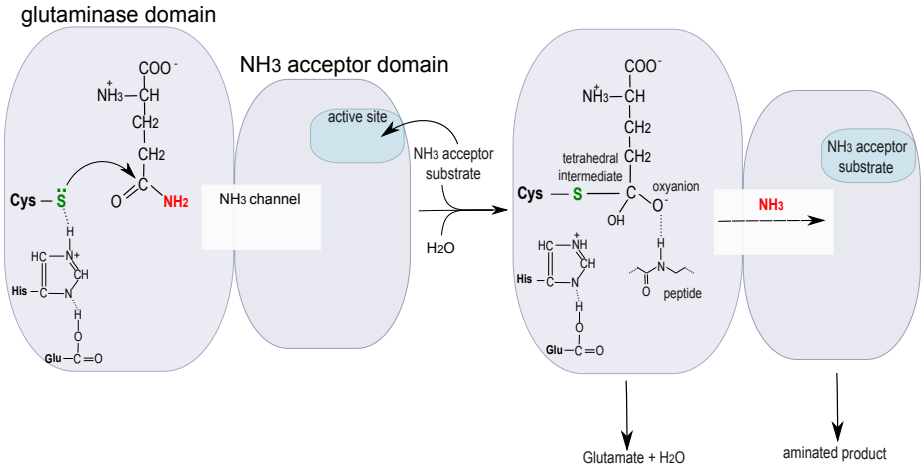

Figure 1.4: Proposed mechanism for class I glutamine amidotransferases. The GATase has two domains: glutaminase and ammonia acceptor. The glutaminase binding domain contains conserved Cys, His and Glu traid residues required for catalytic reaction to the Gln. The thiol group of Cys (green) attacks the amide group of Gln and the γ-amido nitrogen is released as NH_3 (red). A glutamyl-enzyme intermediate is formed at the γ-carbon with tetrahedral geometry. An oxyanion is stabilized by hydrogen bond from a peptide element in the active site. The produced NH_3 is transfered to the active site of the acceptor domain through a channel, where it reacts with an NH_3-acceptor susbtrate. Glutamate and water are the products of the glutamine hydrolysis, while an aminated product is synthesized in the NH_3 acceptor domain.

other with a distance of $\sim$22 Å. As a glutamine amidotransferase enzyme, Pdx2 hydrolyses glutamine and the produced NH_3 in this reaction is subsequently transferred through an ammonia channel to the second active site in Pdx1. It was postulated earlier the ammonia channel localizes inside the $(\beta/\alpha)_8$-barrel of Pdx1 and is lined by flexible methionines [14].

The Pdx1 and Pdx2 interaction was suggested to entail ordering of the helix αN from Pdx1, a helix embeded between the two subunits and is in close proximity to the Pdx2 active site. Helix αN plays a key role in heterodimer formation and activation of Pdx2 [14, 15]. The Pdx1/Pdx2 complex involves also organization of the oxyanion hole in Pdx2 by reorientation of two peptides of amino acid residues Pro45-Gly46-Gly47 (nomenclature for *B. subtilis* Pdx2) [16], when the two subunits interact with each other, Figure 1.5.

1.2.2 The R5P-dependent PLP synthase: Pdx1 with multiple enzymatic reactions

Most of the 3D crystallographic structures of the PLP synthase complex are from the Pdx1 subunit. They are from several prokaryotic organisms such as, *Bacillus subtilis* (PDB code 2NV1, [14]), *Geobacillus stearothermophilus* (PDB code 1ZNN, [17]), *Methanocaldococcus jannaschii* (PDB code 2YZR) and *Thermus thermophilus* (PDB code 2ZBT). The current availabe eukaryotic Pdx1 struc-

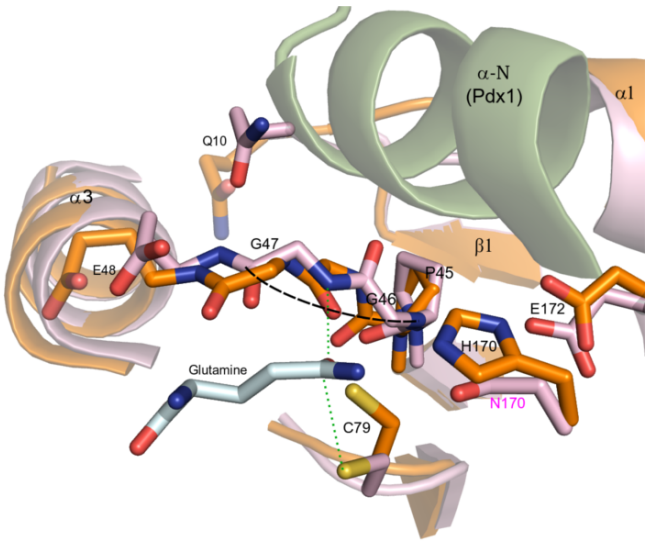

Figure 1.5: Active site and activation of Pdx2. The active site in Pdx2 alone (orange, PBD entry 2NV0, [14]) and in the Pdx1/Pdx2/Glutamine complex (pink, PDB entry 2NV2, [14]) from *Bacillus subtilis*. The triad catalytic is shown in sticks: C79, H170 and E172. H170 residue was replaced by Asn in Pdx2 to stabilize the Pdx1/Pdx2/Gln complex for crystallization [14]. Reorientation of the residues Q10 at loop β1-α1 and E48 implicated in glutaminase activity and complex formation with Pdx1 [16] are shown in sticks. Dashed lines represent the two peptide flip of P45-G46-G47. Two potential hydrogen bonds are shown in green dots: for tetrahedral intermediate (between the sulphydryl of C79 and the γ-carbonyl of Gln) and for stabilization of the oxyanion hole (the O of the Gln amide group and the N of the G47 peptide bond). Part of the Pdx1 α-N is displayed.

ture is from *Saccharomyces cerevisiae* (PDB code 3FEM, [18]). Sequence conservation is mainly observed among Pdx1 proteins with up to 40% identity (see Alingnment D.1).

The Pdx1 monomer has a $(\beta/\alpha)_8$ fold with the location of the active site at the C-terminus of the β-barrel, common in enzymes with this fold [19, 20]. Additional helices and loops surround the $(\beta/\alpha)_8$ core. The bacterial Pdx1 complex has 12 Pdx1 monomers, forming two hexameric rings that dimerise to build a dodecameric core [17, 14]. The protein exists in solution in a hexamer-dodecamer equilibrium. The yeast Pdx1 forms mainly hexamers in solution and the x-ray crystallographic structure has shown the same oligomeric state [18]. Assembly to the dodecamer is mediated by helix α6 and two additional helices, α6' and α6", which protrude from the globular architecture of the $(\beta/\alpha)_8$ barrel. The dodecameric interface in the yeast Pdx1 is disturbed by a lysine residue at the α6-α6" loop absent in other Pdx1 proteins. The implication of this amino acid residue insertion in Pdx1 for enzyme activation and regulation in the hexameric core of the yeast Pdx1 is unknown at present.

Pdx1 uses R5P and G3P and condenses the two phosphorylated sugars and ammonia (NH_3) from L-glutamine to synthesize directly PLP. The biochemistry of Pdx1 comprises several reactions described recently by *Hanes et al 2008*

[21], Figure 1.6. The proposed mechanism suggests that Pdx1 binds the pentose R5P ring, forms an imine between the R5P aldehyde and a lysine in the active site, isomerizes it to ribulose 5-phosphate (Ru5P), incorporates nitrogen from glutamine to the carbon 5 of the Ru5P backbone by an imine formation, performs tautomerization, amine elimination, phosphate ion elimination, G3P incorporation, imine hydrolysis and cyclization to form the pyridinium ring, PLP. Incorporation of ammonia to the R5P adduct leads to the formation of a stable chromophoric intermediate I_{320} with maximum absorbance at 315 nm [22], used commonly to analyse the enzymatic activity of Pdx1 by spectrophotometric experiments. Noteworthy, Pdx1 has the ability to prescind from Pdx2 *in vitro* and synthesize PLP using other NH_3 sources such as, NH_4Cl or NH_2SO_4. There are not cell biology data available to explain whether Pdx1 takes ammonia from the cellular environment or from glutamine hydrolysis in Pdx2 or both. However enzymatic studies *in vitro* have shown that Pdx2 enhances PLP synthesis in Pdx1 [23], suggesting domain comunication is important for catalysis.

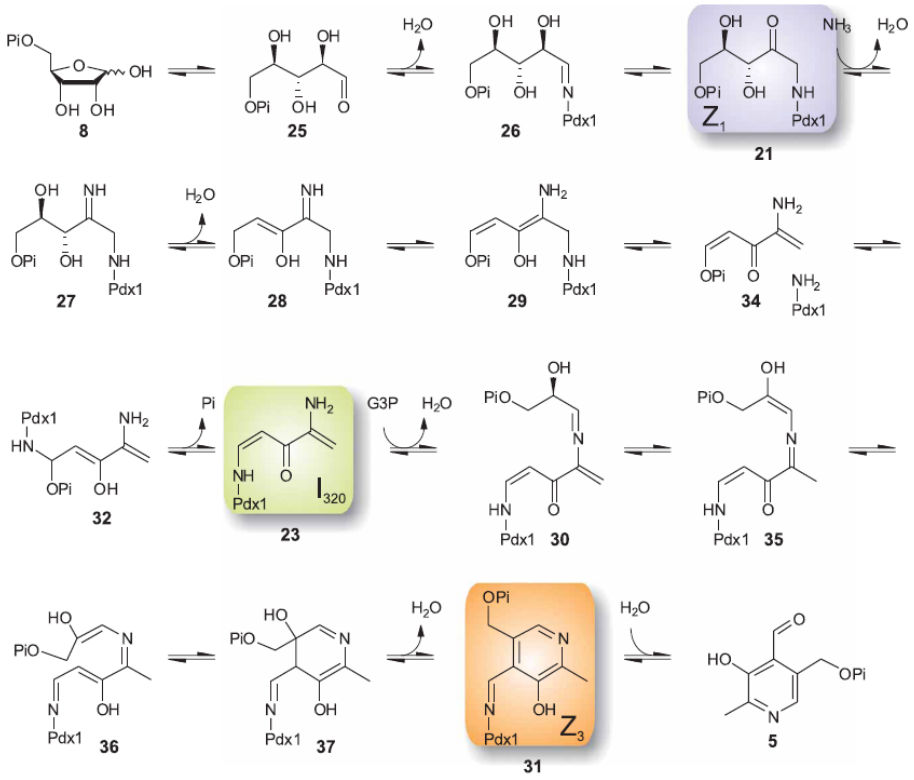

Figure 1.6: Proposed reaction mechanism for PLP biosynthesis via the R5P-dependent route from *Hanes et al 2008* [21]. See text § 1.2.2

1.2.3 Pdx2: the glutaminase of the PLP synthase complex

Known structures of the Pdx2 subunit are solved from *B. subtilis* (PDB codes 1R9G[11], 2NV0[14]), *G. stearothermophilus* (PDB code 1Q7R, [17]), *T. ther-*

mophilus (PDB code 2YWD) and *P. falciparum* (PBD code 2ABW, [24]). Pdx2 is a Rossmann-fold protein with a α/β layer structure common to other members of triad glutamine amidotransferases. Pdx2 is highly variable and insertion sequences are common in eukaryotic homologues with aproximately 35% identity between bacterial and eukaryotic Pdx2 proteins. The eukaryotic Pdx2 structure from *P. falciparum* has structural segments different to the bacterial Pdx2 and was proposed that some of them are possibly involved in protein-protein interaction with Pdx1 [24].

Pdx2 as the NH_3 donor in the PLP synthase complex, has an enzymatic center constituted by the catalytic triad: cysteine, histidine and glutamate (see alignment, Figure D.2) for glutamine hydrolysis, as explained above § 1.2. Pdx2 is functional when interacting with Pdx1, as a manner to control glutamine hydrolysis and therefore optimize glutamine use. Whether Pdx2 activation relies simply on Pdx1 interaction or requires an NH_3 acceptor bound in the active site of Pdx1 is not known at present.

1.3 Current knowledge of PLP biosynthesis in malaria parasites

Plasmodia are protozoan parasites member of the *phylum* apicomplexa and responsible for the protozoal disease, *Malaria*. It is estimated approximately 1 million death anually occurs due to malaria in several countries of Africa, Asia and Latin America [25], caused mainly by *Plasmodium falciparum*.

1.3.1 The elaborate life cycle of *Plasmodium*

Plasmodium species have a complex life cycle involving two hosts, the vector *Anopheles* mosquito and vertebrates such as, humans, rodents, monkeys, etc. The most studied malaria-causing parasite is *P. falciparum*. It develops with several morphological stages in the mosquito and human hosts, each having an asexual proliferation and invasive stage, named sporozoite and merozoite, respectively. To complete its life cycle, *P. falciparum* has a sexual stage shared between both hosts, in which gametes produced in the human are fertilized in the mosquito. Different morphologies of the parasite grow in the erythrocytes: ring, trophozoite, schizont, gametocyte and merozoite, causing a notable necessity for nutrients. In consequence of constant feeding by the parasite, the infected host cells degenerate and release the merozoites into the bloodstream, where they can invade other red blood cells and gametocytes can be taken up by a mosquito during feeding (Figure 1.7, A).

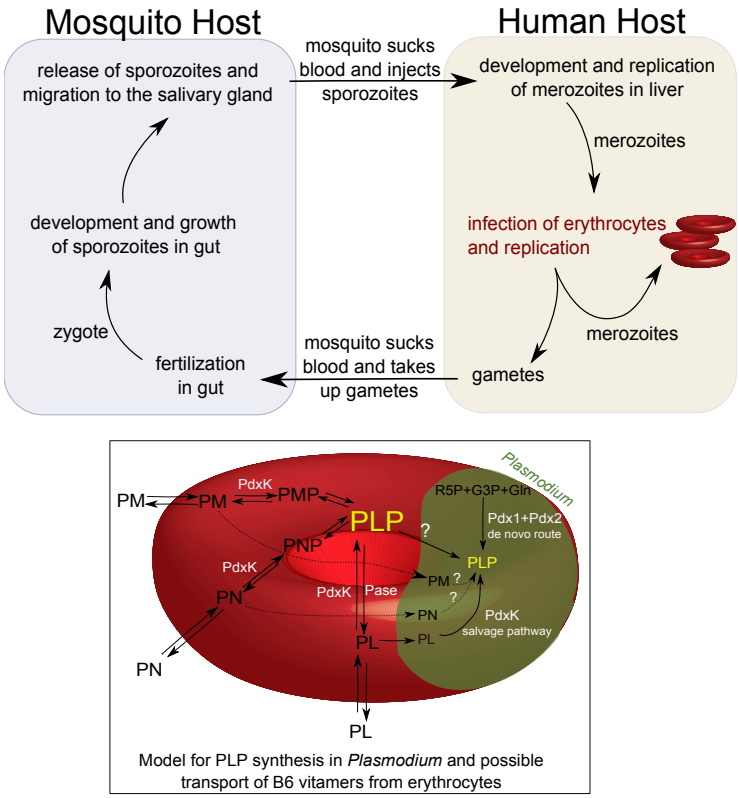

Figure 1.7: The complex life cycle of *Plasmodium falciparum*. A) the sexual cycle of the parasite is developed in the mosquito and human hosts. Two asexual proliferative stages are invasive: merozoites and sporozoites. B) a model for the *de novo* PLP biosynthesis and hypothetical transport of dephosphorylated B_6 vitamers into the parasite is described in a parasite infected-erythrocyte: direct supply of PLP would occur by the R5P-dependent route and/or hemoglobin (Hb) uptake. Dephosphorylated PL, PN, PM vitamers in the red-blood cell would be transported into the parasite and converted into PLP by proteins of the salvage pathway PdxK, transaminases and oxidases. See § 1.1 for more detail of the enzymes involved in the PLP biosynthesis pathways.

1.3.2 Plasmodial PLP biosynthesis in the red blood cell

During intraerythocytic stages, the parasite needs proper survival mechanisms to adapt under different host conditions. Due to the importance of PLP as an essential enzyme cofactor, *Plasmodium* must obtain it and supply cellular PLP demands. *P. falciparum* ingests and degrades more than 75% of the host cell hemoglobin in the acidic vacuole [26] for protein biosynthesis and energy generation [27]. It is known that hemoglobin binds PLP and PL [28] and might serve as a PLP source. However, there are not evidence to date which show the erythrocytes contribute in parasite nutrition in regards to vitamin B_6.

The B_6 vitamers in the form of PN and PM, as well as their phosphorylated forms would require to be converted to PL in the erythrocyte before delivered to the parasite, because human homologues of PNP and PMP oxidases have not

been identified yet in the genome of *Plasmodium*, suggesting that transamination of pyridoxamine 5'-phosphate and oxidation of pyridoxine 5'-phosphate to form PLP might not be possible in the parasite. Therefore PL and/or PLP might be the mayor B_6 vitamers in *Plasmodium* (Figure 1.7, B).

The *pdx1* and *pdx2* genes encoding enzymes of the R5P-dependent pathway are found in *Plasmodium* [29]. Both genes lack a signal targeting sequence. Their protein expression profile in the intraerytrocytic stages of *P. falciparum* shows that Pdx1 and Pdx2 localize in the cytosol [24], suggesting the *de novo* PLP biosynthesis in the parasite might be functional.

1.4 Aim of the PhD Thesis

Pdx1 and Pdx2 proteins from *Plasmodium* are chosen to make this PhD thesis, to gain insights into enzyme function and regulation of the PLP synthase complex, which can contribute in understanding the biology of PLP biosynthesis in the malaria parasite.

The Doctoral thesis was focused on:

- Determination of the first eukaryotic 3D structure of PLP synthase complex
- Insight into the malarial PLP synthase with a vision to drug design
- Study of the assembly of the PLP synthase complex
- Understanding of the mechanism of ammonia substrate tunneling
- Understanding of the PLP biosynthesis reaction mechanism based on structural studies

PLP synthase complex assembly

The R5P-dependent PLP synthase assembles into a multi-enzyme of 24mers with 12 PLP synthase and 12 glutaminase subunits. This high order of organization implies the enzyme is regulated to control enzyme function and activation as a fully occupied complex. Pdx2 for instance enhances the R5P binding in bacterial Pdx1 [18]. However, it is not known whether Pdx2 remains bound to Pdx1 and dissociates from Pdx1 once ammonia is delivered or binding of substrates regulate the Pdx1/Pdx2 assembly. This raises the question whether PLP synthase complex functions as a full 24mer enzyme or Pdx2 transiently interacts with Pdx1 to provide ammonia. In order to describe the assembly process of the enzyme complex, the *Plasmodium* PLP synthase complex is analysed in the presence and absence of substrates, using electron microscopy and isothermal titration calorymetry.

The Pdx1/Pdx2 interface has been analysed in detail in *B. subtilis* [14, 16]. However, eukaryotic systems are not yet available to explain whether there exist differences in the interaction mode between Pdx1 and Pdx2 of the PLP synthase complex from both cellular types. Crystallization of the plasmodial PLP synthase complex is pursued to compare how protein-protein interaction in eukaryotic and prokaryotic PLP synthase complexes is built, based on x-ray crystallographic studies.

Ammonia tunnel in the PLP synthase: a common geometry with slight variations in the packing

A proposed model for ammonia shuttling in *Bs*Pdx1 suggested that methionine residues would be involved in transfer of ammonia from Pdx2 to Pdx1 active site [14]. Although, not all methionines are conserved among Pdx1 proteins, suggesting variations in the tunnel packing maintain a similar function for ammonia delivery. Whether this difference is reflected in the regulation of ammonia transfering is not known. To gain insight into the process of ammonia transfer, residues of plasmodial Pdx1 are mutated by site directed-mutagenesis and the resulting variant proteins are analysed by enzymatic assays. The biochemical analysis should provide insights into the function of conserved and variable residues, to understand ammonia uptake by Pdx1.

PLP synthase activation: views towards the mechanism of PLP biosynthesis

The enzymatic reactions that lead to PLP synthesis in the R5P-dependent route occur mainly in Pdx1. The reaction steps involve a chemistry described by [21]. Participation of some residues in substrate binding and catalysis have been characterized [17, 14, 13, 22, 30], providing important knowledge about PLP biosynthesis. The enzyme requires structural regions to stabilize substrate binding and activate PLP synthesis such as, the C-terminus and helix α2'. The C-terminus plays a role in enzyme function, as seen by the depletion of PLP synthesis in C-terminal deletion mutants of *B. subtilis* and *S. cerevisiae* Pdx1 [23, 18]. Helix α2' orders, when Pdx2 interacts with *B. subtilis* Pdx1 and positions in the vicinity of the active site [14]. Crosslinking studies made in *B. subtilis* Pdx1 suggested that R5P binding is a cooperative process, described by intra-subunit comunication between neighboring subunits [23]. Contributions to understand the role of the Pdx1 C-terminus in enzyme regulation were made by deleting this segment in *P. berghei* Pdx1 and dissecting it in various regions in *P. falciparum* Pdx1 (published in [31]). Additionally, activation and reaction mechanism of the PLP synthase is investigated, using Pdx1 structures in the presence and absence of substrates, as well as in complex with Pdx2 to allow understanding how structural elements such as helix α2' are required for R5P binding and how catalytic residues react with the substrates to produce PLP.

Chapter 2

Materials and Methods

Chemicals. L-Glutamic Dehydrogenase from bovine liver, 3-acetylpyrimidine adenine dinucleotide, D-Ribose 5-phosphate, DL-glyceraldehyde 3-phosphate, L-Glutamine, Glycine, Tris, NaCl, Dithiothreitol (DTT) were from Sigma - Aldrich Vienna - Austria. Imidazol was from Merck Darmstadt-Germany. KCl, NaH_2PO_4 and EDTA were from ApliChem GmbH, Darmstadt-Germany. All other chemicals and reagents were from Roth, Karlsruhe-Germany.

2.1 Molecular biology and protein expression

Heterologous Pdx1 and Pdx2 proteins from *P. falciparum*, *P. berghei* and the archeabacteria *Thermus thermophilus* were used in this study. Vectors containing the desired genes are listed in Table 2.1.

Gene cloning. The plasmodial *pdx1* and *pdx2* genes from *P. falciparum* 3D7 and *P. berghei* cDNA NK65 strains were cloned by M. Gengenbacher, Institute for Hygiene, Heidelberg 2006 as described in [24]. The genes were inserted into NdeI and XhoI restriction sites of the expression vectors pET21a or pET24a (Novagen, Darmstadt-Germany) using enzymes from New England BioLabs (NEB), Frankfurt-Germany.

Point mutations in the wild-type *pbpdx2* (H199N) and *pbpdx1* (M19V, M46I, L82A, L82S, L82F, L82M, M103A, M103F and M148L) genes were introduced using the Quick change muthagenesis Kit (Stratagene, La Jolla, CA, USA). The used primers are listed in Appendix A. Untagged *P. falciparum* Pdx1 and $Pdx2^{H196N}$ constructs were created by PCR amplification using oligonucleotides listed in Appendix A.

Gene encoding for full length *T. thermophilus* Pdx1 protein was amplified by

Table 2.1: Clones and vectors used in this study. Clones marked with an asterisk * were provided by PD Dr. Barbara Kappes, Institute for Hygiene, Heidelberg University.

Clone	Vector	Tag
*Pf*Pdx1*	pET21a	C-terminal 6His-tag
*Pf*Pdx2*	pET21a	C-terminal 6His-tag
*Pf*Pdx2^{H196N}*	pET21a	C-terminal 6His-tag
*Pb*Pdx1*	pET21a	C-terminal 6His-tag
*Pb*Pdx2*	pET24a	C-terminal 6His-tag
*Pf*Pdx1-native	pET21a	-
*Pf*Pdx2^{H196N}-native	pET21a	-
*Pb*Pdx2^{H199N}	pET24a	C-terminal 6His-tag
*Pb*Pdx1^{M19V}	pET21a	C-terminal 6His-tag
*Pb*Pdx1^{M46I}	pET21a	C-terminal 6His-tag
*Pb*Pdx1^{L82A}	pET21a	C-terminal 6His-tag
*Pb*Pdx1^{L82S}	pET21a	C-terminal 6His-tag
*Pb*Pdx1^{L82M}	pET21a	C-terminal 6His-tag
*Pb*Pdx1^{L82F}	pET21a	C-terminal 6His-tag
*Pb*Pdx1^{M103A}	pET21a	C-terminal 6His-tag
*Pb*Pdx1^{M103F}	pET21a	C-terminal 6His-tag
*Pb*Pdx1^{M148L}	pET21a	C-terminal 6His-tag
*Tt*Pdx1	pET21a	C-terminal 6His-tag

PCR from genomic DNA of the *T. thermophilus* HB8 DSM 579 strain purchased from "Deutsche Sammlung von Mikroorganismen und Zellkulturen GmbH", Germany. The *ttpdx1* gene was cloned into BamHI and NotI restriction sites of the PCR®2.1-TOPO® vector (Topo TA cloning kit, Invitrogen). After gene sequencing, the *ttpdx1* gene was excised from the TOPO vector using BamHI (from NEB) and NotI restriction enzymes and further digested with NdeI. The digested product was recloned into NdeI and NotI sites of the expression vector pET21a.

Protein expression. All plasmodial proteins were expressed in *Escherichia coli* BL21-Codon Plus (DE3)-RIL expression cell (Stratagene, USA) transformed with cloned vectors. The *Tt*Pdx1 protein was expressed in *E. coli* BL21-Codon Plus (DE3) expression strain (Stratagene, USA). Cells were grown in LB media at 37°C to an OD_{600} = 0.7 and then induced by addition of 0.1 mM IPTG for 3 hours. After induction, the cells were harvested by centrifugation at 4000xg for 20 minutes at 4°C, flash frozen in liquid nitrogen and stored at -20°C.

2.2 Protein purification

Cell disruption. Pellets from 1 liter expression culture were resuspended in 50 ml lysis buffer (50 mM NaH_2PO_4 pH 8.0, 300 mM NaCl, 10 mM Imidazol). Cells expressing untagged *Pf*Pdx1 and *Pf*Pdx2^{H196N} proteins were resuspended in 200 ml buffer A (50 mM Tris pH 8.0, 10 mM NaCl, 1 mM EDTA, 5% glycerol, 0.5 mM MTG) and cells in suspension were disrupted using a microfluidizer, Microfluidics^{TM} (Newton, Massachusetss, United States). The cellular debris was removed by centrifugation at 26000xg at 4°C. The lysate from *Tt*Pdx1 was incubated at 70°C for 20 minutes and further centrifuged for 20 minutes at 26000xg at 4°C.

1st purification step: Ni affinity for 6His-tagged proteins. Proteins were purified by metal ion affinity chromatography using the Ni-Nitrilotriacetic-acid beads from GE Healthcare, previously equilibrated with lysis buffer and a flow rate of 1 ml/min. The column containing protein-bead mixtures was washed with 50 mM NaH_2PO_4 pH 8.0, 300 mM NaCl, 20 mM imidazol and 50 mM NaH_2PO_4 pH 8.0, 500 mM NaCl, 60 mM imidazol. Proteins were eluted with elution buffer (50 mM NaH_2PO_4 pH 8.0, 300 mM NaCl, 250 mM imidazol). Fractions containing the desired protein were concentrated using Amicon® Ultra filters (Millipore, Ireland) with 30 kDa and 10 kDa cutoff for Pdx1 and Pdx2 proteins, respectively, and applied to a gel filtration column.

Purification of native proteins. Untagged *Pf*Pdx1 and *Pf*Pdx2^{H199N} were purified by anion exchange chromatography, using a self-packed XK26/20 column (GE Healthcare, Uppsala-Sweden) with 5 ml Source 30Q matrix (GE Healthcare, Uppsala-Sweden) and equilibrated with buffer A. The lysate was applied to the column and the column was washed with 3 column volumen (CV) buffer A with a flow rate of 1 ml/min at 4°C. Protein was eluted with a salt gradient from 10 to 800 mM NaCl against buffer B (50 mM Tris pH 8.0, 800 mM NaCl, 1 mM EDTA, 5% glycerol, 0.5 mM MTG). The gradient volume was 20 CV. *Pf*Pdx1 was detected in elution peaks containing 30 mM (peak A), 220 mM (peak B), 410 mM (peak C), 500 mM (peak E) of NaCl (shown in § 3.1.4). *Pf*Pdx2^{H196N} eluted with 286 mM NaCl (Figure B.2). The fractionated proteins from peak A for *Pf*Pdx1 or peak B for *Pf*Pdx2^{H196N} were concentrated using Amicon® Ultra filters with 30 kDa for *Pf*Pdx1 or 10 KDa for *Pf*Pdx2^{H196N} and loaded onto a gel filtration column.

2nd purification step: size exclusion chromatography. For Pdx1 proteins, a Superdex^{TM} 200 26/60 column (GE Healthcare) was used. The column was equilibrated with gel filtration buffer (20 mM Tris/HCl pH 8.0, 200 mM NaCl, 1 mM EDTA, 0.5 mM MTG). The *Tt*Pdx1 gel filtration buffer contained 20 mM Tris pH 8.0, 200 mM KCl. For Pdx2 proteins, a Superdex^{TM} 200 26/60 column (GE Healthcare) equilibrated with 20 mM Hepes pH 7.0, 200 mM KCl, 0.5 mM MTG was used. The elution profiles for *Pb*Pdx1, *Pb*Pdx2 and *Pf*Pdx2 wild types were the same for *Pb*Pdx1 ammonia tunnel mutants, *Pb*Pdx2^{H199N} and *Pf*Pdx2^{H196N}, respectively. Calibration of the gel filtration Superdex 200 26/60 column was done using the calibration standards from Bio-Rad (Bio-

Rad Laboratories, Inc. United States) in the same gel filtration buffer used for protein purification. The gel filtration standard components with respective molecular masses were: Thyroglobulin (bovine) 670 kDa, γ-globulin (bovine) 158 kDa, Ovalbumin (chicken) 44 kDa, Myoglobin (horse) 17 kDa and Vitamin B_{12} 1.35 kDa.

Fractions containing the desired protein were pooled and concentrated for further enzymatic, crystallization, electron microscopy and/or ITC experiments. Protein concentrations were estimated by measuring the absorbance at 280 nm. The predicted extinction coefficients for all proteins used were calculated with the *ProtParam* Tool `http://expasy.org/tools/protparam.html`.

Complex formation analysis by size exclusion chromatography. Purified *Pb*Pdx1 and *Pb*Pdx2^{H199N} proteins at a concentration of 0.15 mM were mixed 1:1 ratio and further loaded on a Superose 6 10/30 (GE Healthcare) previously equilibrated with buffer 20 mM Tris/HCl pH 8.0, 200 mM NaCl, 1 mM EDTA, 0.5 mM MTG. For the analysis of the chimeric *Pb*Pdx1/*Pf*Pdx2^{H196N} complex, proteins were mixed 1:1 molar ratio to a final concentration of $\sim$ 1 mM in buffer 20 mM Tris/HCl pH 8.0, 200 mM NaCl, 1 mM EDTA, 0.5 mM MTG, 10 mM L-glutamine. Calibration of the gel filtration Superose 6 10/30 column was done using the calibration standards from Bio-Rad (Bio-Rad Laboratories, Inc.) as above, in gel filtration buffer 20 mM Tris/HCl pH 8.0, 200 mM NaCl, 1 mM EDTA, 0.5 mM MTG.

2.3 Enzymology

2.3.1 PLP synthase assay

The enzymatic activity for PLP synthesis was monitored spectrophotometrically at λ = 414 nm (ϵ_{PLP}= 5380 M^{-1} cm^{-1}) at 37°C as described [22]. Purified proteins were exchanged to reaction buffer 50 mM Tris/HCl pH 8.0, 20 mM NaCl by centrifugation using Amicon® Ultra filters with 30 kDa and 10 kDa cutoff for Pdx1 and Pdx2 proteins, respectively. PLP synthesis from Pdx1 proteins, including the *Pb*Pdx1 mutants (*Pb*Pdx1^{M19V}, *Pb*Pdx1^{M46I}, *Pb*Pdx1^{L82A}, *Pb*Pdx1^{L82S}, *Pb*Pdx1^{L82M}, *Pb*Pdx1^{L82F}, *Pb*Pdx1^{M103A}, *Pb*Pdx1^{M103F} and *Pb*Pdx1^{M148L}) contained a reaction mixture of 40 μM Pdx1, 1 mM R5P, 1 mM G3P and 10 mM NH_4Cl in a final volume of 300 μl. For Pdx1/Pdx2 complexes, additionally 40 μM Pdx2 was present, and NH_4Cl was replaced by 10 mM L-Gln. Measurements were carried out at 37°C for four hours in 50 mM Tris/HCl, 20 mM NaCl pH 8.0.

2.3.2 Glutaminase assay

The enzymatic activity for glutamine hydrolysis was analyzed using a coupled enzyme assay with glutamate dehydrogenase described by [24]. The reaction mixture contained 5 μM Pdx1 or Pdx1 mutants, 5 μM Pdx2, 10 mM L-Gln, 10 U glutamate dehydrogenase and 0.5 mM $APAD^+$ in 50 mM Tris/HCl pH 8.0, 20 mM NaCl at a final volume of 300 μl. The reduction of $APAD^+$ to APADH was monitored at 363 nm (ϵ_{APADH}= 8900 M^{-1} cm^{-1}) for 20 min at 30°C.

2.4 Biophysical experiments

2.4.1 Isothermal titration calorimetry, ITC

Protein-protein interactions can be characterized by their heat generated or absorbed. ITC is a method that provides information of enthalpy ΔH°, entropy ΔS° and Gibbs free energy ΔG° changes of any reaction under isothermal conditions. In a single ITC experiment, two reactants are titrated against one another generating (exothermic reaction) or absorbing (endothermic reaction) heat during the molecular interaction. The binding constant K_a, enthalpy change ΔH and binding stoichiometry n can be determined by non-linear least squares curve-fitting of the heat change per injection [32]. From the binding constant K_a, the change in free energy of binding ΔG° and entropy change ΔS° at constant temperature can be calculated using the equation 2.1 and 2.2, where R is the gas constant and T the temperature.

$$\Delta G^\circ = -RTlnK_a \tag{2.1}$$

$$\Delta G^\circ = \Delta H - T\Delta S^\circ \tag{2.2}$$

In this work, complex formation between *Pb*Pdx1 or *Pf*Pdx1 with *Pb*Pdx2 or *Pf*Pdx2 were analysed by ITC, using a VP-ITC Microcalorimeter (MicroCal^{TM}, Northampton, USA) as described before [15, 33]. Binding assays were done in absence or presence of 1 mM L-Gln at 25°C. All purified proteins were dialysed overnight in buffer 20 mM Tris/HCl pH 8.0, 20 mM NaCl, 1 mM EDTA, 0.5 mM MTG, +/- 1 mM L-glutamine. The experimental protocol used an initial 5 μl injection followed by 29 injections of 7 μl of Pdx2, typically at a concentration of 350 − 400 μM, against a cell containing Pdx1, typically at a concentration of 40 μM. The binding heat was determined by integration of the areas under the peaks, using the Origin 7.0 graphing/data analysis software [34]. The data were corrected for buffer dilution heats, using measurements in which Pdx2 was titrated into buffer.

2.4.2 Analytical ultracentrigution, AUC

Association of the *Pb*Pdx1 and *Pb*Pdx2^{H199N} in solution in the presence and absence of R5P and L-glutamine were determined by hydrodynamic analysis in analytical ultracentrifugation experiments using a Beckman Optima XL-A ultracentrifuge equipped with absorbance optics and an An60 Ti rotor (Beckman Coulter, Fullerton, CA). Sedimentation velocity studies were carried out at 42,000 rpm at 20°C using proteins with absorbance of 1 at λ=280 nm. Centrifugation was done in buffer 20 mM Tris pH 8.0, 20 mM NaCl, 1 mM EDTA, 0.5 mM MTG, +/- 1 mM R5P and +/- 1 mM L-glutamine.

Buffer density ρ and viscosity η were calculated using the program SEDNTERP, Version 1.09 (University of New Hampshire). Sedimentation coefficients were derived from the c(s) distribution of the raw data processed in Sedfit [35]. The theoretical and expected molecular weights were calculated using the aminoacid sequence with and without substrate(s) and from the molar mass distribution using Sedfit [36, 35], respectively.

2.5 Crystallization and Structure determination

Fundamentals of X-ray diffraction

X-rays are electromagnetic waves with wavelengths in the order of atomic distances 0.1 nm = 1 Å. The suitable x-rays used in crystallography are in the range between 0.5 Å and 1.6 Å, because the x-rays can interact and be scattered by electrons of atoms in protein crystals [37]. Crystals contain molecule(s) within a unit cell, which is periodically repeated in three dimensions. Interaction of the incoming X-ray with the atom electrons produces X-ray scattering. The conditions for constructive interference of scattered waves are given by Bragg's Law (equation 2.3):

$$n\lambda = 2dsin\theta \tag{2.3}$$

where n is integer, d the spacing distance between scattering planes, θ the scattering angle and λ the wavelenght of the x-ray.

A reflexion for each set of parallel lattice planes is observed only if the distance d and θ between parallel lattice planes follow Bragg's Law. The diffracted beam produces spots, whose intensity $I \propto A^2$ can be measured by the detector. However, the phase of the beam wave cannot be measured directly, because detectors are sensitive only to the incoming energy and this energy is independent of the wave phase. If the phases are known, the electron density of the diffracting atoms in the unit cell can be obtained by Fourier Transformation.

2.5.1 Protein crystallization and data collection

*Pb*Pdx1, *Pb*Pdx1-R5P, *Pb*Pdx1/*Pb*Pdx2^{H199N} and *Pb*Pdx1/*Pf*Pdx2^{H196N} and *Tt*Pdx1 were crystallized by sitting or hanging drop vapor diffusion at 19°C under the conditions written in Tables 2.2. Crystals of *Pb*Pdx1 with R5P were obtained by co-crystallization. Before setting drops, the protein was incubated with 10 mM R5P in gel filtration buffer for 1 hour at room temperature. The *Tt*Pdx1 crystals were soaked in mother liquor containing substrates as detailed in Tables 2.2. Crystals were flash frozen in liquid nitrogen, using respective cryoprotectants (Tables 2.2). Datasets were collected in the European Synchrotron Radiation Facility in Grenoble, France. For complete data collection, optimal starting angle and oscillation range were calculated using the "Strategy" option implemented in the software i*MOSFLM* graphical user interface [38].

	***Pb*Pdx1** (ga48-3)	***Pb*Pdx1-R5P** (ga50-3)	***Pb*Pdx1/ *Pf*Pdx2^{H196N}** (ga38-5)
Protein (mg/ml)	20	20	15
Beamline	ID23-2	ID14-4	ID23-1
Crystallization condition	0.1 Bicine pH 8.5, 1.6 M LiCl	0.1 Bicine pH 8.5, 1.2 M LiCl	0.1 NaK/Phosphate pH 6.2, 0.2 M NaCl, 6% PEG8000
substrate added (mM)		10 mM R5P in the condition	
Cryoprotectant	15 % glycerol	15% glycerol	20% EG

	***Tt*Pdx1-R5P** (i6-2)	***Tt*Pdx1-PLP** (i20-5)
Protein (mg/ml)	30	30
Beamline	ID29	ID14-4
Crystallization condition	0.1 MES pH 6.0, 0.8 M LiCl, 10% PEG6000	0.1 NaAcetate pH 5.5, 0.2 M MgAcetate, 20% MPD
substrate added (mM)	15 mM R5P	10 mM PLP
incubation time	1 day	15 hours
Cryoprotectant	20 % PEG400	MPD

Table 2.2: Crystallization conditions for the plasmodial and *T. thermophilus* structures.

2.5.2 Crystallographic data processing

Fundamentals of data processing

Indexing. The indexing procedure consists of assigning the unit cell parameters a, b and c and corresponding angles α, β and γ based on the symmetry of the diffracted reflections. The software reads the spot positions from one or more diffraction images, considering the crystal distance to detector. The spot position provides information about the crystal lattice, that can enclose several posibilities. The task is to find the lattice vectors with the highest Bravais lattice symmetry and lowest penalty. Once the lattice symmetry is chosen, parameter refinement (unit cell parameters, crystal orientation, the crystal-to-detector distance and position) is constrained to the chosen lattice symmetry.

Integration and scaling. After the unit-cell parameters and orientation are known, integration of the spots can be performed. During integration, all raw pixel intensity of full reflections, as well as partial reflections spread over multiple images are converted into single reflections by considering a defined pixel area (peak/background area) of the reflections. The proccess consists of estimating the intensities of the reflected spots and error value to each intensity by substracting the x-ray background. The background is measured in a region around the reflection. At the end all values for the intensities are listed in the form of Miller indices *hkl* with respective intensities $I(hkl)$ and estimated errors $\sigma I(hkl)$ for each observed reflection.

Many measured reflections from identical reflections or symmetry-related reflections are further scaled and merged in a process called data reduction, in order to generate unique reflections dataset that corresponds to the asymmetric unit of the reciprocal space. The indicators of data quality will be reflected in the R_{merge} (equation 2.4), redundancy and the signal-to-noise ratio ($I/\sigma I$) in each shell and in the entire dataset. The statistical values for each dataset processed in this work are shown in Tables 3.7 and 3.9.

$$R_{merge} = \frac{\sum_h \sum_{i=1}^{N} |I(h)_i - \bar{I}(h)|}{\sum_h \sum_{i=1}^{N} I(h)_i} \tag{2.4}$$

where N is the number of redundant observations of a given reflection h and $\bar{I}(h)$ is the average intensity of each reflection.

Datasets collected from *Pb*Pdx1and *Pb*Pdx1-R5P crystals were indexed in R32 and for *Pb*Pdx1/*Pf*Pdx2^{H196N} crystals in P6$_1$22 space groups. The indexed data were reduced using *Denzo* and *Scalepack* from HKL 2000 software [39]. Datasets from *Tt*Pdx1 crystals were indexed in the R32 space group and integrated with i*MOSFLM* [38]; scaling was performed using *Scala* [40]. Details of data processing from all structures are listed in Tables 3.7 and 3.9.

2.5.3 Structure solution and refinement

Fundamentals of structure determination and refinement

Three methods exist to calculate experimental phases:

- Molecular Replacement
- Multiple Isomorphous Replacement
- Multiple Anomalous Dispertion

3-Dimensional structure models were available to permit the use of the molecular replacement method to solve the structures of this study.

Molecular Replacement

The phases are obtained using the coordinates of a model with sufficient homology to the structure to be solved. To calculate the amplitudes F_{calc} and the phases Φ_{calc}, the coordinates of the solved model are positioned in the unit cell by rotation and translation functions. With the help of the Patterson map, intramolecular vectors - which depend on the orientation of the molecule - are used in the rotation function. The Patterson map of the unknown structure is compared to the Patterson maps of the known structure in different orientations. The correlation between the two maps is obtained when the two vectors have similar orientation. Subsequently, when the orientation of the molecule is known the translation function - based on the intermolecular vectors - places the molecule to the correct coordinates in the assymetric unit. The phases derived from the model and the experimental observed amplitudes F_{obs} are used to calculate an electron density map. The model is further built manually and refined to find the differences between the model and the target and establish an agreement to the experimental data.

In this study, the structures of *Pb*Pdx1 and *Pb*Pdx1-R5P at 2.4 Å resolution were solved by molecular replacement using *MOLREP* from *CCP*4 suite [41]. *Bs*Pdx1 (PDB entry 2NV1, [14]) was used as starting model for the *Pb*Pdx1 structure. Iterative model building of the chains in the asymmetric unit and refinement were carried out with *Coot* [42] and *REFMAC*5 [43]. Water molecules were added to the model using *ARP/wARP*. The chimera *Pb*Pdx1/*Pf*Pdx2^{H196N} structure was solved by molecular replacement using *Phaser* [44] with the refined *Pb*Pdx1 as a search model. The 6 *Pf*Pdx2^{H196N} subunits were found one by one, using the solution obtained from *Phaser* in *MOLREP* as fixed input model and *Pf*Pdx2 (PDB entry 2abw, [24]) as a search model. All obtained models were refined in *REFMAC*5 (Table 3.6). The *Tt*Pdx1 structures were solved by molecular replacement using *imosflm* [38] and phases from *Tt*Pdx1 (PDB entry 2ZBT).

Structure refinement. Considerations of refinement at low resolution

After a macromolecular structure model is obtained from molecular replacement, the model can be refined. Refinement consists of minimizing errors in the geometry and stereochemistry of bond lengths and angles, which remain after real space model building [45]. The parameters of a model are refined against the experimental data to obtain the best fit between the structure factor amplitudes of the observed F_{obs} and calculated F_{calc} model, quantified by the R_{work} (Equation 2.5):

$$R_{factor} = \frac{\sum_h |F_{obs} - F_{calc}|}{\sum_h F_{obs}} \tag{2.5}$$

A cross-validation against a subset of unused experimental data (5% of the

data) is monitored by the R_{free} value, which has the same equation as the R_{work} (Equation 2.5).

Crystals that diffract to high resolution produce interpretable electron density maps because the diffraction data contains information of atomic distances d $<$ 2.5 Å (e.g. *Pb*Pdx1, *Tt*Pdx1 and their corresponding derivatives solved in this work). For low-resolution crystal structures (e.g. *Pb*Pdx1/*Pf*Pdx2^{H196N} structure), side chains cannot be easily placed. The problem stems from the lack of sufficient number of observations contained in the diffraction data required to define the position of atoms at high resolution. The availability of high resolution structures as molecular replacement models (i.e., *Pb*Pdx1 at 2.4 Å resolution and *Pf*Pdx2 at 1.6 Å resolution [24]) served as useful starting point for the refinement at low resolution (i.e. *Pb*Pdx1/*Pf*Pdx2^{H196N} structure). C_α fragments are traced of regions such as, loops and α-helices not possible to visualize in places where they are disordered in the individual subunits. The regions can be modelled manually in the electron density maps with programs like *Coot* and then refined using non-crystallographic symmetry (if symmetry related molecules are present in the assymetric unit), rigid body refinement and/or secondary structure restraint using algoritms available in *Phenix* and/or *CCP4i* suites to improve experimental phases. Details of refinement statistics from all structures are listed in Tables 3.7 and 3.9.

2.5.4 Structure analysis

Structural superposition
Differences between *Pb*Pdx1/*Pf*Pdx2^{H196N} and *Bs*Pdx1/*Bs*Pdx2^{H170N} complexes were seen by superposition of the C_α backbone of a single Pdx1 from the two structures, using the *lsqkab* program from the CCP4 suite [41]. The program calculated the root main square deviation of the Cα atoms (rmsd). The resulting coordinates were recorded and used to superpose individual Pdx2 chain from *Pb*Pdx1/*Pf*Pdx2^{H196N} onto a single Pdx2 from *Pb*Pdx1/*Pf*Pdx2^{H196N} in *lsqkab*, providing both the rotation matrix and translation distance between centroids. The rotation matrix was used to calculate the rotation angle.

Electrostatic surface analysis
Comparison of the electrostatic surfaces between *Pb*Pdx1 (solved in this study) and *Pf*Pdx1 from the *Pf*Pdx1/*Pf*Pdx2 model described by [15] were done by superposition of the two structures in *Pymol* and further calculation of the electrostatic map using Adaptive Poisson-Boltzmann Solvent (APBS) tool `www.umich.edu/~mlerner/Pymol`.

Ligand-protein building and representation
The R5P and PLP coordinates were sketched with the CCP4 library sketcher [41]. The monomer library files were used as input coordinates for manual building in *Coot* of the R5P in the active site of *Pb*Pdx1 and *Tt*Pdx1, as well as PLP in *Tt*Pdx1 and further refinement in *Refmac*5. Schematic diagrams of

ligand-protein interaction were generated with the program *ligplot* [46].

2.5.5 Electron microscopy analysis

Protein samples of *Pb*Pdx1 in complex with *Pb*Pdx2 or *Pb*Pdx2^{H199N}, as well as *Pf*Pdx1 and *Pf*Pdx1/*Pf*Pdx2^{H196N} complex were prepared in reaction buffer used for enzymatic assays (§ 2.3), containing 50 mM Tris pH 8.0, 20 mM NaCl and -/+ 10 mM Gln. The samples in a concentration of 20 $\mu g/ml$ were stained with 2 % uranyl acetate and placed onto a carbon-coated grid using the sandwich technique as detailed in [47]. The data were recorded either with a CM120 Biotwin electron microscope at 100 kV and a nominal magnification of 53,000x on a 4kx4k Tietz-CCD-camera or with a FEI F20 electron microscope at 200 kV with a nominal magnification of 29,000x on a Tietz 8kx8k CMOS camera. The nominal pixel size was 2.36 Å/pixel for the CM120 and 2.8 Å/pixel for the F20, respectively. For image analysis, particle images were semi-automatically selected with the autobox option of Boxer [48]. Subsequent alignment and classification were done with IMAGIC 5 [49].

Chapter 3

Results

3.1 Assembly of the PLP synthase complex in *Plasmodium*

3.1.1 Crystallization of the plasmodial PLP synthase complex

Structural studies in the bacterial Pdx1/Pdx2 complex have shown that several conformational changes occur in the two subunits upon complex formation [14, 16]. Some of these are implicated in mediating the protein-protein interface e.g., the αN terminus of Pdx1 and structural changes leading to a peptide flip in Pdx2 (described in § 1.2.1).

To understand what promotes a stronger protein-protein interaction in the plasmodial Pdx1/Pdx2 when compared to the bacterial complex, a structural model was built based on the known bacterial complex and *P. falciparum* Pdx2 structures. This model proposed possible regions required at the interface not present in the bacterial complex and explained the variations seen in the protein sequence between the bacterial Pdx1 and plasmodial *Pf*Pdx1 (54% identical), Alignment D.1. However, a true structure was necessary to characterize these differences in more detail.

Several crystallization attempts were pursued with the *P. falciparum* PLP synthase complex and failed. Instead, proteins from the rodent malaria parasite *P. berghei* were succesfully crystallized, obtaining different forms: needle-, star-, rombohedral- and spear- crystals. Crystallization was carried out using purified *Pb*Pdx1 and *Pb*Pdx2 or *Pb*Pdx2^{H199N} proteins in the presence and absence of L-glutamine. Crystals were obtained from different preparations:

- *Pb*Pdx1 and *Pb*Pdx2^{H199N} were mixed 1:1 ratio and gel filtered before crystallization (Figure 3.1, upper panel)

- the mixed proteins were subjected to crystallization in the presence of glutamine (Figure 3.1, lower panel *a*, *c* and *d*) and,

- a protein mixture containing *Pb*Pdx1/*Pb*Pdx2 was crystallized in the absence of glutamine (Figure 3.1, lower panel *b*).

All crystal forms were tested by x-ray crystallography, giving weak and anisotropic diffraction at low resolution ($\geq$ 4.5 Å). The highest resolution was obtained by the needle crystals grown from a mixture of *Pb*Pdx1/*Pb*Pdx2^{H199N} gel filtered previous to crystallization (Figure 3.1, upper panel). Several crystallization conditions such as, temperature, purification buffer and protein ratio variations were tried, in order to improve diffraction resolution, but were unsuccessful and structure solution was not pursued.

Due to the crystallization problems encountered with the Pdx1/Pdx2 complexes from *P. berghei* described above, a chimera consisting of Pdx1 from *P. berghei* and Pdx2^{H196N} from *P. falciparum* was subjected to crystallization. The synthase and glutaminase from the different parasites formed a complex *in vitro*, as seen in size exclusion chromatography (Figure 3.2). The two Pdx1 and Pdx2 proteins from the human and rodent parasites share high similarities in protein sequence, 84.5% between *Pf*Pdx1 and *Pb*Pdx1 and 63.8% between *Pf*Pdx2 and *Pb*Pdx2. The chimera *Pb*Pdx1/ *Pb*Pdx2^{H199N} complex succesfully crystallized (Figure 3.2, top right) and diffracted to 3.6 Å resolution.

3.1.2 Reciprocal activation and interaction of Pdx1 and Pdx2 from different plasmodial species

Earlier studies described the importance of helix αN of Pdx1 for heteromeric Pdx1/Pdx2 interaction and glutaminase activation [14, 15]. Furthermore, the role of αN showed species specific properties, when analysing the interaction of a *Pf*Pdx1 "swap mutant" containing the αN helix from *Bs*Pdx1 by isothermal titration calorimetry [15]. The mutant interacted and activated the *Bs*Pdx2 glutaminase subunit but not *Pf*Pdx2. Additionally, in vivo complementation and in vitro studies showed PLP synthesis is depleted when the parasite Pdx1 and bacterial Pdx2 interaction is induced [24], suggesting there are species-specific features for the PLP synthase complex activation.

To test whether the *P. falciparum* and *P. berghei* Pdx1/Pdx2 complexes share similar activation properties that would allow to validate the chimeric *Pb*Pdx1/ *Pf*Pdx2^{H196N} complex as an apropiate system to study the plasmodial PLP synthase complex, enzymatic and thermodynamic experiments by ITC were carried out with the genuine complexes and the two possible chimeras *P. berghei* Pdx1 with *P. falciparum* Pdx2 and viceversa.

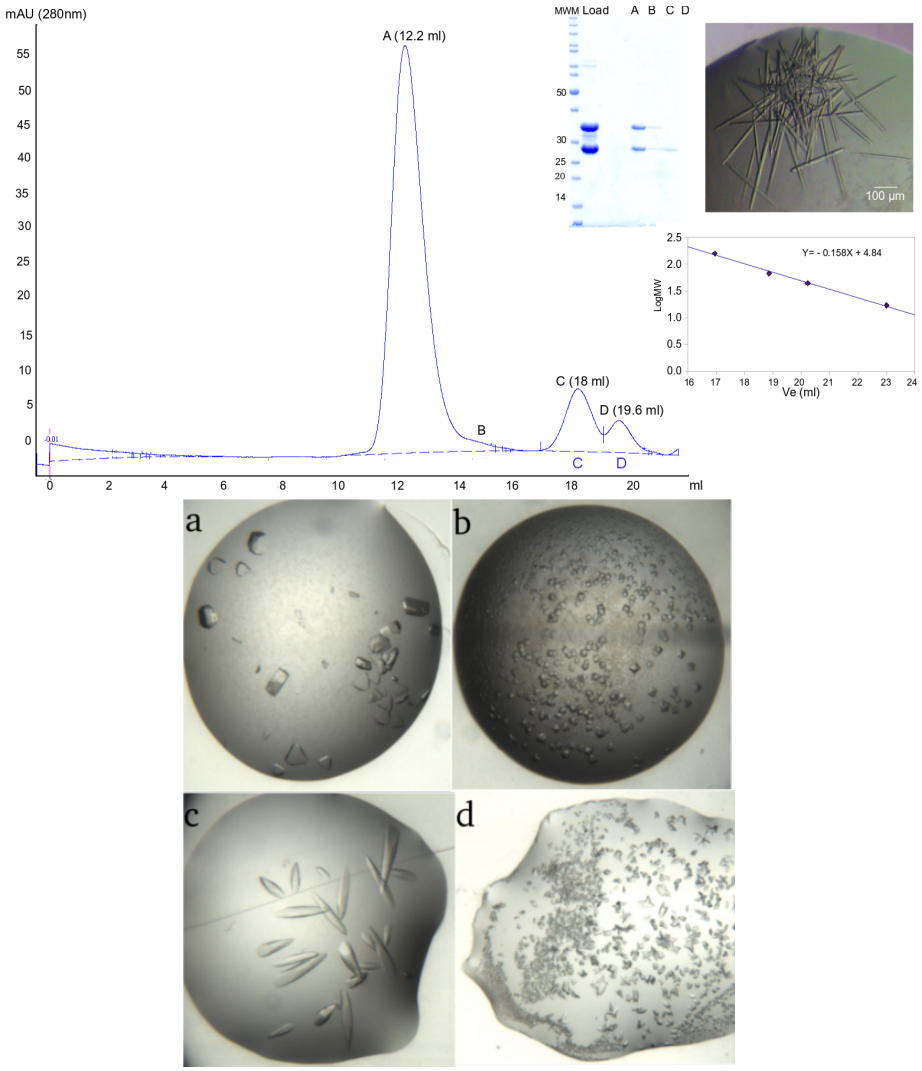

Figure 3.1: Purification and crystallization of the *P. berghei* Pdx1/Pdx2 complex. Upper panel, purified *Pb*Pdx1 and *Pb*Pdx2^{H199N} proteins were mixed 1:1 ratio to a final concentration of 0.5 mM and loaded onto a Superose 6 10/300 GL (GE Healthcare). The elution profile is shown and collected fractions from corresponding A, B, C and D peaks were evaluated by SDS-PAGE (middle). The apparent molecular weight of peak A is 817 kDa, for the 24 mer of Pdx1/Pdx2 (theoretical value 708 kDa) calculated with the calibration curve (lower, right). Needle crystals (upper, right) from the pooled peak A fractions appeared under the condition containing 0.1 M Hepes pH 6.0, 0.2 M $NaNO_3$, 1.9 M NH_2SO_4. The needle crystals diffracted anisotropically to 4.5-5.5 Å resolution. Lower panel, the purified *Pb*Pdx1 and *Pb*Pdx2 or *Pb*Pdx2^{H199N} were mixed 1:1 ratio to a final concentration of 0.5 - 1 mM in the absence and presence of 10 mM glutamine and crystallized under the conditions: *a*, 0.1 MES pH 6.0, 5% PEG6000; *b*, 0.1 Hepes pH 7.0, 5% PEG6000; *c*, 0.1 M Bicine pH 9.0, 2 M NaCl, 10% PEG6000; and *d*, 0.1 M Tris pH 8.0, 1 M LiCl, 10 % PEG6000. Crystals obtained in *a*, *c* and *d*, contained variant *Pb*Pdx2^{H199N} in the presence of glutamine and, crystals obtained under the condition *b*, contained Pdx2 in the absence of glutamine. All four crystal forms diffracted to poor resolutions lower than 8 Å resolution.

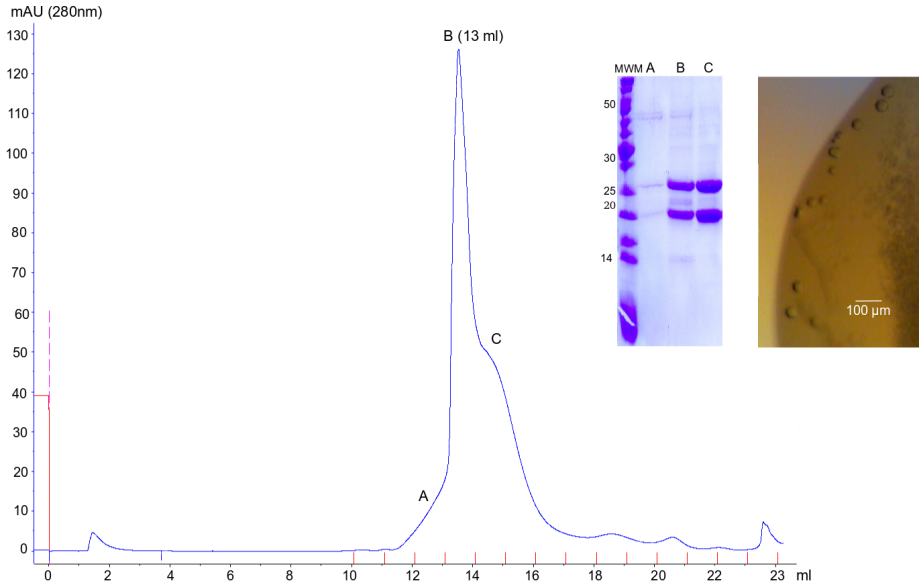

Figure 3.2: Purification and crystallization of the chimeric PbPdx1/PfPdx2^{H196N} complex in the presence of glutamine. Purified PbPdx1 and PfPdx2^{H196N} were mixed 1:1 molar ratio to a final concentration of $\sim$ 1 mM in the presence of 10 mM glutamine and loaded onto a gel filtration column Superose 6 10/300 GL (elution profile is shown). Samples from peak fractions A, B and C were evaluated by SDS-PAGE (middle). Elution peak B corresponded to the PbPdx1/PfPdx2^{H196N} complex with a molecular mass of 610 kDa, calculated using the calibration curve shown in Figure 3.1. The sample from fraction peak was concentrated to 15 mgml and used for crystallization. Crystals of the PbPdx1/PfPdx2^{H196N} complex with $\sim$ 20 μm appeared under 0.1 M Na/K Phosphate pH 6.2, 0.2 M NaCl, 10% NaCl at 19°C (right).

Activation of Pdx1 and Pdx2 from *P. falciparum* and *P. berghei*

PLP synthesis and glutaminase activity were monitored under saturating conditions of substrates, as described in § 2.3. The PbPdx1/PfPdx2 complex showed an overall PLP and glutaminase activities similar to the genuine complexes PbPdx1/PbPdx2 and PfPdx1/PfPdx2, respectively (Table 3.1). The control PfPdx1/PbPdx2 complex had a PLP activity similar to PfPdx1/PfPdx2. Glutamine hydrolysis showed a slight dependency of the subunit origin, for example, the chimera containing *P. falciparum* Pdx2 had a slight increase of glutaminase activity, whereas the chimera containing PbPdx2 was decreased like the PbPdx1/PbPdx2, each with activities similar to the genuine complexes (Table 3.1). The results suggest that variations in the Pdx2 activity are independent on the plasmodial Pdx1 subunit used.

Interaction between Pdx1 and Pdx2 subunits from *P. falciparum* and *P. berghei*

The Pdx2 substrate L-glutamine was reported to play a major role in strengthening the Pdx1 / Pdx2 interaction, leading to 23-fold increased affinity of the *B.*

	PLP synthesis	**Glutaminase activity**
***Pf*Pdx1/*Pf*Pdx2**	0.7 ± 0.1	260 ± 28
***Pb*Pdx1/*Pb*Pdx2**	1.1 ± 0.2	150 ± 12
***Pb*Pdx1/*Pf*Pdx2**	1.3 ± 0.1	233 ± 14
***Pf*Pdx1/*Pb*Pdx2**	0.9 ± 0.1	175 ± 20

Table 3.1: PLP synthesis and glutaminase activities of *P. falciparum* and *P. berghei* complexes (in nmol/min.mg)

subtilis and to 29-fold increased affinity of the *P.falciparum* proteins [15, 33]. To test the influence of L-Gln on complex formation, the chimera *Pb*Pdx1/*Pf*Pdx2 and controls *Pb*Pdx1/*Pb*Pdx2 or *Pf*Pdx1/*Pb*Pdx2 complexes were analysed by ITC as described in § 2.4.1. Pdx2 (or catalytically inactive Pdx2: *Pb*Pdx2^{H199N} and *Pf*Pdx2^{H196N}) was used as the titrant in the presence or absence of 1 mM glutamine at 25°C. The titration data for all analysed complexes are shown in Figure 3.3. In contrast to *P. falciparum* PLP synthase complex [15], addition of L-glutamine to *P. berghei* proteins did not show significant increase in affinity as judged from the similar dissociation konstant (K_d) values in the presence and absence of glutamine (Table 3.2). Chimeric complexes behaved like complexes from *P. berghei* and showed no (*Pb*Pdx2 vs. *Pf*Pdx1) or little (*Pf*Pdx2 vs. *Pb*Pdx1) dependence on addition of L-glutamine, according to the K_d values (Table 3.2). The ITC data suggest that in all cases the proteins become more ordered when substrate glutamine binds as entropy loss occurs and additional interactions are formed, seen as enthalpy gain.

	N	Kd (nM)	ΔG (kJ/mol)	ΔH (kJ/mol)	-TΔS (kJ/mol)
PfPdx1/PfPdx2	1±0.1	2000±300	-33±1	12±3	-44±3
PfPdx1/PfPdx2/Gln	0.9±0.1	70±40	-41±1	-34±6	-6±6
PbPdx1/PbPdx2	0.84±0.1	83.1±30.4	-41.1±0.9	-16.0±1.1	-25.2±1.1
PbPdx1/PbPdx2/Gln	0.8±0.12	45.9±17.6	-42.5±1.3	-52.7±11.5	10.2±10.5
PbPdx1/PfPdx2	1.1±0.07	90.9±9.0	-40.2±0.3	9.8±1.1	-50.0±1.3
PbPdx1/PfPdx2/Gln	0.9±0.13	36.3±9.9	-42.6±0.7	-42.8±2.2	-0.2±1.6
PfPdx1/PbPdx2	0.6	143	-39	-25	-14
PfPdx1/PbPdx2/Gln	0.8	130	-39	-58	-19

Table 3.2: Interaction of Pdx1 and Pdx2 from *P.falciparum* and *P. berghei* in absence and presence of glutamine

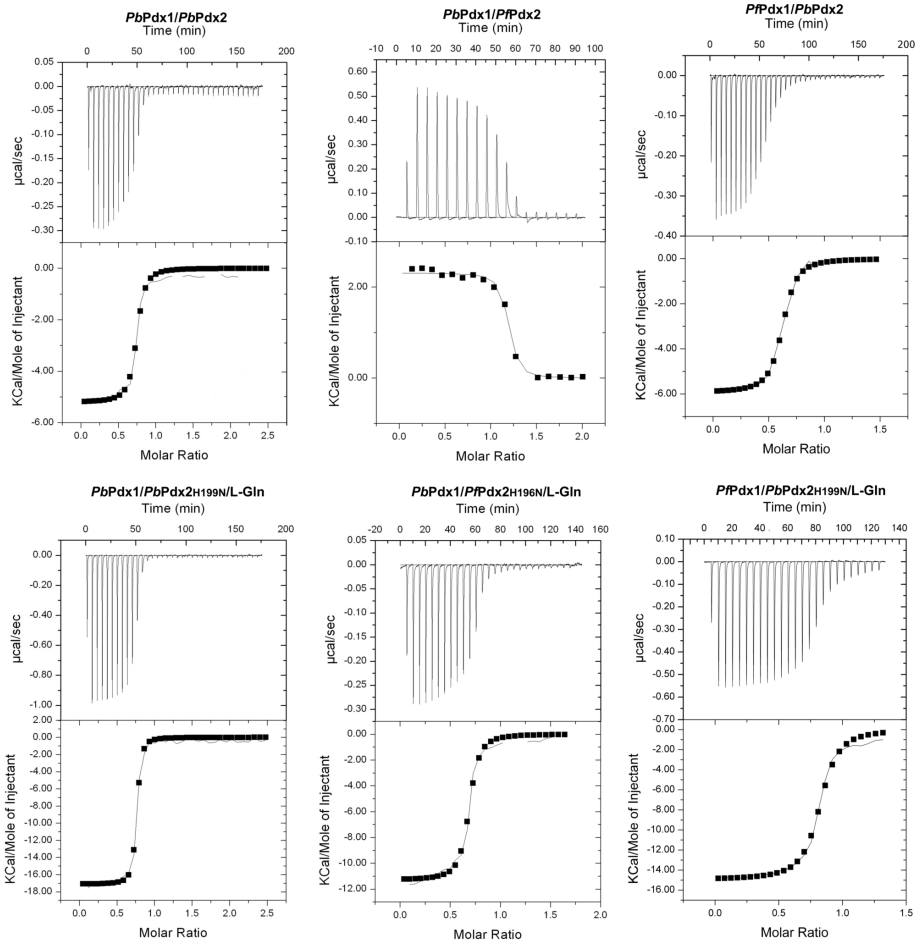

Figure 3.3: Isothermal titration calorimetry of the plasmodial PLP synthase complexes in absence or presence of 1 mM L-glutamine. Upper pannel shows the ITC results of the *Pb*Pdx1/*Pb*Pdx2, *Pb*Pdx1/*Pf*Pdx2 and *Pf*Pdx1/*Pb*Pdx2. In the lower panel, the ITC results of the same complexes in the presence of glutamine are shown, using inactive Pdx2 with a mutation at the His residue for Asn (*Pb*Pdx2^{H199N} and *Pf*Pdx2^{H196N}). Binding assays and fitting of the heat signals were performed as described in § 2.4.1.

3.1.3 Reciprocal interaction of Pdx1 and Pdx2 for enzyme activation

Effect of Pdx1 in glutamine binding by Pdx2

Activation of Pdx2 requires the presence of Pdx1 [50]. Basal glutamine hydrolysis is observed in the absence of Pdx1 and is enhanced in the presence of the PLP synthase (Table 3.3). To test whether Pdx2 can bind glutamine before complex formation with Pdx1, ITC measurements were done at 25°C. When glutamine was titrated into *Pb*Pdx1 or *Pb*Pdx2^{H199N}, no heat was observed, while titration into a mixture of 1:1 molar ratio of *Pb*Pdx1/*Pb*Pdx2^{H199N} did

produce heat of binding generated by the substrate (Figure 3.4). This suggests that the substrate glutamine does not bind tightly to the autonomous Pdx2 subunit, and instead requires a preformed Pdx1/Pdx2 complex.

	Glutaminase activity
***Pb*Pdx2**	24 ± 6
***Pb*Pdx1/*Pb*Pdx2**	150 ± 12

Table 3.3: Glutaminase activity of *P. berghei* Pdx2 influenced by Pdx1 in nmol/min.mg

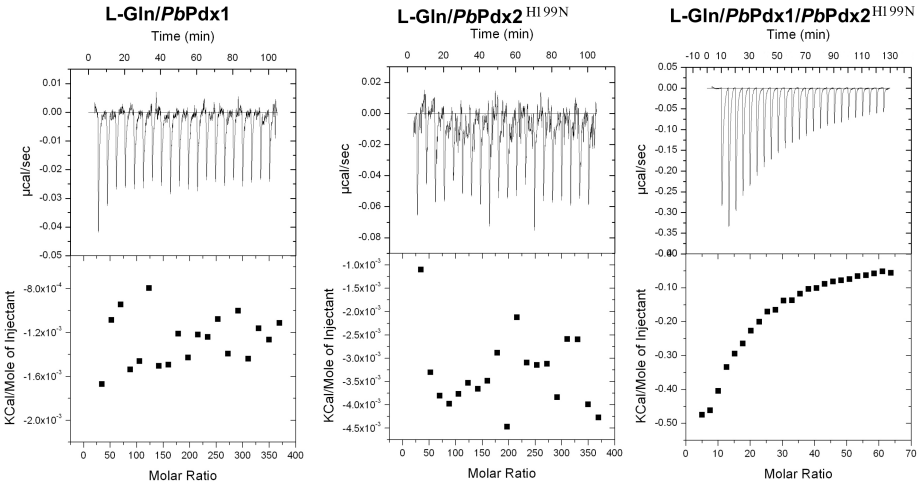

Figure 3.4: Isothermal titration calorimetry of glutamine into the plasmodial PLP synthase complex. Titration of 100 mM glutamine into 40 μM *Pb*Pdx1 (left), 40 μM *Pb*Pdx2^{H199N} (middle) or 40 μM *Pb*Pdx1/*Pb*Pdx2^{H199N} (right). No significant heat change is observed after titration of glutamine into the autonomous Pdx1 and Pdx2 proteins.

Effect of R5P in Pdx1/Pdx2 interaction and glutaminase activation

A particular feature of glutamine amidotransferases is an acceptor domain for ammonia. Usually, it is expected that this ammonia acceptor promotes the activation of the glutaminase. In contrast, the glutaminase rate in the PLP synthase complex is not influenced by an ammonia acceptor [12]. Whether the substrate R5P is required to enhance protein complex assembly is not known. To discard the possibility Pdx1 had bound R5P from the bacterial cytosol during protein expression, the purified Pdx1 was incubated with 1 mM G3P and 10 mM NH_4Cl at room temperature, followed by dialysis and gel filtration to remove remnants of substrates and PLP. The protein free of R5P adduct was used in the enzymatic and interaction assays. The activity of Pdx2 was tested in the presence or absence of R5P and was similar in both assays (Table 3.4). In addition, unbound Pdx1 was used for interaction studies by ITC (Table 3.5) and analytical ultracentrifugation (AUC) (Figure 3.5). The results showed Pdx1 and Pdx2 can interact in the same manner independent on the presence and absence of the sugar.

	Glutaminase activity
***Pb*Pdx1/*Pb*Pdx2**	183 ± 39
***Pb*Pdx1/*Pb*Pdx2/R5P**	179 ± 14

Table 3.4: Glutaminase specific activity of *P. berghei* PLP synthase complex in the presence or absence of R5P (in nmol/min.mg)

	N	Kd (nM)	ΔG (kJ/mol)	ΔH (kJ/mol)	-TΔS (kJ/mol)
*Pb*Pdx1/*Pb*Pdx2	0.84±0.1	83.1±30.4	-41.1±0.9	-16.0±1.1	-25.2±1.1
*Pb*Pdx1/*Pb*Pdx2/R5P	1	99.0±25	-40±0.6	-14.2±2	-26±0.4
PbPdx1/PbPdx2/R5P/Gln	0.94±0.02	85±28	-40.4±	-49±	-8.2±10.5

Table 3.5: Effect of R5P on the interaction of Pdx1 and Pdx2 from *P. berghei* analysed by isothermal titration calorimetry.

	ρ^a (g/cm^3)	η^b (cP)	$S_{exp}{}^c$ (S)	$M_{exp}{}^d$ (kDa)	$M_{calc}{}^e$ (kDa)
*Pb*Pdx1/*Pb*Pdx2	0.9	0.001	19.3 2.5	611 28.02	720.12 26.5^f
*Pb*Pdx1/*Pb*Pdx2/R5P	1	0.001	19.4 2.53	590.4 27.7	721.872 26.5^f
PbPdx1/PbPdx2/R5P/Gln	1	0.001	19.2 2.5	582 27.26	724.536 26.5^f

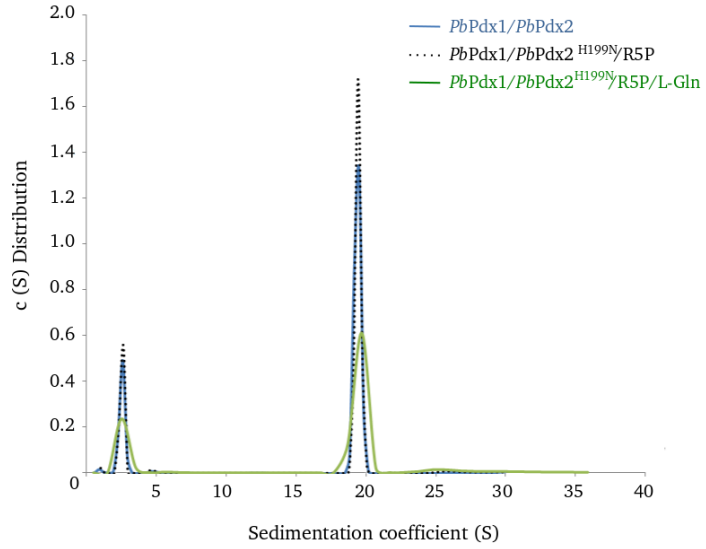

Figure 3.5: Analysis of the R5P effect in the *Pb*Pdx1/*Pb*Pdx2^{H199N} complex in the presence of L-Gln by AUC. Sedimentation velocity runs at 35000 rpm at λ=280 nm. Sample concentration was with an absorbance of 1 at 280 nm. The frictional ratio for all Pdx1/Pdx2 complexes were 1.3.
^{a} and ^{b}, buffer density and viscosity, respectively calculated using SEDNTERP version 1.09 (University of New Hampshire).
^{c}, sedimentation coefficients calculated from the c(s) distribution of the raw data processed in Sedfit [35].
^{d}, molecular weight derived from molar mass distribution using Sedfit.
^{e}, molecular weights calculated from aminoacid sequence with and without substrate(s).
^{f}, corresponds to the molecular weight of *Pb*Pdx2 calculated from the protein sequence.

3.1.4 Pdx2 occupies the Pdx1 dodecamer randomly

Since crystallization attempts of the *Pf*Pdx1/*Pf*Pdx2 or *Pf*Pdx1/*Pf*Pdx2^{H196N} complexes in the presence and absence of glutamine did not give any crystal hits, electron microscopy (EM) studies [1] were caried out in the presence of glutamine and catalytic inactive *Pf*Pdx2^{H196N}. Unexpectedly, the *Pf*Pdx1/*Pf*Pdx2/L-Gln complex formed high order of fiber-like aggregates constituted by stacked heteromeric 24mer Pdx1/Pdx2 complexes, as shown by the densities in the class averages (see Figure 3.6, *a*). The protein aggregation was dependent on *Pf*Pdx1, since the protein alone also formed fibers (Figure 3.6, *b*). Interestingly, the high molecular aggregates of *Pf*Pdx1 were not seen in size exclusion chromatography. To discard the possibility that modified His-tag proteins would form aggregates, native proteins were also analysed. However, the untagged *Pf*Pdx1 formed fibers. During the protein purification Pdx1 eluted under different salt concentrations, i.e., different ionic species were present, as shown in the ionic exchange purification profile (Figure 3.7) and each fraction peak showed the same elution profile after gel filtration (Figure 3.8, example for one purification profile). Neither of these protein samples were crystallizable. The electrostatic surface at the interface of opposite Pdx1 subunits using the *Pf*Pdx1/*Pf*Pdx2 model [15] and *Pb*Pdx1 did not show differences in the contact of the two Pdx1 proteins (Figure 3.9), difficult to discern the cause of fiber formation in the *P. falciparum* PLP synthase.

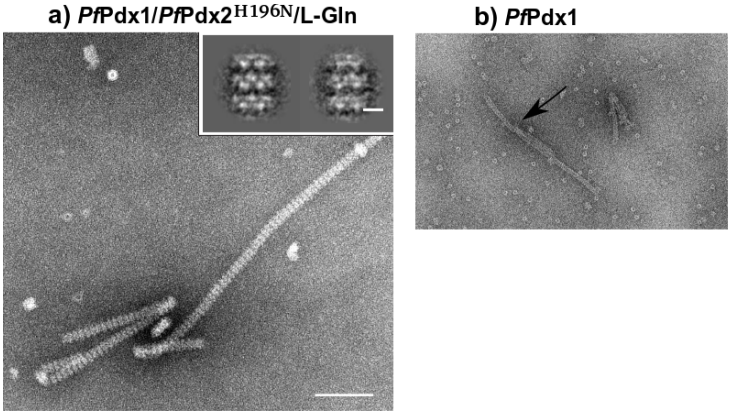

Figure 3.6: Fiber formation in the *Pf*Pdx1/*Pf*Pdx2 complex shown by EM. Purified native *Pf*Pdx1 and *Pf*Pdx2^{H196N} proteins were mixed 1:1 ratio and analysed in the presence of 10 mM glutamine by EM. In *a*) *Pf*Pdx1/*Pf*Pdx2^{H196N} in the presence of glutamine; *b*) *Pf*Pdx1 protein. Protein preparation for the EM contained 20 μg/ml. The arrows show fiber-like aggregations of the proteins.

When analysing the *B. subtilis* Pdx1/Pdx2 complex, it was noticed that the complex requires the catalytically inactive Pdx2 variant in the His residue of the catalytic triad to stabilize the Pdx1/Pdx2 interaction [14]. Due to fiber formation with the *P. falciparum* Pdx1 and Pdx2 proteins and poor diffraction encountered with the *P. berghei* Pdx1/Pdx2 crystals, the *P. berghei* proteins

[1] EM class averages and pictures shown in this study were made by Dr. Katharina Hipp, formerly European Molecular Laboratories (EMBL), now at the University of Edinburgh, UK

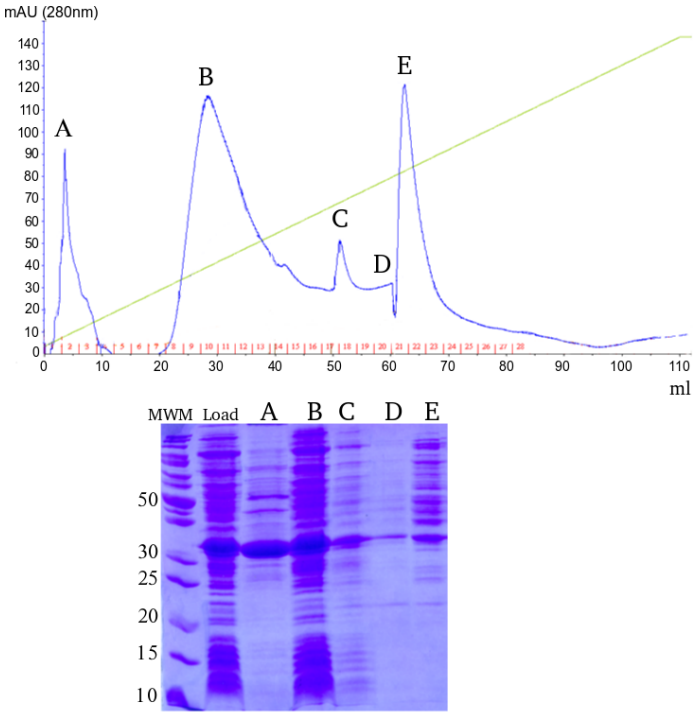

Figure 3.7: Elution profile of native *Pf*Pdx1 by AEC using a Source 30Q matrix. *Pf*Pdx1 eluted with a NaCl gradient from 10 to 800 mM at different concentrations: 28.2 (peak A), 221 (peak B), 408 (peak C) and 499 (peak E). The green line represents the gradient elution. Each peak fraction was pooled and loaded onto Superdex S200 26/60. An example of the purification by size exclusion chromatography is shown in 3.8.

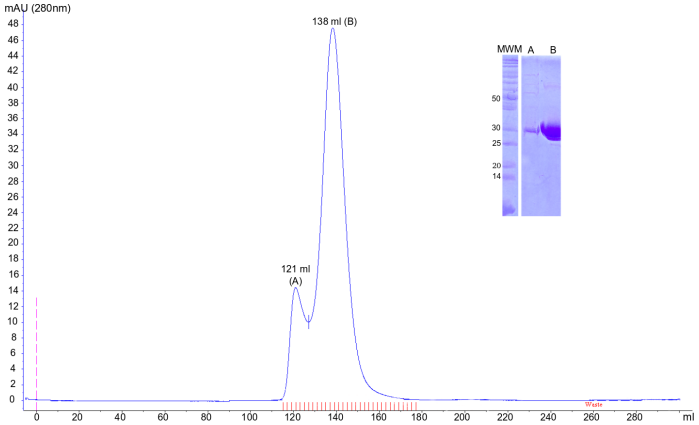

Figure 3.8: Elution profile and purification of *Pf*Pdx1. Elution profile of *Pf*Pdx1 from a Superdex S200 26/60 column shows two elution peaks A and B at 121 and 138 ml with molecular mass of 707 and 435 KDa, respectively, calculated using the calibration curve shown in Figure B.1. Theoretical value of one *Pf*Pdx1 subunit is 33.013 KDa (accession code C6KT50 `http://www.uniprot.org/`) and for 12 Pdx1 subunits, 396.01 kDa. Evaluation of the fraction peaks by SDS-PAGE is shown (right). Peak B corresponds to the elution of *Pf*Pdx1 dodecamer.

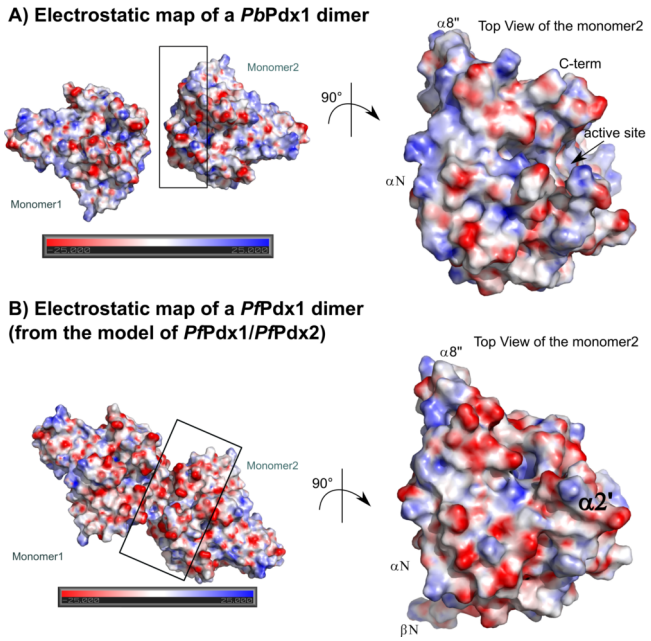

Figure 3.9: Electrostatic surface analysis of *Pf*Pdx1 and *Pb*Pdx1. A) Two opposite monomers, 1 and 2, of *Pb*Pdx1 (left), indicating the interface with a rectangle. Monomer2 is rotated 90° to show the electrostatic surface of the two monomers interface (right). Surface regions of structural elements such as, αN, C-terminus (C-term) and α8" as well as, position of the active site are labelled. B) Two opposite monomers of *Pf*Pdx1 from the *Pf*Pdx1/*Pf*Pdx2 described in [15] are shown as in A). The electrostatic surface of additional segments (βN and α2') not visible in *Pb*Pdx1 are labelled. The electrostatic surface was generated with the APBS tool in *Pymol*, as described in § 2.5.4. Blue and red patches correspond to positively and negatively charged residues, respectively. The molecular surface was setted to -25 to 25 to visualize the electrostatic map.

were analysed by electron microscopy to see whether these homologue proteins formed fibers as the *P. falciparum* proteins. For the assay, active and inactive Pdx2 were used. The *Pb*Pdx1 and *Pb*Pdx2 proteins were mixed in equimolar concentrations and visualized by electron microscopy. Unexpectedly, few Pdx2 subunits of the active protein ocuppied the Pdx1 ring, even in the presence of glutamine (Figure 3.10, a). The control experiment, consisting of *Pb*Pdx1 and inactive *Pb*Pdx2^{H199N} showed Pdx1 dodecameric particles fully occupied with Pdx2 in the presence of glutamine (Figure 3.10, b), as observed by size exclusion chromatography analysis (Figure 3.1).

The fiber formation observed with *Pf*Pdx1 and *Pf*Pdx1/*Pf*Pdx2 not seen when using the *P. berghei* homologue proteins might be a time and concentration-dependent process and would explain why autonomous *Pf*Pdx1 or in complex with *Pf*Pdx2 complex failed to crystallize. The results also showed Pdx1/Pdx2 complexes require the inactive Pdx2 to stabilize the heterodimers, as seen in the bacterial complexes because clearly a different pattern distribution is possible to see when active Pdx2 is used, in which Pdx2 attaches to Pdx1 complexes randomly.

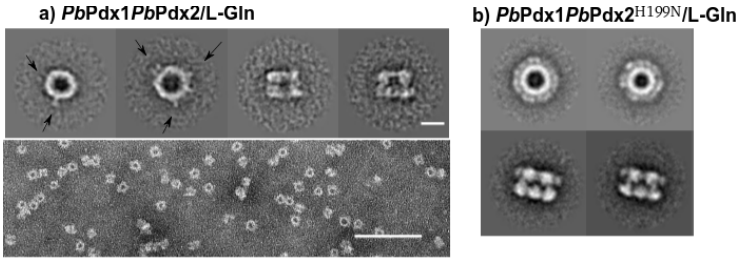

Figure 3.10: EM analysis of the *Pb*Pdx1 / *Pb*Pdx2 complex in the presence of glutamine: (*a*) EM image taken from a *Pb*Pdx1/*Pb*Pdx2 sample. The scale bar represents 100 nm. The class average (3.098 particles: four out of 100 classes) shows Pdx1 dodecameric core particles differentially occupied with Pdx2. Full occupancy of the Pdx1 dodecamer with Pdx2 is not observed, indicated with black arrows. The scale bar on the class averages represents 10 nm; (*b*) class average of the *P. berghei* PLP synthase complex with the *Pb*Pdx2^{H199N} variant, showing higher occupancy of Pdx1 with *Pb*Pdx2^{H199N}.

3.2 The plasmodial Pdx1/Pdx2 structure

Initial attempts to determine the *Pb*Pdx1/*Pf*Pdx2^{H196N} structure by molecular replacement (MR) failed when using *Bs*Pdx1/*Bs*Pdx2 (PBD code 2NV2, [14]) as a template in the form of hetero-dodecamers (6 Pdx1 and 6 Pdx2 subunits) or heterodimers of Pdx1/Pdx2. The experimental phases were then obtained by consecutive MR, using high resolution structures from *P. berghei* Pdx1 at 2.4 Å (determined in this work, Table 3.7) and *P. falciparum* Pdx2 at 1.6 Å (PBD code 2AWB, [24]) as search models. Initially, the Pdx1 hexamer was searched by MR, giving a refinable solution. The packing of the hexamer in the unit cell showed clear space for the placement of Pdx2 subunits. On this MR solution, 6 subunits of *Pf*Pdx2 (PDB 2ABW) structure were added by their superposition onto the bacterial complex as a reference. Using this model in MR also failed, suggesting from this result and the previous MR attempt with the bacterial dimer or hetero-dodecamer that Pdx2 position in the plasmodial complex differs from the bacterial system. Therefore, MR was performed fixing the Pdx1 model as input coordinates and searching for Pdx2. The Pdx2 subunits were found consecutively and refined as rigid bodies after every MR solution (Table 3.6). The last Pdx2 subunit (chain 6) found in the asymmetric unit after MR had low occupancy, due to the absence of crystal contact and is reflected by the slightly change of the figure of merit (FOM) and $R_{factors}$ shown in Table 3.6. A final model containing 6 Pdx1 and 6 Pdx2 subunits in the asymetric unit and 59 % solvent content was refined at 3.6 Å resolution (Table 3.7).

The overall architecture of the complex resembles the complexes described from *T. maritima* [13] and *B. subtilis* [14]. It consists of 12 Pdx1 subunits forming a dodecamer of two hexameric rings occupied by 12 Pdx2 subunits interacting with each Pdx1 (Figure 3.11). Differences on Pdx1 and Pdx2 are seen when the bacterial and plasmodial complexes are superposed, with an rmsd of 0.931 Å calculated over the main chain of 261 residues out of 297, belonging to the $(\beta/\alpha)_8$ core of one Pdx1 subunit in the two structures and excluding the residues at the N and C-terminal regions. Superposition of the Pdx1 subunits showed

$P6_122$	Pdx2	R_{work}	R_{free}	FOM
6 Pdx1	-	41.8	42.2	0.61
	1	41.8	41.3	0.61
	2	40.8	40.2	0.64
	4	38.0	38.2	0.68
	5	36.8	37.0	0.69
	6	**37.2**	**37.7**	**0.68**

Table 3.6: Molecular replacement and refinement statistics of the PbPdx1/PfPdx2^{H196N} structure. Molecular replacement was performed as described in § 2.5.3. Models containing 6 Pdx1 ($P6_122$) with 1, 2, 4, 5 or 6 Pdx2 subunits were refined with each Pdx1 and Pdx2 domains as rigid bodies, using $Refmac5$ from $CCP4i$ [41]. R_{work} and R_{free} are defined in equation 2.5. Figure of merit (FOM) represents the phase probability distribution, tending to 1 when the phase angles are well defined and to 0 when the error of the measured phase angles increases. Highlighted values correspond to the final model consisting of 6Pdx1 and 6Pdx2.

	ga48-3 *Pb*Pdx1	**ga50-3 *Pb*Pdx1-R5P**	**ga38-5 *Pb*Pdx1/ *Pf*Pdx2^{H196N}**
Space group	R32	R32	$P6_122$
Unit cell a, b, c (Å) α, β, γ (°)	180, 180, 102 90, 90, 120	181, 181, 102 90, 90, 120	160, 160, 583 90, 90, 120
Solvent content (%)	49	54	54
# of mol in AU	2	2	12
Resolution (Å)	50 - 2.42	62.2 - 2.4	138.6 - 3.6
Unique reflections	23093	23988	77437
R_{merge} **(%)**	3.6 - 44.7	4.2 - 44	10.6 - 37.6
Completeness (%)	100 - 98.5	99.9 - 99.38	96 - 93.7
$I/\sigma I$	48.7 - 3.2	9 - 2.3	10 - 2
Redundancy	6.7	6.1	5.1
Refinement			
R_{free} **(%)**	23.2	28	29
R_{work} **(%)**	18.5	21	28
# of amino acids	539	555	2988
# of Water	107	68	3
# ligands	2	4	12
# of protein atoms	4189	4168	23094
Ligand/ion atoms	20[a]	26[b]	60[c]
Ramachandran most favored (%)	93.2	92.1	68.5
Ramachandran additional allowed (%)	6.6	6.8	20.3
Ramachandran generously allowed (%)	0.2	0.8	6
Ramachandran disallowed (%)	0	0.2	5.2
RMSD bonds (Å)	0.022	0.0168	0.016
RMSD angles (°)	1.984	1.8482	1.668

Table 3.7: Crystallographic analysis of the plasmodial structures. R_{merge}, R_{work} and R_{free} are defined in equations 2.4 and 2.5. R_{free} was calculated by excluding 5% of the experimental data.
[a] and [c] values were calculated for phosphate ions; [b] values were calculated for ribose 5-phosphate

Pdx2 backbone is displaced 1.6 Å and rotated 8.5° with respect to Pdx1 (Figure 3.12, left).

Analysis of the electron density maps of PbPdx1/PfPdx2^{H196N} structure showed regions not resolved in the electron density of autonomous proteins, difficult for the intrepretation of amino acid side chain position at 3.6 Å resolution. However, backbone of the main chain of secondary structure regions such as, loops and

α-helices not visible in the autonomous subunits were possible to trace and build manually in the electron density map, using the high resolution structures *Bs*Pdx1/*Bs*Pdx2, *P. berghei* Pdx1 and *P. falciparum* Pdx2 as references. The use of non-crystallographic symmetry in *Coot* and rigid body refinement with multiple rigid bodies (each chain considered as a rigid body) in *Phenix* [51] were used to improve experimental phases.

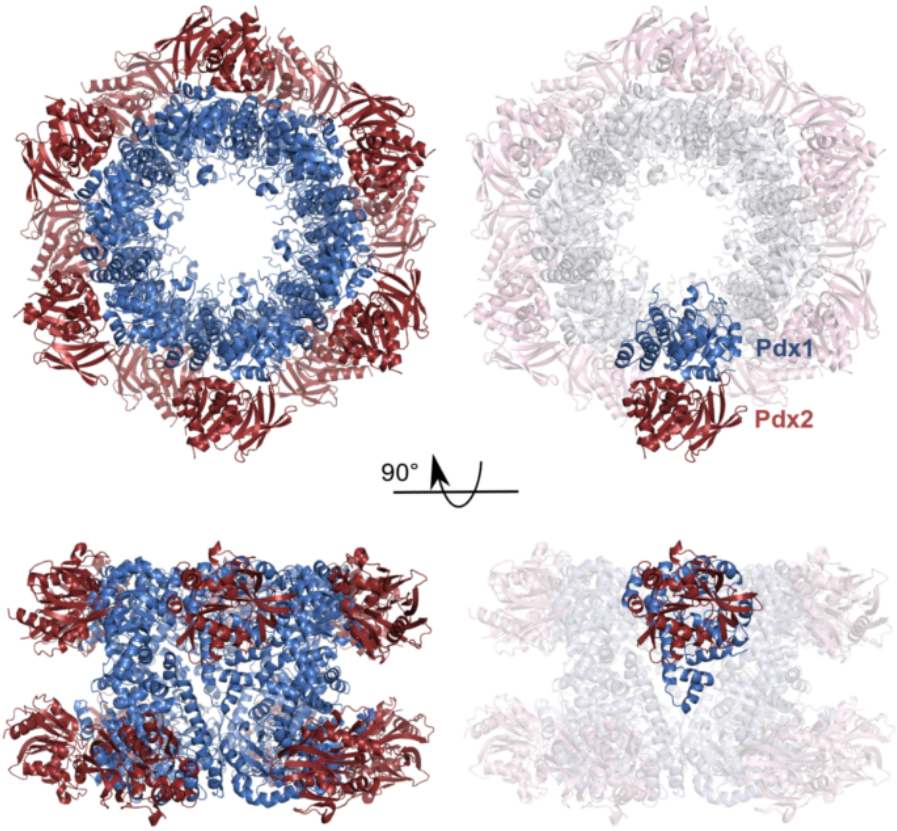

Figure 3.11: Structure of the plasmodial PLP synthase complex. Pdx1 forms a dodecamer-like structure with 12 Pdx1 subunits (blue). Pdx2 (brown) attaches to each Pdx1 subunit. One Pdx1/Pdx2 heterodimer is highlighted (right side). Top and side views are shown by rotating the complex by 90°.

3.2.1 Plasmodial Pdx1/Pdx2 interface: structural changes induced by complex formation

Helix αN of Pdx1 required for complex formation and glutaminase activation [14, 15] is partially ordered and becomes stabilized once Pdx1 interacts with Pdx2. An earlier model of the PLP synthase from *P. falciparum* proposed that helix αN would be preceeded by a small beta strand (named βN) that orients to the Pdx2 subunit and runs parallel to the β7 of the central beta sheet of this protein, as shown in *T. maritima* and *B. subtilis* [13, 14]. Interestingly, the very N-terminus in the chimeric complex differed in this important region and was not oriented towards Pdx2, instead is oriented to Pdx1 (Figure 3.12, right), suggesting the very N-terminus can acquire a different conformation in eukaryotic PLP synthase complexes.

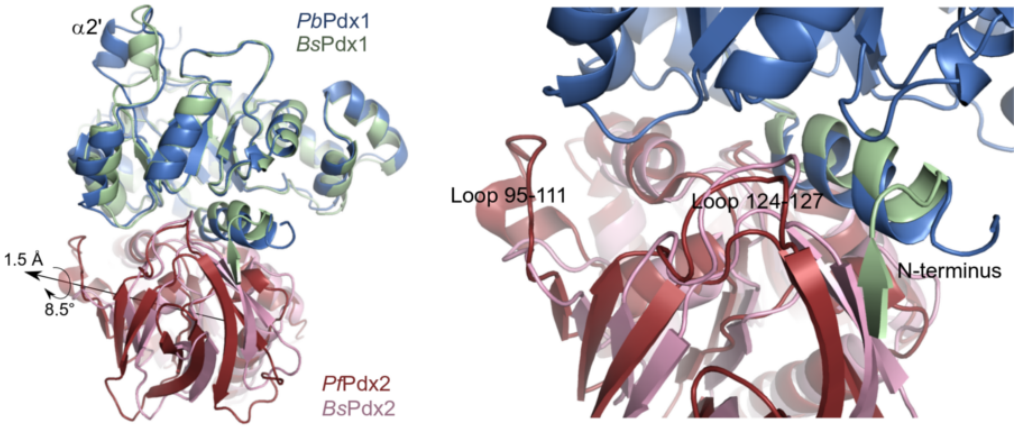

Figure 3.12: Comparison between bacterial and plasmodial Pdx1/Pdx2 heterodimers. Superposition of Pdx1 from *Plasmodium* (blue) onto Pdx1 from *B. subtilis* (green) reveals the displacement and rotation of the plasmodial Pdx2 subunit (brown) 1.6 Å and 8.5°, respectively, with respect to bacterial Pdx2 (pink). Helix α2' of Pdx1 is seen also in a different position. Pdx1/Pdx2 interface is zoomed in to show the position of the N-terminus and loops 95-111 and 124-127 of the plasmodial heterodimer.

A particular loop that connects β5 and β6 in Pdx2 (residues 95-111) is extended by additional seven residues not observed in the bacterial homologues, and forms a helical turn α5-1 (Figures 3.13). This segment contacts the loop α2-β3 in Pdx1 (Figure 3.12, right), a conserved region in *P. falciparum* Pdx1.

Pdx1/Pdx2 complex formation induces additional changes in the interface. Two loops in Pdx2 important for glutaminase activation [16], i) loop Q12 connecting α1 and β1 and ii) oxyanion hole loop (Figure 3.13), acquire a similar conformation as seen in the bacterial Pdx2 complexed to Pdx1. In addition, a loop β6-β7 (amino acid residues 124-127) not resolved in electron density of the 1.6 Å Pdx2 structure alone is visible in the chimeric complex (Figure 3.13), and is located at the interface region with Pdx1 (Figure 3.12, right).

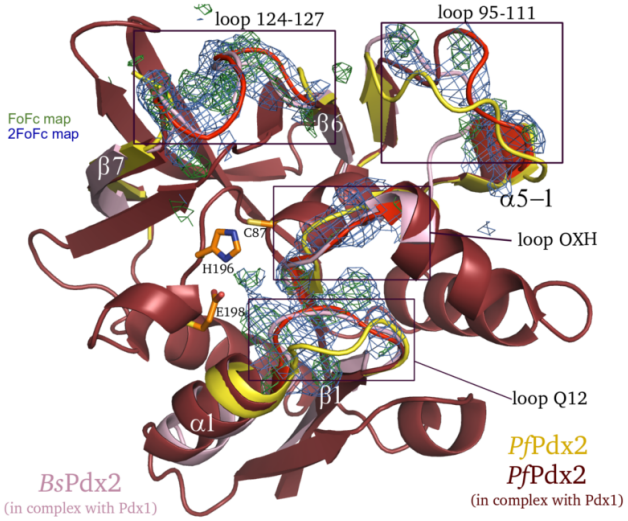

Figure 3.13: Comparison between bacterial and plasmodial Pdx2 Structures. Superposition of autonomous *Pf*Pdx2 (yellow, PDB 2ABW) and *Bs*Pdx2 from the Pdx1/Pdx2 complex (pink, PBD 2NV2) onto *Pb*Pdx1/*Pf*Pdx2^{H196N} complex (brown) reveals structural changes in the Pdx2 subunit upon complex formation. Regions that remain the same in *Bs*Pdx2 and *Pf*Pdx2 structures after supersposition are ommited for clarity. The structural differences are highlighted in red color and enclosed in rectangles: the insertion sequence in plasmodial Pdx2 is shown as Loop 95-111. Loop 124-127 is disordered in autonomous *Pf*Pdx2. The critical activation loop regions: loop Q12 (located between β1 and α1) and loop OXH (oxyanion hole region) are highlighted. Both loops in the plasmodial PLP synthase complex acquires a similar conformation like in the bacterial *Bs*Pdx2. Electron density 2mFo-DFc (blue, after refinement) and Fo-DFc (green, before refinement) omit maps contoured at 1.2sigma and 2.2sigma, respectively, for each respective region. Position of the active site shows the catalytic triad in stick representation.

3.3 Activation of the PLP synthase: helix α2' and C-terminus of Pdx1 are key players in catalysis

The Pdx1 C-terminus plays a key role in catalysis and oligomerization of the hexameric Pdx1 ring [18, 23]. It has low protein sequence conservation (Figure D.1), although its biochemical function in catalysis seems to be conserved. Structure of the full C-terminus is not known because of its high flexibility [13, 14, 18]. In this study, the solved *Pb*Pdx1 structure shows the C-terminus forming an extended loop close to loop α2′-α2 of an adjacent Pdx1 monomer (Figure 3.14). The 14 C-terminal residues are not defined in electron density of either *Pb*Pdx1 or *Pb*Pdx1 in complex with Pdx2. Deletion of 23 residues at the C-terminal loop in *Pb*Pdx1 abolished I_{320} formation and therefore no PLP activity was detected by enzymatic studies, without interfering with the glutaminase activity, Table 3.8. However, dodecameric conformation of this deletion mutant was not disrupted as seen for the wild-type *Pb*Pdx1 (Figure 3.15, upper panel), according to the elution profile in size exclusion chromatography (Figure 3.15, lower panel).

	I_{320} (% Activity)	PLP synthesis (% Activity)	Glutaminase (% Activity)
***Pb*Pdx1**	0.9	0.9	-
***Pb*Pdx1$_{\Delta 275}$**	no activity	no activity	-
***Pb*Pdx1*Pb*Pdx2**	1.2	1.5	179
***Pb*Pdx1$_{\Delta 275}$*Pb*Pdx2**	no activity	no activity	187

Table 3.8: Functional analysis of the *Pb*Pdx1$_{\Delta 275}$ deletion mutant. Specific activities of I_{320} formation, PLP synthesis and glutaminase in the absence and presence of *Pb*Pdx2.

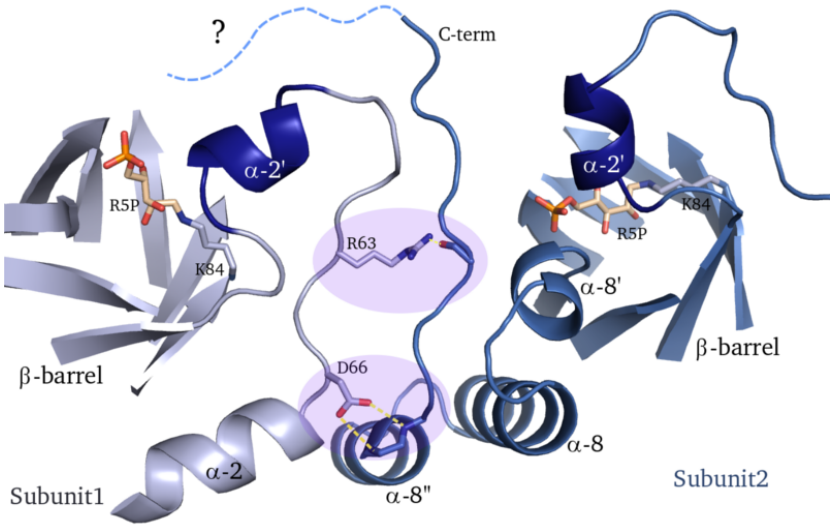

Figure 3.14: Architecture of the C-terminus in plasmodial Pdx1. Two Pdx1 protomers are shown in light and dark blue. C-terminus of the subunit 2 is oriented toward the adjacent Pdx1 in close proximity to helix α2'. Highlighted hydrogen bonds make contact between subunit 1 and 2 along the C-terminus and loop α2′-α2. The dashed line represents one possible orientation the C-terminal region of subunit 2 might take towards subunit 1. Covalently bound R5P to Lys 84 is shown as stick model.

To characterize the function of different regions of Pdx1 C-terminus in R5P binding and PLP synthesis, several C-terminal deletion variants of *P. falciparum* Pdx1 (Alignment shows the mutation position D.1) were analysed with respect to PLP and hexamer/dodecamer formation. Contributions to this knowledge were published in *Derrer, et al 2010* [31]. The results demonstrated that 5 amino acid residues after helix α8" are involved in R5P binding and I_{320} intermediate formation, and efficient PLP synthesis requires the residues onward. Furthermore, formation of the hexamers requires the C terminal helix α8", which helps to maintain the oligomeric state of Pdx1. The *Pb*Pdx1 structure at 2.42 Å resolution is used here to describe the results. The C-terminus runs parallel to the loop which connects α8 and α8' of the same protomer (Figure 3.14). When this C-terminal region was deleted, R5P binding was abolished. As helix α8' is required to tighen R5P in the active site [13], the initial C-terminal segment might assist α8' in the sugar binding.

Furthemore, the C-terminus and loop α2′-α2 run parallel with each other (Figure

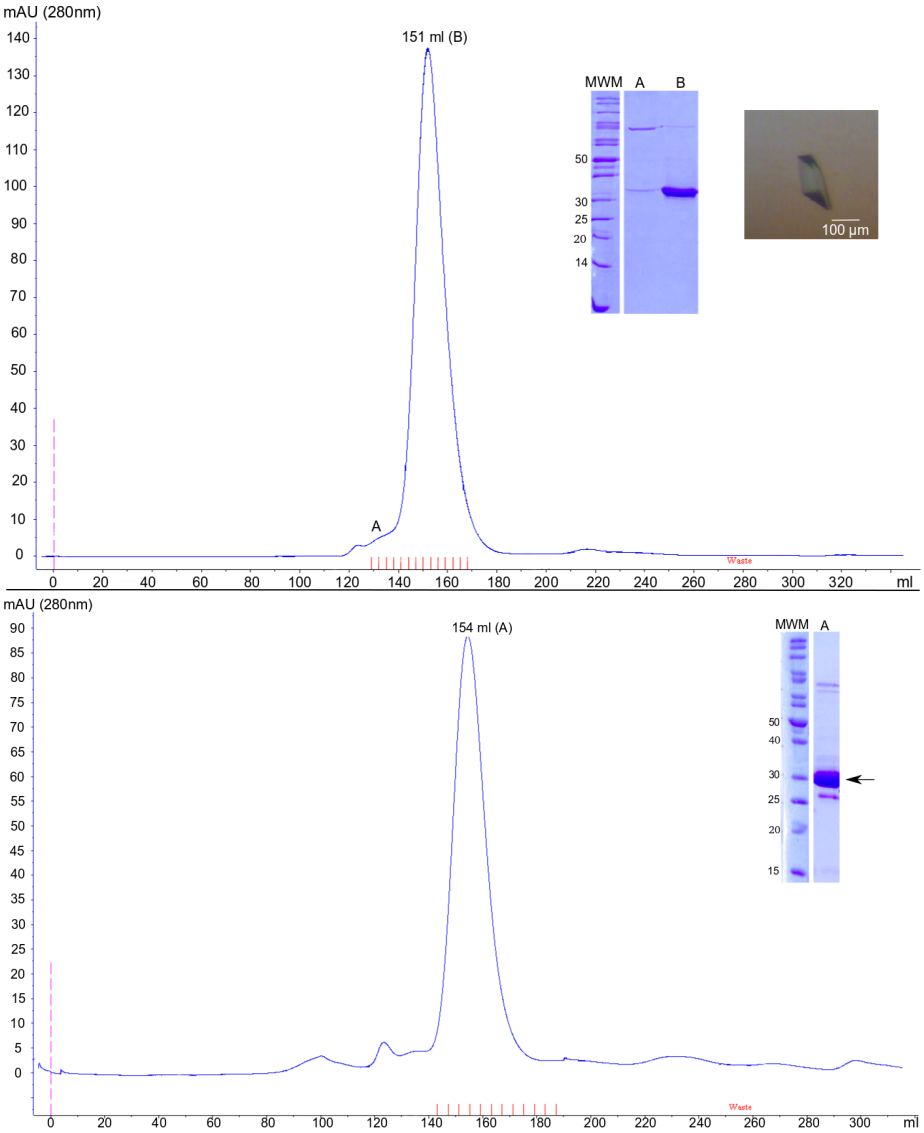

Figure 3.15: Purification of *Pb*Pdx1 and *Pb*Pdx1$_{\Delta 275}$ C-terminal deletion mutant. Elution profiles *Pb*Pdx1 and *Pb*Pdx1$_{\Delta 275}$ from a Superdex S200 26/60 column. Upper panel, elution profile of *Pb*Pdx1 shows two fraction peaks (A and B), evaluated by SDS-PAGE (middle). *Pb*Pdx1 eluted at 151 ml, with a molecular mass of 352 KDa for a dodecamer, calculated using the calibration curve shown in Figure 3.19. Rhomboid crystals of *Pb*Pdx1 (right) were obtained with size ∼200 μm and diffracted to 2.5 Å resolution (Table 3.7). Lower panel, Elution profile of *Pb*Pdx1$_{\Delta 275}$ shows a fraction peak (A) evaluated by SDS-PAGE (right). The deletion mutant eluted at 154 ml, with a molecular mass of 319.2 KDa for a dodecamer, calculated using the same calibration curve as *Pb*Pdx1. Theoretical values for one protomer of *Pb*Pdx1 and *Pb*Pdx1$_{\Delta 275}$ are 32.689 and 30.17 KDa, respectively, calculated with the `http://www.uniprot.org/` server, accession code of *Pb*Pdx1: Q4Z0E8.

3.14), forming two main hydrogen bond contacts with distances of 2.9-3.3 Å: two nitrogens of two peptide bonds right after α8" with the carboxyl group of Asp66

in loop $\alpha 2'$-$\alpha 2$, and the guanidinium group of Arg63 with the carbonyl group of Met 278 peptide bond at the C-terminal loop. Arg63 is a highly conserved residue that might stablish an important contact to stabilize the conformation of loop upward $\alpha 8$" at the adjacent subunit. Biochemical analysis of deletion variants of *Pf*Pdx1 lacking the residues onward Met278 showed a decrease in PLP synthesis. This C-terminal region is in close proximity to $\alpha 2$' of an adjacent protomer (Figure 3.14), an additional segment involved in the initial steps for R5P binding [14], it appears the C-terminus extends towards the adjacent active site and assists in R5P binding, a cooperative regulatory process in Pdx1 core proposed by *Raschle, et al 2009* [23].

Conformational changes in helix $\alpha 2$' of Pdx1 [14] are important for PLP synthase activation. The helix is ordered in the bacterial Pdx1 upon interaction with Pdx2 and most likely prepares enzyme for catalysis [14]. In the plasmodial Pdx1/Pdx2 complex solved at 3.6 Å resolution, $\alpha 2$' is also ordered and seen in a different orientation, compared with the Pdx1/Pdx2 structure from *B. subtilis* (Figures 3.12 and 3.16). Since Pdx1 can bind R5P in the absence of Pdx2, crystallization of *Pb*Pdx1 in the presence of R5P was tried to understand the importance of this helix in the R5P binding. The Pdx1-R5P structure at 2.44 Å resolution showed the sugar covalently bound in the active site to lysine 84 and $\alpha 2$' is visible oriented towards the active site, closed to the sugar phosphate. Hence, the three structural conformations of helix $\alpha 2$' suggest that there is an alternative positioning for this helix and this might be relevant with respect to the catalytic cycle of covalent R5P attachment.

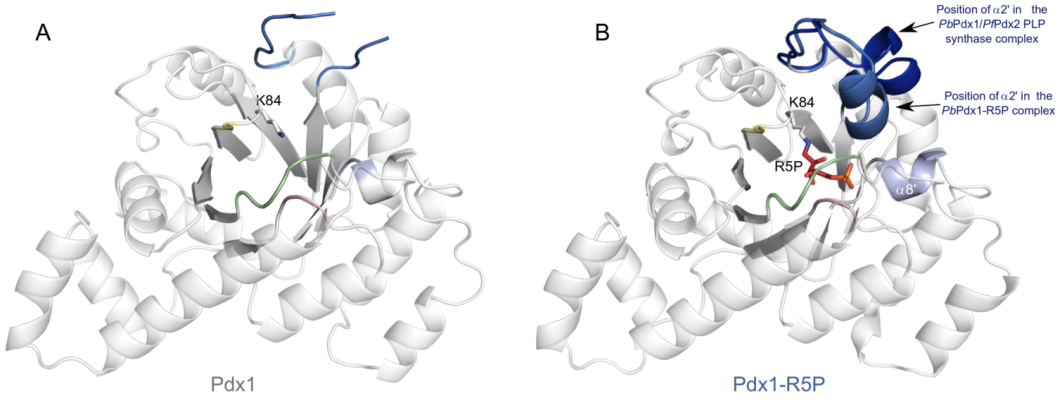

Figure 3.16: Ordering of helix $\alpha 2$' for Pdx1 activation. A) Pdx1 alone showing lysine 84 as stick model. The loop region of $\alpha 2$' is shown in blue. B) This pannel indicates the position of helix $\alpha 2$' as observed in the *Pb*Pdx1-R5P complex (blue) and in the *Pb*Pdx1/*Pf*Pdx2 PLP synthase complex (dark-blue). Loops that change position upon R5P binding towards the sugar phosphate are colored green, pink and yellow. Helix $\alpha 8$' is also shown, as this helix orients towards the sugar, as explained in § 3.5.1. The covalently bound substrate ribose 5-phosphate on lysine 84 is represented as stick model.

3.4 Ammonia enters through an "unrestricted" tunnel in Pdx1

Ammonia is an essential substrate for PLP synthesis in the enzyme Pdx1. How it enters to the active site is not really understood. Glutamine is a source of ammonia when is hydrolysed by Pdx2 and can be substituted *in vitro* conditions for ammonium salts e.g., NH_4Cl and $NH(_4)_2SO_4$. The Pdx1/Pdx2 complex carries out a coupled reaction, in which glutamine hydrolysis by Pdx2 leads to production of ammonia, which subsequently reacts with R5P in Pdx1. Since the two active sites are remote from each other, a model based on the structure of *B. subtilis* Pdx1 was proposed and suggested that ammonia might enter the β-barrel under the movement of flexible methionine residues [14]. The Pdx1 structure from *P. berghei* solved in this study shows that some methionine residues vary with respect to the position or conservation when compared to the bacterial Pdx1 (Figure 3.17, compare left and right in B). Enzymatic experiments were done in order to investigate the functional role of the residues within the β-barrel in ammonia transfer.

Methionine residues involved in ammonia transfer from Pdx2 to Pdx1

Helix αN of Pdx1 was assigned as a key segment placed at the interface of both subunits, probably as the gate for ammonia entrance from Pdx2. Superposition of Pdx1 from *B. subtilis* alone and from the complex with Pdx2 showed no mayor changes in the conformation of αN, despite some side chain residues of the helix are not fully resolved in the autonomous *Bs*Pdx1 [14]. However, the functional groups of two methionines (Met #13 and #16) on the helix displayed different conformation in the two Pdx1 structures (figure 3.17, B right). Mutation of Leu30 in *Arabidopsis thaliana*, a residue in equivalent position to Met13 in *B. subtilis*, reduced the coupling between Pdx1 and Pdx2 by increasing the glutaminase activity [50]. The *Pb*Pdx1 structure solved in this study has a tryptophan in place of Met13 (Trp16), which is conserved in all plasmodial Pdx1 proteins (see Alignment D1). Met16 on the contrary, is conserved in the *P. berghei* Pdx1 (corresponds to Met19) and other Pdx1 proteins and in the *Pb*Pdx1 structure adopts a similar conformation (Figure 3.17, A) to the one seen in the *B. subtilis* Pdx1 alone (Figure 3.17, B left). This Met19 was mutated to valine (based on the inactive Pdx1.2 of *A. thaliana*) and the PLP synthase activity was evaluated with and without *Pb*Pdx2. The mutant had an increase of PLP synthesis in the absence of Pdx2 and produced a similar amount of PLP like wild-type in the presence of the glutaminase (Figure 3.18). Ammonia uptake from Pdx2 was efficient, despite the decrease of glutaminase activity in *Pb*Pdx2 (Figure 3.18).

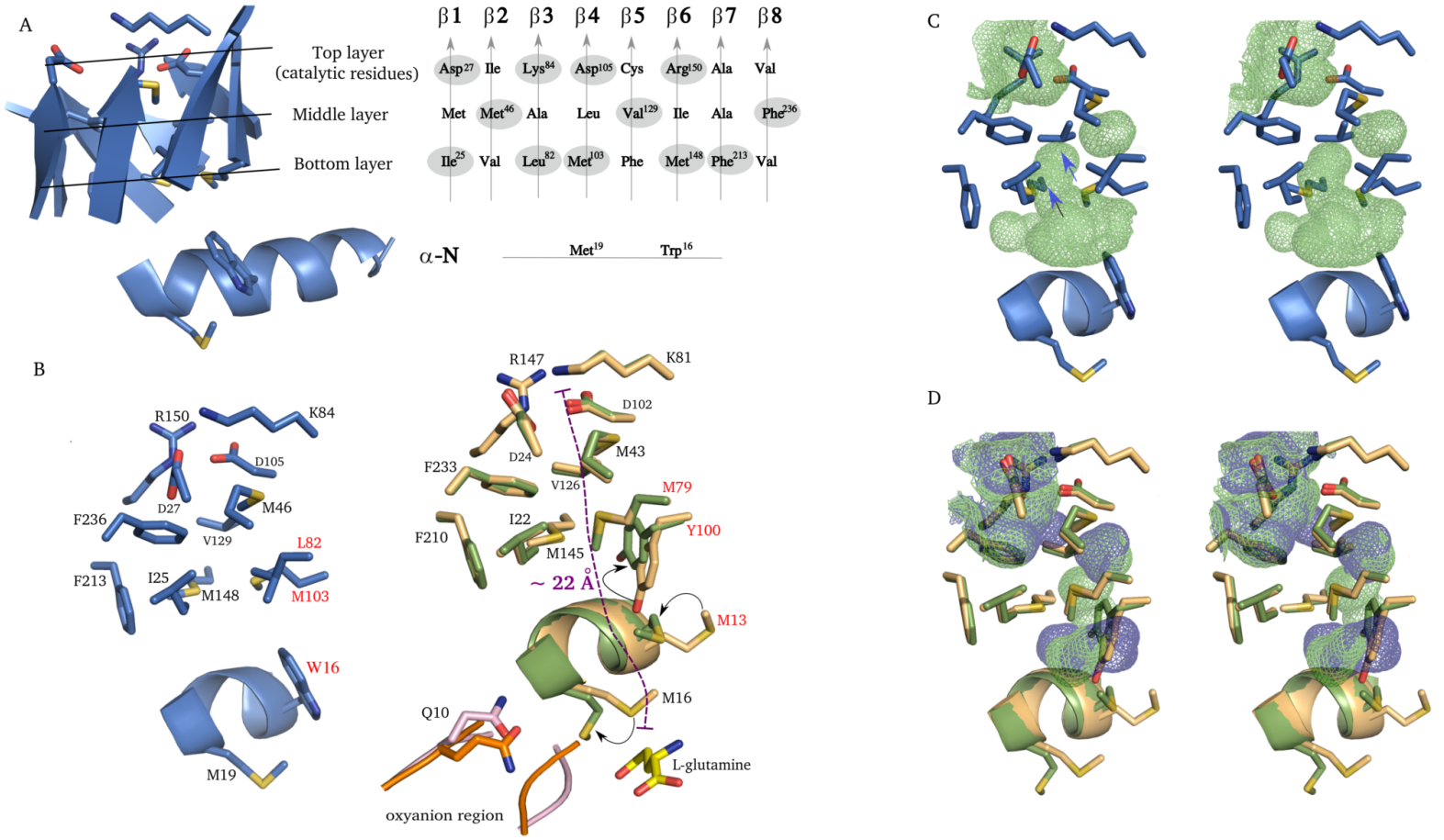

Figure 3.17: Comparison of the ammonia tunnel in *Pb*Pdx1 and *Bs*Pdx1. A) View of the *Pb*Pdx1 β8-barrel divided by three layers and αN helix with residues possibly involved in ammonia transfer. Scheme of the residue organization in the β-barrel in *Pb*Pdx1: residues in the inner β8-barrel are highlighted in gray circles. B) Stick representation of the residues in the inner barrel of *P. berghei* Pdx1 (left) and the superposed *B. subtilis* Pdx1 (right) in the absence (yellow, PBD code 2NV1[14]) and presence of Pdx2 (green, PDB code 2NV2[14]). Dashed line represents the distance of $\sim$ 22 Å between the active sites of Pdx1 and Pdx2. The oxyanion region of Pdx2 is shown for *Bs*Pdx2 (orange, PDB 2NV0) and *Bs*Pdx2 (pink, PDB 2NV2) from the complex with Pdx1. Half of the α-N terminus is shown for the three Pdx1 structures. Aminoacids exchanged in *Pb*Pdx1 and *Bs*Pdx1 are labelled in red color. Glutamine from the *Bs*Pdx1/*Bs*Pdx2 structure is shown in stick representation. C) and D) Stereo views of the residues whithin the β-barrel for *Pb*Pdx1 (C) and *Bs*Pdx1 (D), as seen in the absence (yellow) and presence of *Bs*Pdx2 (green). Cavities in the barrels produced with a solvent radius probe of 1.2 Åcalculated using *Pymol*. Cavities of the *Pb*Pdx1 and *Bs*Pdx1 alone are shown in green. Cavities of the *Bs*Pdx1 in the complex with Pdx2 are shown in blue. The two cavities in *Pb*Pdx1 not seen in the bacterial Pdx1s are indicated with blue arrows.

	PLP synthesis with NH_4Cl as NH_3 donor (% Activity)	PLP synthesis with Pdx2/Gln as NH_3 donor (% Activity)	Glutaminase activity (% Activity)
PbPdx1	0.9±0.0 (100)	1.4±0.2 (100)	183±6 (100)
M19V	2.0±0.8 (222)	1.8±0.1 (130)	87±1 (48)
M46I	1.5±0.2 (161)	2.8±0.8 (207)	294±15 (155)
L82A	0.3±0.2 (28)	1.2±0.1 (89)	115±12 (63)
L82S	0.3±0.0 (34)	1.3±0.1 (93)	194±20 (104)
L82F	0.4±0.3 (44)	1.2±0.9 (89)	138±15 (74)
L82M	0.7±0.2 (72)	1.2±0.2 (82)	179±3 (96)
M103A	0.3±0.0 (34)	0.4±0.1 (30)	178±18 (97)
M103F	no activity	no activity	126±37 (69)
M148L	0.8±0.4 (89)	3.7±1.2 (274)	229±7 (125)

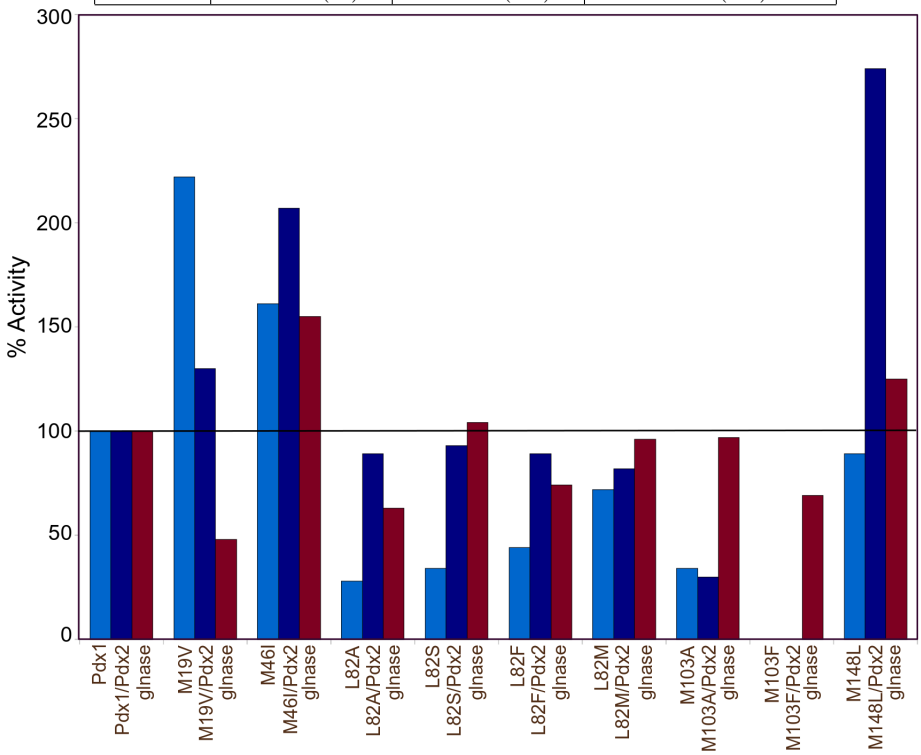

Figure 3.18: Functional analysis of residues in NH_3 tunneling in *Pb*Pdx1. Specific activities are indicated in nmol/min.mg for PLP synthesis of the NH_3 tunnel mutants in the absence and presence of *Pb*Pdx2. Glutaminase specific activities were also determined in nmol/min.mg with corresponding NH_3 tunnel mutants. Percentage of PLP synthesis and glutaminase activities were calculated based on the wild type (*Pb*Pdx1 or *Pb*Pdx1/*Pb*Pdx2) specific activities and displayed in a bar plot: *light blue*, variants using NH_3 from NH_4Cl source; *dark blue*, variants using NH_3 from L-glutamine hydrolyzed by Pdx2, and *brown*, glutaminase activities in the presence of the NH_3 tunnel mutants.

Residues in the β-barrel of *Pb*Pdx1 are organized in three layers represented in Scheme 3.17, A. The bottom layer is constituted by Ile25, Leu82, M103, M148 and Phe213. The two residues Leu82 and Met103 are exchanged among Pdx1 proteins by a conserved Met or an aromatic residue (Tyr or Phe), respectively but conserved among plasmodial Pdx1s (see Alignment D.1). An example is shown in *Bs*Pdx1 (figure 3.17). The middle layer is formed by conserved residues Met46, Val129 and Phe236 (see Alignment in D.1). The upper layer at the C-

terminal end of the β-barrel has invariant residues of the active site, described in more detail in § 3.5.

Interestingly, the reciprocal amino acid exchanges of *Pb*Pdx1Met103 for *Bs*Pdx1 Tyr100 at the bottom layer and *Pb*Pdx1Trp16 for *Bs*Pdx1Met13 in αN give the plasmodial Pdx1 ammonia tunnel a different construction, compared to the *B. subtilis* protein. At the interface of αN and bottom layer of the *Pb*Pdx1 barrel, a cavity is visible protruding at the proximity of Leu82, Met103 and Met148, when the tunnel is probed with a solvent surface radius of 1.2 Å (Figure 3.17, C). This cavity is not seen in the *Bs*Pdx1 barrel (Figure 3.17, D). To understand the function of the residues aligned within the barrel, point mutations were introduced by site-directed mutagenesis. The ability of the variants to produce PLP was tested in the absence and presence of Pdx2. Replacement of Met103 for Phe (based on the occuring of this residue in *Tm*Pdx1) and Ala resulted in no (Figure 3.18) or halved PLP synthesis, respectively. Pdx2 glutaminase activity in the presence of the *Pb*Pdx1^{M103F} mutant was decreased to half of the activity. Replacement of Leu82 with Met (highly conserved residue in other Pdx1s) did not show difference in the PLP synthesis activity in the ammonia or Pdx2-dependent reactions. On the contrary, L82A, L82S or L82F showed significant changes in PLP synthase activities in the range of 50 % in the absence of Pdx2 (Figure 3.18), restoring their activities in the presence of Pdx2 (Figure 3.18). However, the exchanged Met148 and Met46 residues for Leu and Ile, respectively, led to two-three fold production of PLP when Pdx2 supplied the ammonia. The variant Met46Ile had also an increased PLP synthesis in the ammonia-dependent assay, suggesting this residue functions in ammonia transfer but not in Pdx1/Pdx2 comunication. The results suggest that residues at the lower layer (L82 and M103) might function as a control point for ammonia uptake, and more precisely at M103 position according to the lost or decrease PLP synthase activity when the residue is mutated to Phe or Ala, followed by the conserved M46 and M148. These two methionines would control the ammonia movement once it enters the tunnel, otherwise their mutations would not make more accessible the tunnel for ammonia.

3.5 Insights into the reaction mechanism of PLP biosynthesis in Pdx1

Biosynthesis of PLP *de novo* in Pdx1 involves a chemistry currently described by *Hanes et al 2008* [21, 52]. The authors characterized three key intermediates by NMR studies, incubating Pdx1 with ^{13}C and ^{15}N labeled substrates in a stepwise manner to prove: firstly, R5P or Ru5P adduct intermediate is bound to Pdx1 through its C1 carbonyl at the early steps of the reaction; this revises an earlier finding in the crystal structure of *T. maritima* at 2.9 Å resolution, where the sugar was thought to bind through a Schiff base at the C2 atom [13]. Secondly, it was confirmed that a chromophoric intermediate (I_{320}) with maximum absorbance at 315 nm previously observed by *Raschle et al 2007* [22] is bound to Pdx1 via C5, suggesting a C1 to C5 imine migration. And thirdly, a final intermediate formed after addition of G3P was characterized as PLP bound through C5 to Pdx1 via an imine. These characterizations permitted to construct the several chemical steps in the PLP synthase mechanism as shown in Figure 1.6.

The highest resolution structure at 1.62 Å of Pdx1 deposited in the Protein Data Bank (`http://www.pdb.org/`, PDB entry 2ZBT) belongs to the extreme thermophile *Thermus thermophilus* from the HB8 strain. *T. termophilus* is a gram-negative bacterium that can grow at temperatures from 50°C to 82°C [53]. To gain insight into the sequence of the chemical reactions that encompasses PLP biosynthesis in the R5P-dependent route at atomic resolution, Pdx1 protein from this organism was cloned, expressed and purified as described in § 2.1 and § 2.2 (Figure 3.19), with the expectation to produce diffracting crystals at higher resolutions than the obtained with plasmodial *Pb*Pdx1-R5P complex.

The protein was crystallized under the conditions specified in Table 2.2, using $\sim$ 1 mM of protein. Crystals for different experiments were soaked in ligands with 10 to 15 excess for R5P or PLP than protein concentration.[2]. Data collection statistics are listed in Table 3.9.

3.5.1 Architecture of the active site in PLP synthase: R5P binding state

In previous work, elucidation of the bacterial 3D Pdx1 structure at 2.9 Å (PDB 2ISS, [13]) in the presence of Ru5P allowed to assign the active site and the residues possibly involved in the sugar binding and catalysis [13]. This site was located at the C-terminal region of the β-barrel and was referred to P1, constituted by highly conserved residues: D23, K80, D101, S103, Arg146, G152, G213, G234 and S235, see Alignment D.1. The *Tt*Pdx1-R5P complex structure solved in this study at 1.7 Å resolution higher than the *Tm*Pdx1-Ru5P complex structure gave additional details of the sugar binding site, P1. At the early steps of

[2]nomenclature of amino acid residues mentioned throughout this § 3.5 are from *T. thermophilus Pdx1*

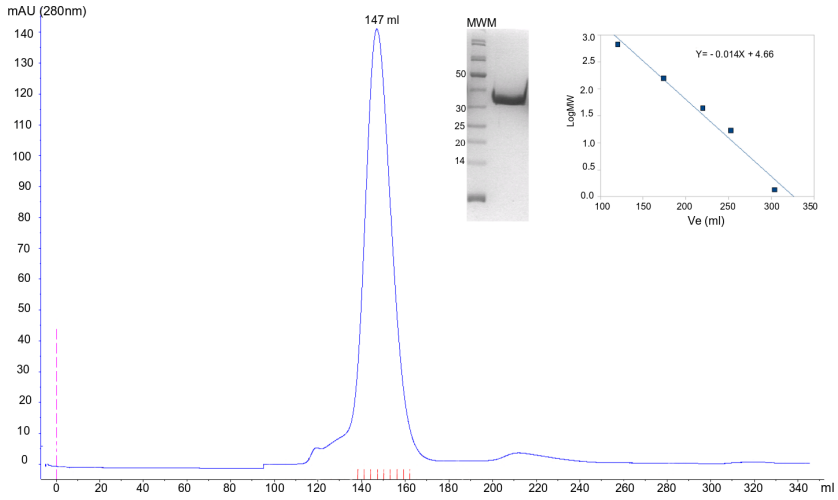

Figure 3.19: Elution profile and purification of *Tt*Pdx1. Elution profile of *Tt*Pdx1 from a Superdex S200 26/60 column shows a fraction peak of 147 ml with molecular mass of 400 KDa calculated using the calibration curve (right). Theoretical value of one *Tt*Pdx1 subunit is 32.026 KDa (accession code Q5SKD9 `http://www.uniprot.org/`). The molecular weight for a dodecamer is 384.312 kDa (peak 147 ml). Evaluation of the fraction peak by SDS-PAGE is shown (middle).

	tt6-2 Pdx1-R5P	**i20-5 Pdx1-PLP**
Space group	R32	
Unit cell a, b, c (Å)	183, 183, 97	
α, β, γ (°)	90, 90, 120	
Solvent content (%)	51	
# mol in AU	2	
Resolution (Å)	46 - 1.7	90.9 - 2.1
Unique reflections	62742	77155
R_{merge}	19.8 - 98.1	19.8 - 32.6
Completeness (%)	99.8	99.0
$I/\sigma I$	4.5 - 2.5	4.7 - 2.4
Redundancy	8.4	4.7
Refinement		
$\mathbf{R}_{free}$ **(%)**	21.7	27.8
$\mathbf{R}_{work}$ **(%)**	17.1	21.7
# of amino acids	552	548
#Water	732	351
# ligands	2^a	2^b, 2^c
Ramachandran most favored (%)	94	93.3
Ramachandran additional allowed (%)	5.6	6.5
Ramachandran generously allowed (%)	0.2	0.1
Ramachandran disallowed (%)	0.2	0
RMSD bonds (Å)	0.026	0.022
RMSD angles (°)	2.1	1.9

Table 3.9: Crystallographic analysis of the *Tt*Pdx1 structures. R_{merge}, R_{work} and R_{free} are defined in equations 2.4 and 2.5.
[a] values were calculated for R5P ligand. [b] and [c] values were calculated for PLP and phosphate ions, respectively. R_{free} was calculated by excluding 5% of the experimental data.

PLP biosynthesis, R5P is opened, by an still unknown mechanism, with formation of an R5P adduct at *Tt*Pdx1Lys80 and loss of H_2O, as was demonstrated

by mass-spectrometry analysis in *Bs*Pdx1 [22]. The hydrolysis occurs to lead a Schiff base linkage between the ε-N of Lys80 and the C1 carbonyl of R5P. This adduct has a visible electron density in the active site before refinement, when the map is contoured with 2σ (Figure 3.20, green map). Modelling of the sugar in the electron density and further refinement cycles, led to the backbone of the sugar well fitted into the density. Its carbonyl group at C2 is visible and not at C1 (Figure 3.20, light map), whose carbonyl would be expected to be lost during the imine reaction. A water molecule represented by water 1 in Figure 3.20 (see also the diagram in the same figure) is well defined at the high resolution electron density, forming hydrogen bonds with the ε-N of Lys80, Asp101 and Ser103. Asp23 is positioned closer to the hydroxyl group of C2 of the R5P adduct. Although Asp23 does not form direct contact with the sugar, it might function in general acid/base catalysis, because its mutation (i.e., in *B. subtilis* and *P. falciparum* Pdx1 [14, 54]) inactivated the PLP synthesis in Pdx1, confirming its catalytic importance.

Comparison of the apo and *Tt*Pdx1-R5P structures shows that sugar binding induces several conformational changes in the surrounding of the P1 site (Figure 3.20). These structural changes lead to the formation of a pocket, where the phosphate group of R5P forms H-bonds with: the nitrogen of the peptide bond of three glycines (G152, G213 and G234), the hydroxyl group of S235 and three water molecules 2, 3 and 4 (Figure 3.20). The residues orient towards the phosphate ion i.e., residues G234 and S235 in helix α8' and G156 in loop β6-α6 (Figure 3.20). Helix α2' also is displaced to the bound sugar (as seen in the *Pb*Pdx1 structure, Figure 3.16) and closes the active sites.

3.5.2 From P1 to P2: PLP synthesis

A second active site in Pdx1, named P2, was predicted to be composed by H114, R129, E137, R136, R137, K148 and K186 from a neighboring subunit (Figure 3.21) based on *Tm*Pdx1 structure [13]. Recently, H114, R136 and R137 were confirmed to be required for PLP synthesis [30]. After R5P ring opens in P1 site, an imine adduct is formed. Ammonia enters P1 active site and reacts with the ketone of the adduct. This reaction releases water, forming a second imine in C2 with the incoming ammonia, Figure 1.6. The reaction would follow a phosphate elimination that leads to the I_{320}. A particular chemical step of imine migration was described in the PLP reaction mechanism [21]: the imine linkage between Lys80 and the adduct shifts from the C1 to C5 position, Figure 1.6). It would represent a mechanism for the movement of the intermediate to the P2 active site. As Lys148 is located at P2 site of Pdx1, it was proposed earlier that Lys148 main chain would rotate and approach the P1 site [13]. The reaction proceeds from the chromophoric I_{320} intermediate to PLP synthesis by addition of G3P. A free form of PLP in the active site has been reported in P2 of the yeast Pdx1 structure [55], but not explanation was given about the reaction step that leads to the release of PLP nor the residues implicated in catalysis. To gain insight into the PLP formation site, Pdx1 crystals were soaked in PLP solution. The obtained *Tt*Pdx1-PLP structure at 2.1 Å resolution showed an

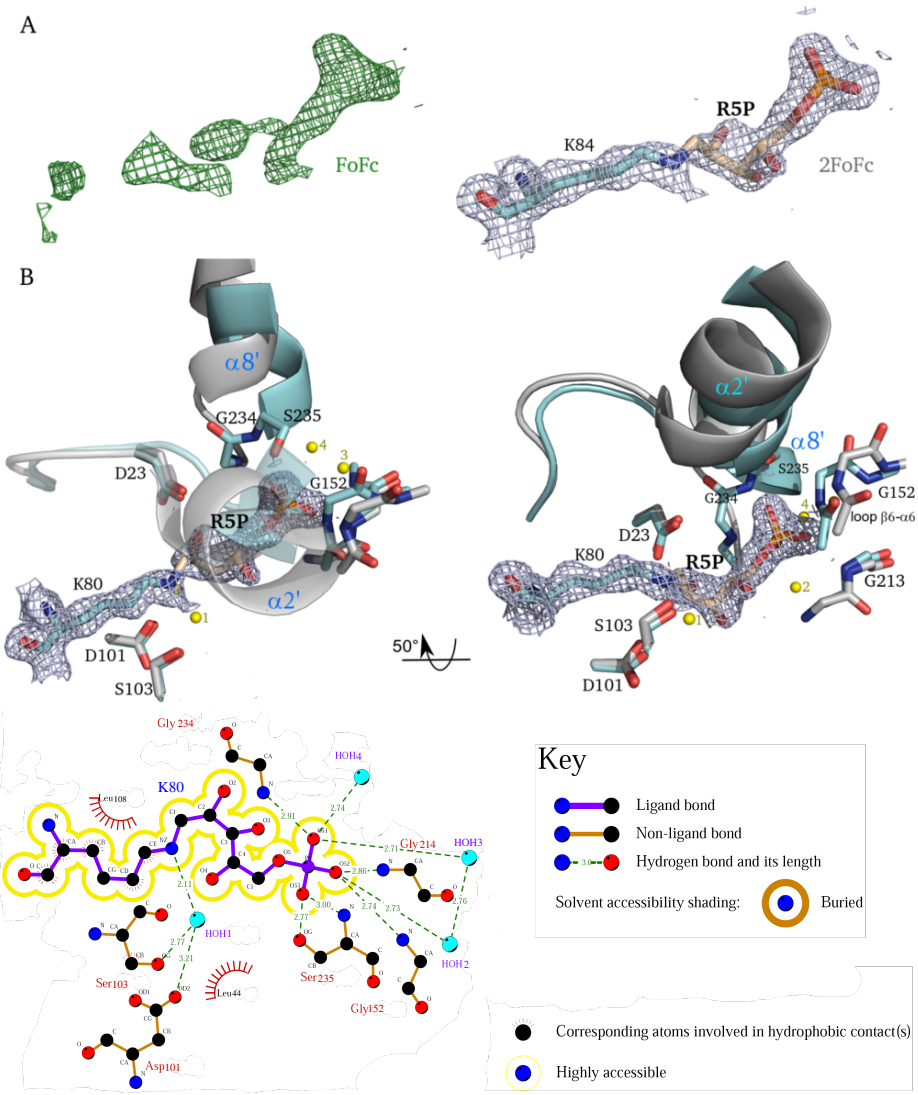

Figure 3.20: R5P bound state in the active site of Pdx1. A) Electron density maps F_oF_c (green mesh) before refinement and $2F_oF_c$ (light mesh) after refinement of R5P bound to Lys80. B) Two views of the active site of *Tt*Pdx1 (blue) at 1.7 Å resolution with refined electron density of Lys80 bound to opened R5P. The F_oF_c and $2F_oF_c$ maps are contoured with 2.5σ and 1.2σ, respectively. Apo Pdx1 structure (grey) is used to observe the conformational changes upon R5P binding in helices α2', α8' and loop β6-α6. Catalytic residues are represented in sticks. Waters (yellow dots) are enumerated: 1, 2, 3 and 4, according to the scheme shown below. Bottom panel, schematic diagram of R5P-Lysine interaction in P1 active site of Pdx1. Residues and waters in contacto to Lys80 bound to the C1 of opened R5P via a Schiff base are shown with the hydrophobic interactions and hydrogen bonds and respective length.

electron density protruding from Lys148 (Figure 3.22, A) with similar shape to the pyridinium ring of PLP. PLP was modelled in the density and refined. The resulting structure shows PLP forming an imine bond with its C4' and the ε-N of Lys148 (Figure 3.22, B). In this PLP-Pdx1 complex clearly the side chains of

Arg136 and Arg137, as well as Lys186 from an adjacent protomer are in polar contacts with the phosphate of PLP (Diagram 3.22).

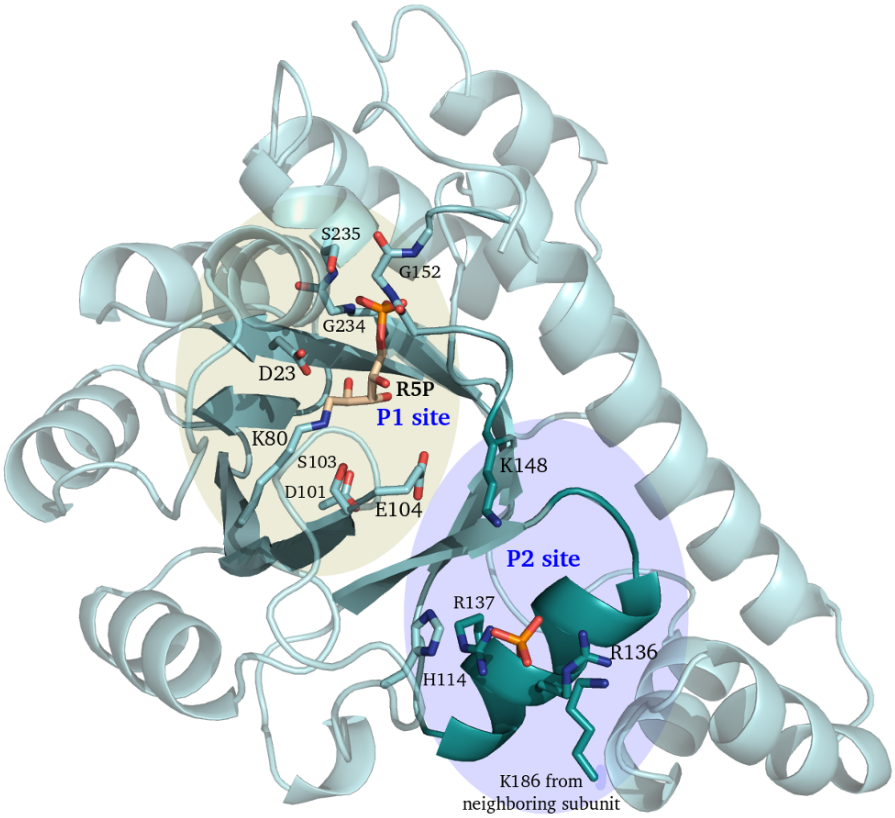

Figure 3.21: P1 and P2 active sites of Pdx1 with R5P bound in P1. A Pdx1 subunit with the two active sites highlighted in green (P1) and blue (P2) with respective catalytic residues in stick representation. R5P covalently bound to Lys80 in P1 and phosphate ion in P2 are shown in stick representation.

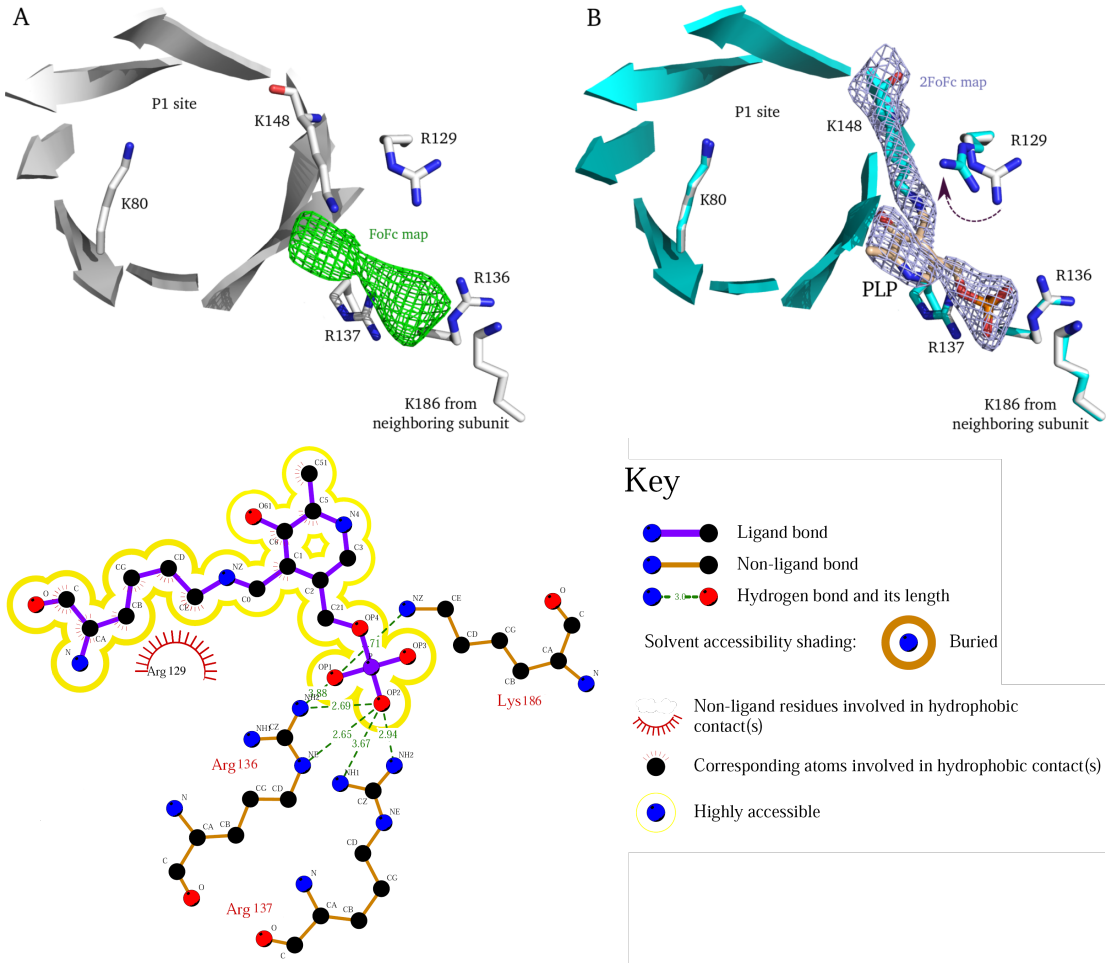

Figure 3.22: PLP bound state in the active site of Pdx1. Top Panel, A) Pdx1 active sites showing electron density map F_oF_c (green mesh) of the main chain of Lys148 before refinement in P2 site. Location of P1 shows Lys80. Residues of P2 site are displayed in stick representation. B.- The refined electron density $2F_oF_c$ of modelled PLP in the active site of Pdx1 (blue), superposed onto the unrefined structure as shown in A. Rotation of R129 is represented by dashed arrow. F_oF_c and $2F_oF_c$ maps in A and B are contoured with 3.0σ and 1.2σ, respectively. Bottom Panel, schematic diagram of PLP-Lysine interaction in P2 active site of Pdx1. Hydrophobic interactions and hydrogen bonds with respective length are shown of the residues and waters in contact to Lys148 bound to C1' of PLP via a Schiff base.

Chapter 4

Discussion

Direct *de novo* biosynthesis of pyridoxal 5'-phoshate requires the three substrates ribose 5-phosphate, glyceraldehyde 3-phosphate and L-glutamine as a source for ammonia. The biochemical mechanism consists of the condensation of the two phosphorylated sugars with ammonia in the PLP synthase. The mayority of the knowledge available to date about the enzyme describes the activation mode of Pdx2, in which Pdx1 is essential to induce glutamine hydrolysis. However, Pdx1 catalyses most of the chemical steps for PLP biosynthesis and it needs to be understood how the enzyme is activated in order to carry out the catalytic reactions to finally synthesize PLP.

4.1 Activation of the PLP synthase

R5P entrance and organization of the catalytic center for enzyme activation

R5P binding entails reorganization of the active site, in which segments such as, helices α2' and α8", move towards the sugar. The structural changes induce the formation of several hydrogen bonds with the substrate mainly at the phosphate group. This leads to the formation of a closed environment surrounding the sugar (Figure 4.1). Earlier structural studies showed that helix α2' is ordered when Pdx1 interacts with Pdx2 [14, 13] and this was later assumed to occur as an allosteric effect induced by Pdx2 to enhance R5P binding [23]. There are three structural states for α2' described in this study, which explain how helix α2' functions in the activation of the PLP synthase. The helix is disordered in the *Pb*Pdx1 structure and orders in the plasmodial Pdx1/Pdx2 structure. Interestingly, the helix is seen in a different position, when compared to bacterial Pdx1/Pdx2 complexes and does not cover the P1 site. Here, this state is proposed as the open conformation of α2' to allow access for R5P.

Co-crystallization of the plasmodial *Pb*Pdx1-R5P complex showed a third conformation of the helix, closer to what was observed for bacterial PLP synthase complexes from *B. subtilis* and *T. maritima* [14, 13]. When the sugar enters the catalytic center, it binds convalently to lysine 84 and helix α2' closes the active site. It explains helix α2' has a crucial function in sequestering the substrate intermediate from the solvent, most likely to prepare the enzyme for further catalytic steps.

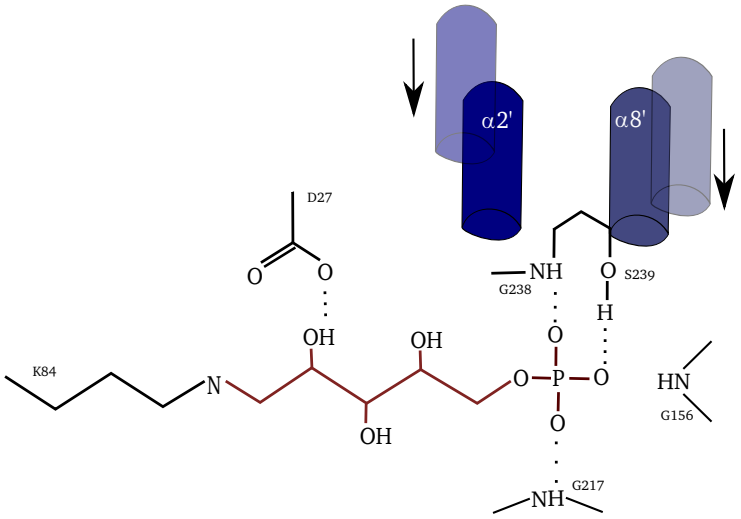

Figure 4.1: Scheme for R5P binding in the active site. The open R5P is attached to Lys84 with its C1 atom. H-bonds are shown between the phosphate group and residues G217, G238 and S239. H-bonds with G156 can also be formed (not shown). Displacement of α2' and α8' induced by R5P binding are indicated by arrows. Asp27 is shown as a potential residue involved in isomerization of the R5P adduct into Ru5P intermediate, as this residue is seen in close proximity to the oxygen atom of C2 in the R5P-Pdx1 complex.

The activation mechanism of Pdx1 seems to be supported by simultaneous intra and inter subunit communication in the Pdx1 core, by the C-terminus of a Pdx1 protomer. This assumption is not a direct interpretation from the crystal structures of Pdx1 proteins solved in this study or from other known structures, in which the C-terminus is partially resolved in the electron density. Instead, biochemical and mass spectrometry analyses carried out in C-terminal deletion mutants of *Pf*Pdx1 showed that the five residues dowmstream of helix α8" of the C-terminus (Figure 4.2), are essential for R5P binding and therefore PLP synthesis (results published in [31]). This result and the available data of the partially C-terminal region seen in the *P. berghei* Pdx1 structure, are consistent to assign a function to the C-terminus of Pdx1 in catalysis. The C-terminus of one Pdx1 subunit forms an extended loop at the interface of the adjacent Pdx1 subunit. The cooperative mechanism for PLP biosynthesis might occur by the active role of the C-terminus in pentose binding at two active sites: firstly, mediating the displacement of the N-terminal dipole of helix α8' towards the substrate phosphate of the same subunit with its initial region (Figure 4.2), and secondly, assisting in sugar binding at the neighboring protomer with the onward region (Figure 4.2), by repositioning helix α2'.

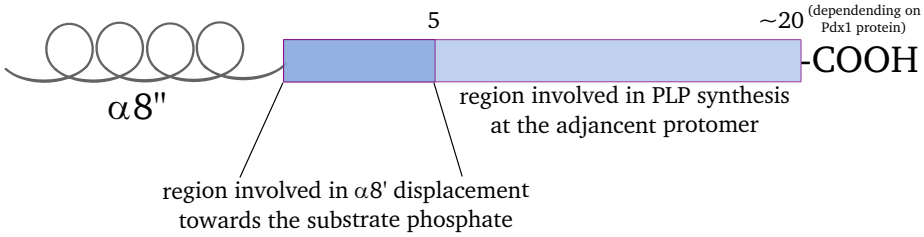

Figure 4.2: C-terminal regions of Pdx1 involved in catalysis. The length of two regions with assigned functions are indicated.

4.1.1 Intermediates of the PLP synthase reaction mechanism

Biochemical evidence for NH_3 tunneling in the β/α-barrel

The PLP synthase is classified as a glutamine amidotransferase with two remote active sites, one for the ammonia production and the other for PLP synthesis. The resulting ammonia from glutamine hydrolysis in Pdx2 is channeled to the Pdx1 active site [14] by an unknown mechanism. Structural analyses proposed methionine residues are involved in NH_3 transfer. Pdx1 is functional in the absence of Pdx2 under *in vitro* conditions in the presence of ammonium salts. Furthermore, enzymatic reports have shown that deletion of helix αN of Pdx1, a key segment for glutaminase activation, does not affect PLP synthesis in ammonia-dependent reactions [14, 55]. The ability of Pdx1 to function in the absence of Pdx2, even when lacking its helix αN, indicates the N-terminal side of the β-barrel functions as the ammonia gate. The Pdx1 β-barrel is hydrophobic and encloses the appropiate environment for the passage of reactive ammonia. However, a defined route within the β-barrel to connect the two active sites is not discernible, suggesting opening of the tunnel is transient for ammonia transfer.

Several residues at the inner side of the barrel or within helix αN terminus were exchanged by site-directed mutagenesis in *Pb*Pdx1 and resulting proteins were evaluated by enzymatic assays. The results from these assays gave evidences the β-barrel channels ammonia to the acceptor intermediate in the P1 active site. They also explained which residues are required for ammonia transfer. The residues were chosen based on structural analysis for two reasons: 1) because they showed changes in side chain conformation upon Pdx1 and Pdx2 interaction; 2) to prove their function as the residues formed cavities in the β-barrel that would form - in principle - the place of ammonia. The variants indicated the β-barrel of Pdx1 plays a role in ammonia tunneling, as shown by their significant changes in the PLP synthesis rate. The ammonia tunnel residues were grouped here according to three functions: i) residues involved in the uptake of nascent ammonia from the Pdx2 active site e.g., Met19; ii) residues of the ammonia gate in Pdx1 in the β-barrel (e.g., Leu82, Met103 and M148) and, iii) residues controling the ammonia transfer to the catalytic center (e.g., Met46). Met19 showed to be involved in glutamine hydrolysis, since a severe effect was observed

on glutaminase activity of Pdx2 on exchanged of this residue. Met19 lies on αN helix exposed to the Pdx2 catalytic center, close to the peptide required to stabilize the oxyanion region formed during glutamine hydrolysis. It appears this methionine has an influence on the arrangement of the Pdx2 active site, forming a path for the nascent ammonia. The ammonia would then pass helix αN and encounter the ammonia gate at the bottom of the β-barrel. This gate consists of Leu82, Met103 and Met148. Mutations of Leu82 and Met103 showed notable defects in ammonia-dependent PLP synthesis, restoring the enzymatic activity in the Leu82 mutants when ammonia was supplied from the glutaminase. Interestingly, Met103 was unique in this respect showing drastic activity loss in the Pdx2 dependent and independent assays, when substituted either by Phe or Ala. Introduction of a bulky side chain blocked the tunnel completely, however a replacement for alanine still showed a decrease to less than 50% PLP activity with a minor effect on the glutaminase rate, suggesting Met103 serves as a control point for ammonia uptake. An interesting result from the Met148Leu variant showed that the PLP synthesis rate increased aproximately five-fold in the glutaminase-dependent assay, therefore this residue directly links glutamine hydrolysis, ammonia transfer and PLP synthesis. The path for ammonia is followed by Met46, which is close to the catalytic Lys84 at the upper part of the β-barrel. Replacement of this conserved methionine upregulated the PLP synthesis in both enzymatic assays, suggesting ammonia can move within the β-barrel until it encounters Met46, which controls the ammonia entrance to the catalytic center of Pdx1.

R5P binding at the catalytic center

Earlier steps of the PLP biosynthesis require the catalytic reaction of R5P with a lysine in the P1 site followed by isomerization of the R5P adduct. NMR experiments demonstrated that the sugar is bound with its C1 carbon to the lysine via a Schiff base [21]. In a recent investigation made by *Moccand et al* [30], it was suggested that an arginine (Arg288, nomenclature of *Bs*Pdx1) positioned at the flexible C-terminal region (not visible in Pdx1 structures) would coordinate the binding of R5P at the adjacent protomer, by functioning as a general base activated by Asp24 (nomenclature for *B. subtilis*) of Pdx1 [30]. The activated Arg288 would function as a proton abstractor at C5 prior to phosphate elimination [30] on the way of the chromophoric intermediate formation. This residue is not highly conserved and is substituted by lysine in plasmodial Pdx1 proteins (Alignment D.1). The authors also tested an R288K variant which behaved as the wild type. If the Arg functions as a proton acceptor, Lys might have the same chemical function in plasmodial Pdx1 proteins. Crystallographic structures of *Pb*Pdx1 and *Tt*Pdx1 solved in this study confirmed the R5P substrate is attached to the catalytic lysine with its C1. The aspartate is in close proximity to the C2 carbon of the R5P adduct in the active site, indicating the aspartate might be the proton acceptor from the hydroxyl group of C2 for R5P adduct isomerization into Ru5P. Arg288 could function in substrate isomerization and not for proton shuffling at C5, more precisely, as a proton acceptor at Asp24 subsequently Asp24 functioning as a base in the isomerization to give a carbonyl group at C2.

Intermediate migration from P1 to P2: PLP biosynthesis

The enzymatic reaction after R5P binding continues when the second substrate, NH_3, reacts with the pentose adduct to form the chromophoric intermediate I_{320} after release of water and phosphate ion. The question was if the final steps of PLP biosynthesis take place in the P2 site of Pdx1 and Lys152 (nomenclature for *Pb*Pdx1) is involved in the chemical reactions, how the intermediate would be transfered from P1 to P2. A proposed mechanism was suggested after elucidation of the bacterial PLP synthase in complex with an Ru5P adduct and later supported by chemical analyses with NMR experiments [13, 21]: since Lys152 is located in the P2 site, the residue would have to rotate and approach the P1 site [13], to reposition the intermediate in a new environment [21, 56]. This residue was confirmed to play a role in catalysis, as mutants of it were unable to synthesize PLP [13, 22]. Interestingly, mutation of this lysine into arginine did not hinder the enzyme to produce I_{320}, unlike mutation to alanine that incapacitated Pdx1 to produce the chromophoric intermediate [22]. This finding was an initial indication that Lys152 might play a role in catalysis and has been recently confirmed by electrospray ionization mass spectrometry studies [30]. The Pdx1-PLP structure solved in this work shows the PLP attached with its C4' carbon to the catalytic lysine via a Schiff base in the P2 site, giving structural evidence of the P2 site for PLP biosynthesis. Still, it is unclear at what stage of the reaction the intermediate is transfered from P1 to P2, where the PLP is observed. The mechanism remains to be characterized by which the imine migrates from C1 to C5. A hypothetical mechanism based on [21, 56] is illustrated in Figure 4.3.

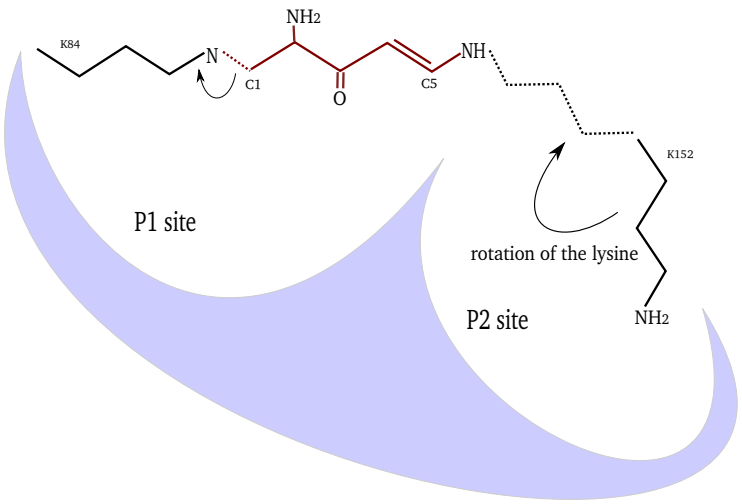

Figure 4.3: Proposed mechanism for migration of the intermediate to P2 site. As postulated by *Hanes et al 2008*, an imine migration mechanism takes place from C1 to C5 of the intermediate. Lys152 approaches P1 site by rotation and reacts with the intermediate at C5.

4.2 Assembly of the PLP synthase complex

Studies of the multienzymatic assembly of the PLP synthase complex are sparse. The structural and biochemical data available show the full assembly of the enzyme forms a complex of up to ∼700 kDa [13, 14, 18, 31] and the association of the Pdx1 or Pdx1/Pdx2 subunits relies on critical structural and functional segments. The core of the PLP synthase complex is constituted by Pdx1 forming a dodecamer, as seen in the crystal structures of bacterial Pdx1 [13, 14]. However, hexamers can be formed in solution for bacterial and eukaryotic systems [13, 14, 31], and smaller oligomers are absent. The *Plasmodium* structure solved in this study confirms that eukaryotic Pdx1 proteins, in general, can assemble into dodecameric structures, in contrast to the yeast Pdx1 from *S. cereviciae* that was hexameric in the crystal structure and almost exclusively hexameric in solution [18]. The presence of a unique sequence insertion in the yeast Pdx1 protein is responsible for the different oligomerisation behavior [18]. The Pdx1 complex assembly depends on the additional helices that surround the $(\beta/\alpha)_8$ barrel and delimit the interface of the hexamer/dodecamer [18, 31]. This assembly determines a catalytically active complex as the Pdx1 quaternary conformation is required for pentose substrate binding and catalysis in a cooperative manner [23, 31].

Pdx2 assembles randomly to the Pdx1 dodecameric core

The mechanism by which Pdx2 assembles to the Pdx1 core has not been studied in detail. Fully occupied PLP synthase complexes could be obtained *in vitro* using substrates of the enzymes (Ru5P or glutamine), which allowed crystal structure determination [13, 14] and in this study (Figure 4.4, A). Biophysical studies have shown the substrate glutamine streghtens the Pdx1/Pdx2 interaction in prokaryotic and eukaryotic complexes [14, 15, 33]. All tested PLP synthase complexes from *B. subtilis* [33], *P. falciparum* [15] and *P. berghei* show a high entropy gain in the absence of glutamine that decreases when glutamine is added to the system, suggesting Pdx1/Pdx2 complexes lose conformational freedom tending to the stabilization of the complex. Furthermore, an increase of enthalpy change occurs in the presence of glutamine, most likely due to the additional interactions formed at the protein-protein interface and glutamine binding in the active site. Hence, it can be deduced that the substrate glutamine modulates the complex formation by entropy loss and enthalpy gain.

The mechanism by which the two enzymatic subunits associate / dissociate in the presence of glutamine is not discernible from the ITC studies. It is unknown whether glutamine binding modulates the assembly of Pdx2 with Pdx1 in the complex, as the ITC assays tested complexes using the catalytic inactive Pdx2 to stabilize the complex. Previous pull out assays to analyse the interaction of native Pdx1 and His-tagged Pdx2 from *B. subtilis* in the presence of acivicin [12] showed that Pdx1/Pdx2 complexes were no longer formed after preincubation of the proteins with acivicin. Particularly, it was observed that the complexes dissociated due to transient interactions, allowing Pdx2 to bind acivicin and the

modified acivicin-Pdx2 complexes could not longer interact with Pdx1. Crystallization studies of the *B. subtilis* Pdx2 in complex with acivicin showed that the relevant regions for complex formation and Pdx2 active site organization are distorted [57]. These structural changes caused by acivicin alter the protein-protein interface, decreasing the affinity of Pdx2 with Pdx1 and therefore, a Pdx1 and Pdx2 interaction analysis with acivicin is not compatible to explain the assembly of the PLP synthase complex.

Visualization of the PLP synthase complex by electron microscopy analysis proves that Pdx1 and Pdx2 assemble transiently. Few Pdx2 subunits occupied the Pdx1 dodecameric core, without a defined pattern for this association, despite the presence of glutamine in the assay. In contrast, fully assembled complexes were observed, when the catalytic inactive Pdx2 was used. If the measured ITC data in the absence of glutamine are considered together with the EM analysis using active Pdx2 and L-glutamine, it can be deduced the Pdx1/Pdx2 assembly has a high rate of association/dissociation and the substrate glutamine does not modulate a subsequent binding of the Pdx2 subunits on the Pdx1 dodecamer.

Substrates do not determine the Pdx1/Pdx2 assembly *in vitro*

GATases are regulated in several ways to control glutamine hydrolysis [9]. For example, in enzymes such as, Anthranilate synthase [58], glucosamine 6- phosphate synthase [59] or imidazole glycerol phosphate synthase [60] the glutaminase domain requires an acceptor substrate bound to the synthase domain to activate glutamine hydrolysis allosterically. It was reported earlier for the PLP synthase complex that Pdx1 is sufficient to stimulate the glutaminase; addition of the Pdx1-substrates did not enhance the rate of glutamine hydrolysis [12]. Moreover, it is known that Pdx1 catalyzes PLP synthesis with sub-optimal activity, as observed in this study with *Pf*Pdx1 or *Pb*Pdx1; more precisely, the glutaminase and synthase reactions seem not to be synchronized as most of the produced NH_3 is not used for PLP synthesis. Recent evidence shows PLP release from Pdx1 depends on the presence of a PLP-depedent enzyme [30] as a regulatory mechanism to control PLP biosynthesis by Pdx1. Biochemical and biophysical (ITC and AUC) analyses presented in this study show that Pdx2 can interact with Pdx1 independent of the substrates R5P or L-Gln. In particular, glutamine does not bind to Pdx2 alone, rather it requires a preformed Pdx1/Pdx2 complex. This implies Pdx2 interaction with Pdx1 and glutamine binding in the Pdx1/Pdx2 complex do not modulate PLP synthesis.

In summary, the interpretation that a Pdx1/Pdx2 complex is required for glutamine binding, together with EM analysis leads to the proposal that the composition of Pdx2 can vary in the multi-enzymatic Pdx1/Pdx2 complexes and would not require neighboring Pdx1 proteins to promote sequential occupancy with Pdx2. In addition, encounter complexes can associate independent of the presence of glutamine or NH_3-acceptor substrate, i.e, Pdx2 can interact with Pdx1, subsequently bind glutamine and hydrolyse it without an stimulatory

signal provided by an NH_3 acceptor and then Pdx2 leaves the complex (Figure 4.4, B). Another interpretation would be that Pdx2 binds Pdx1, hydrolyses glutamine and remains in complex with Pdx1 in the presence or absence of an ammonia acceptor (Figure 4.4, B). The resulting NH_3 could be stored until a substrate acceptor enters the active site. The synchronization of ammonia transfer for PLP synthesis would be further regulated by a PLP-dependent enzyme.

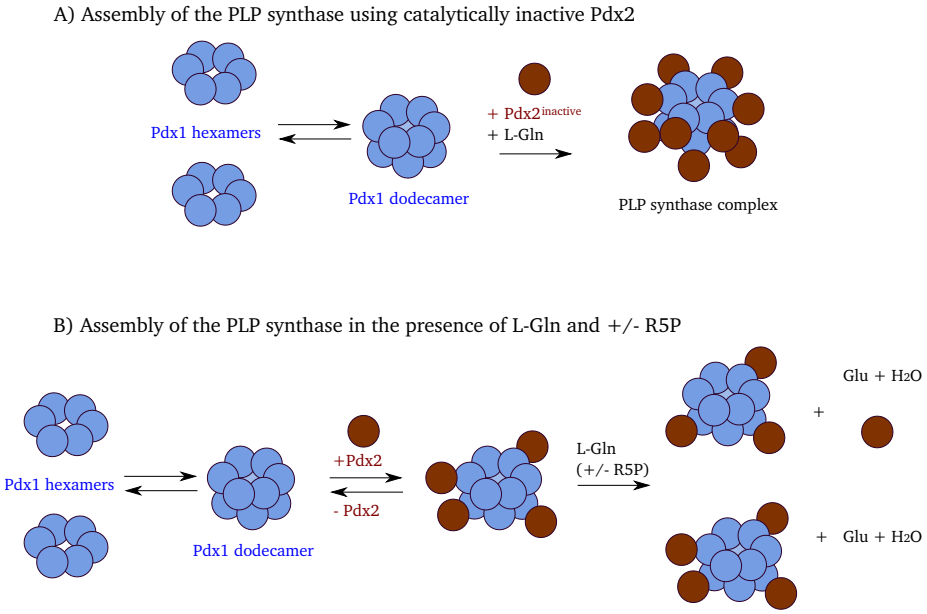

Figure 4.4: Assembly of PLP synthase from Pdx1 and Pdx2 proteins.

Pdx1/Pdx2 interaction in prokaryotes and eukaryotes

The main motivation of this PhD Thesis was to obtain the crystal structure from *P. falciparum* PLP synthase complex and understand how this enzyme functions for its potential use in drug design to treat malaria. However, *P. falciparum* PLP synthase proved a difficult target for crystallographic 3D structure determination due to the aggregation into fibers *in vitro* observed in electron microscopic analysis, not seen with the proteins from the rodent parasite *P. berghei*. The fibers were seen when using *Pf*Pdx1, which also aggregated into fibers in the absence of *Pf*Pdx2, Figure 3.6. Comparison of the electrostatic surface at the interface of two opposite Pdx1 subunits from the *Pf*Pdx1/*Pf*Pdx2 model[1] and *Pb*Pdx1 dodecamer did not show differences in the contact of the two Pdx1 proteins (Figure 3.9). One can speculate the C-terminus of *Pf*Pdx1, that has eluded structural determination and has high protein sequence variability, might be involved in the fiber formation, since it is known that this region plays a key role in reciprocal activation between two Pdx1 subunits [23, 31]. Future investigations could use C-terminal deletion mutants of *Pf*Pdx1 in crys-

[1] structural model described in [15]

tallographic and electron microscopy experiments to understand the cause of *Pf*Pdx1 aggregation.

The observed aggregation into fibers was a limitant for continuing crystallization trials with the *P. falciprum* PLP synthase complex. Instead, structural studies were continued on a chimeric complex between *P. berghei* Pdx1 and *P. falciparum* Pdx2. The proteins are highly similar, with more than 60% identity in sequence among the autonomous Pdx1 and Pdx2 from both parasites. The complex sucessfully crystallized and diffracted to 3.6 Å resolution and is composed of 24 subunits, as seen in the bacterial strutures [13, 14]. The plasmodial Pdx1/Pdx2 chimera proved to be a proper system to study an eukaryotic PLP synthase complex because this reconstituted complex was functional, hydrolysing glutamine and synthesizing PLP with catalytic rates similar to the natural *P. falciparum* and *P. berghei* PLP synthase complexes.

Elucidation of the 3D structure from this eukaryotic complex revealed two major advances related to enzyme interaction and activation: i) the importance of insertion sequences for protein-protein interaction in eukaryotic systems, and ii) the importance of key structural conformational changes in the interface for the Pdx2 glutaminase activation, common in prokaryotic and eukaryotic systems. The insertion sequences determine the differences in the Pdx1/Pdx2 interaction. A particular loop named loop 95-111 [24] of Pdx2 was seen in the interface with Pdx1. This region is prone to variation in eukaryotic proteins (Figure D.2) and is absent in bacterial Pdx2, therefore the contact to Pdx1 is abolished. It might explain why the strength of Pdx1/Pdx2 association between bacterial and plasmodial Pdx1/Pdx2 interfaces is different in ITC experiments. Rigid body rotation of Pdx2 was seen in the structure, compared to bacterial systems. This should not be surprising, since changes in the shape of multi-subunit complexes are common for the function and regulation of the proteins in the cell, e.g, chaperonins [61, 62], piruvate kinase [63]. The structural alteration of the Pdx2 position in the chimeric complex could explain another step of the complex formation process, as changes were also seen in the Pdx1 subunit, i.e., helix α2' was observed in an open conformation, discussed above § 4.1. Despite this positional difference of the Pdx2 subunit, the active site is organized at the interface with Pdx1, similar to the position observed for bacterial complex structures. Its surrounding showed the same structural changes required for Pdx2 activation such as, ordering of loop 124-127 and organization of the critical oxyanion region, supported by the activation loops Q12 and OXH. This suggests the mechanism of Pdx2 activation is conserved in prokaryotic and eukaryotic proteins.

4.2.1 Targeting PLP synthase complex for drug design

Inhibitor-based approaches to combat diseases should be based on the premise that the selected or designed inhibitors should target biological components absent in the host genome, in order to avoid harmful side effects with proteins from the host. Vitamin B_6 is essential for all living organisms. The mayority

of organims can synthesize vitamin B_6 *de novo* but humans must take it from the diet. The genes *pdx1* and *pdx2* of the R5P-dependent pathway are present in several pathogenic organisms, such as *Plasmodium*, *Toxoplasma gondii* [64] and *Mycobacterium tuberculosis* [65, 66]. Recently it has been reported that disruption of the *pdx1* gene in *M. tuberculosis* is lethal for the bacterium [66]. Moreover, it has been reported that *P. falciparum* expresses pdx1 and pdx2 during blood stages [24], the ones that cause the malaria disease. The PLP synthase Pdx1/Pdx2 complex from *Plasmodium* was studied here for its potential use as a drug target.

Targeting the PLP synthase complex for drug design should be based on knowledge about the 3D structure of the enzyme more than substrate-based approaches to avoid side effects because, the PLP synthase complex shares substrates (R5P, G3P and Gln) with other essential metabolic enzymes eg., ribose 5-phosphate isomerase[2], glyceraldehyde 3-phosphate deshydrogenase[3], glutamine-PRPP[4] amidotransferase[5] [67]. Given that the assembly and activation of the PLP synthase complex depends on α-helices such as, αN or α2', these represent an useful information for drug development. Compounds such as small peptides, designed to inhibit protein-protein formation must affect the protein surface selectively, despite protein-protein interfaces having a large surface area. For instance, approaches to disrupt the assembly of the hexameric gp41[6] core using C-terminal heptad repeat peptides of HIV-1 gp41 have been successful [68], and have been confirmed by x-ray crystallography from which the peptide is shown bound to the hydrophobic pocket on the surface of HIV-1 gp41 [68].

Interestingly, Pdx1 and Pdx2 depend on each other for activation and also to provide substrates to the other, marking the importance of the ammonia tunnel entrance as a vulnerable site for drug design. This would circumvent the problem of identifying drugs based only on protein-protein interaction. Taking advantage of the fact that αN is fundamental for Pdx1/Pdx2 assembly and is at the interface of the ammonia gate of the β-barrel, this region could be considered for developing inhibitors of the PLP synthase complex, i.e., inhibitors (e.g., compounds or peptides) that block the protein-protein interaction and concomitant block the ammonia entrance to the β-barrel.

In addition to the above strategy, targeting the PLP synthase catalytic center in Pdx1 would be suitable for structure-based inhibitor design for the following reasons: PLP synthesis involves more than 20 enzymatic steps with intermediates uncommon in other enzymatic processes such as I_{320}. I_{320} is a very stable intermediate and could guide drug development.
Studies of structure-based drug design will also enrich our understanding of the PLP synthase reaction mechanism.

[2] an enzyme involved in the pentose phosphate pathway
[3] an enzyme involved in the breakdown of glucose in glycolysis
[4] 5-phosphoribosyl 1-pyrophosphate
[5] an enzyme involved in *de novo* purine nucleotide synthesis
[6] a glycoprotein of the HIV-1 envelope

Chapter 5

Future Directions

Plasmodial PLP synthase has emerged as an attractive drug target due to the absence of this biosynthetic enzyme in humans. The possibility of translocation of B_6 vitamers from the host cell and conversion into PLP by the kinase PdxK in the parasite is considered as a likely survival mechanism under PLP depletion, although genetic manipulation trials are needed to prove that, i.e., knockdown experiments of the gene encoding Pdx1 in the erythrocyte-infecting stages of the malaria parasite to observe the requirement of Pdx1 for cell growth. Regardless of alternative strategies to supply vitamin B_6 to the parasite, PLP biosynthesis seems to be an important pathway during the blood stages of *P. falciparum*, because Pdx1 and Pdx2 proteins are expressed constitutively [24], and both enzyme genes are upregulated when the parasite is subjected to oxidative stress conditions [29].

Future investigations to provide additional knowledge of the enzymatic mechanism of plasmodial PLP synthase e.g., PLP release from the Pdx1 catalytic center, in the presence of PLP-dependent enzymes, might contribute in understanding enzyme regulation and its dependency on certain cellular conditions eg., oxidative stress, PLP demands.

As electron microscopic studies proved to be an useful technique to gain insight into enzyme assembly, additional experiments can be done with this technique to visualize how substrates such as, R5P, G3P, or product like PLP, modulate the Pdx1/Pdx2 assembly *in vitro*.

Elucidation of the PLP synthase 3D structure with its entire C-terminus would improve the understanding of how residues of the C-terminus are involved in the cooperativism of the Pdx1 core, for example, using cross-linkers "to trap" the enzyme in a conformation with the C-terminus bound at the adjacent Pdx1 protomer.

Another interesting question to answer is whether Pdx1 synthesizes PLP in the

absence of Pdx2 *in vivo*, as shown in the *in vitro* assays using ammonia sources.

In particular, characterization of the PLP biosynthetic mechanism by microspectrophotometry, substrate analogues and x-ray crystallography to get snapshots of the catalytic steps as well as, advances in unraveling the molecular mechanism by which ammonia is transfered along the $(\beta/\alpha)_8$-barrel in the PLP synthase, can be used as basis for drug design against malaria.

Appendix A

Oligonucleotides

Table A.1: List of oligonucleotides used for cloning genes and point-mutants. Codon mutations are highlighted and restriction sites for endonucleases recognition are underlined.

Name	Oligonucleotide
PbPdx1^{M19V} for	CTTAAGCATGGATGGTGTGAA**GTG**TTAAAAGGGGGAGTCATAATG
PbPdx1^{M19V} rev	CATTATGACTCCCCCTTTTAA**CAC**TTCACACCATCCATGCTTAAG
PbPdx1^{M46I} for	GGCTGGTGCAATAGGTGTA**ATC**ATTTTAGAAAATATTCCATC
PbPdx1^{M46I} rev	GATGGAATATTTTCTAAAAT**GAT**TACACCTATTGCACCAGCC
PbPdx1^{L82M} for	GAAAATGCATTTCTATAAATGTA**ATG**GCTAAAGTTAGAATAGGC
PbPdx1^{L82M} rev	GCCTATTCTAACTTTAGC**CAT**TACATTTATAGAAATGCATTTTC
PbPdx1^{L82A} for	CATTTCTATAAATGTA**GCA**GCTAAAGTTAG
PbPdx1^{L82A} rev	CTAACTTTAGC**TGC**TACATTTATAGAAATG
PbPdx1^{L82F} for	CATTTCTATAAATGTA**TTC**GCTAAAGTTAG
PbPdx1^{L82F} rev	CTAACTTTAGC**GAA**TACATTTATAGAAATG
PbPdx1^{L82S} for	CATTTCTATAAATGTA**TCC**GCTAAAGTTAG
PbPdx1^{L82S} rev	CTAACTTTAGC**GGA**TACATTTATAGAAATG
PbPdx1^{M103A} for	GAACTCAAAGTTGAT**GCA**CTTGATGAAAGTG
PbPdx1^{M103A} rev	CACTTTCATCAAG**TGC**ATCAACTTTGAGTTC
PbPdx1^{M103F} for	GAAGAACTCAAAGTTGAT**TTC**CTTGATGAAAGTGAAG
PbPdx1^{M103F} rev	CTTCACTTTCATCAAG**GAA**ATCAACTTTGAGTTCTTC
PbPdx1^{M148L} for	GAATATCAGAAGGAGCTTCT**CTG**ATAAGAACCAAAGGTGAAGC
PbPdx1^{M148L} rev	GCTTCACCTTTGGTTCTTAT**CAG**AGAAGCTCCTTCTGATATTC
PbPdx2^{H199N} for	ATTGTATGGGAACAATTTTTT**AAC**CCAGAATTAATGCCATAT
PbPdx2^{H199N} rev	ATATGGCATTAATTCTGG**GTT**AAAAATTGTTCCCATACAAT
TtPdx1NotIrev	ATAAGAGCGGCCGCCCATCCTCTCTTTGCAAGCCTTTC
TtPdx1BamHINdeI for	AAAAGGATCCATATGGAGGGCGGGATGGAAAAGGGC
PfPdx1BamHINdeI for	GAAGAAGGATCCATATGGAAAATCATAAAGATGATGCAG
PfPdx1Stop XhoI rev	CAACAACTCGAGTCATTGTGGTGTTAAAAATTTGGTG
PfPdx2^{H196N}NheI for	ACTAGTGGAGCTAGCATGTCCGAAATAACTATAGGGGTATTAT
PfPdx2^{H196N}Stop XhoI rev	TAATAACTCGAGTTATGAATATTTGTAATTTTTAACCTTC

Appendix B

Purification of Pdx2 from *P. berghei* and *P. falciparum*

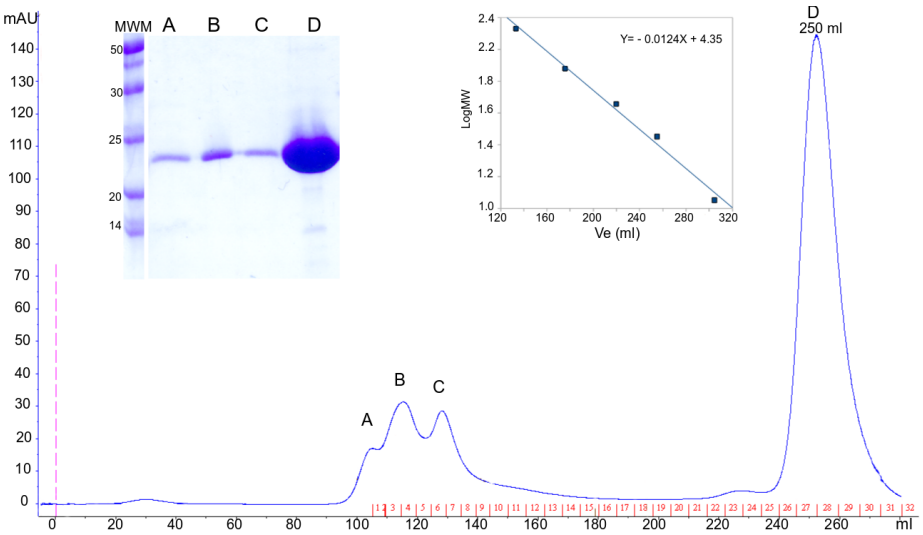

Figure B.1: Elution profile and purification of PbPdx2^{H199N} by SEC. Elution profile of PbPdx2^{H199N} from a Superdex S200 26/60 column shows four fraction peaks (A, B, C and D), which were evaluated by SDS-PAGE (left). Peaks A, B and C correspond to high molecular weight aggregates. Monomers of PbPdx1 eluted at 250 ml, corresponding to a molecular mass of 18 KDa. Theoretical value of PbPdx2^{H199N} is 25.675 KDa (accession code Q4PJX5 `http://www.uniprot.org/`). The calibration curve (middle) of the column was performed as described in § 2.2.

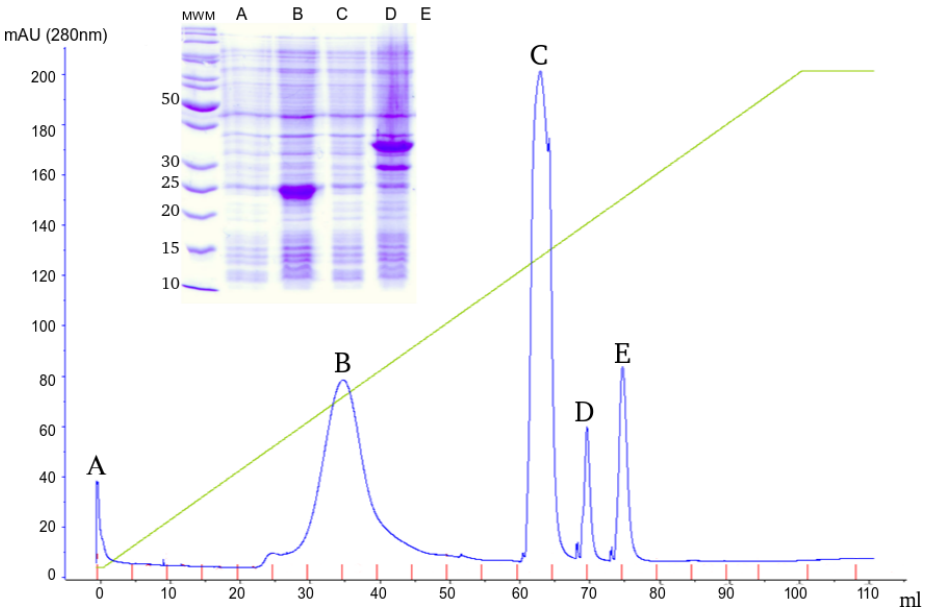

Figure B.2: Elution profile of native PfPdx2^{H196N} by AEC using a Source 30Q matrix. PfPdx2^{H196N} eluted from a 10-800 mM NaCl gradient at a concentration of 286 mM NaCl (peak B).

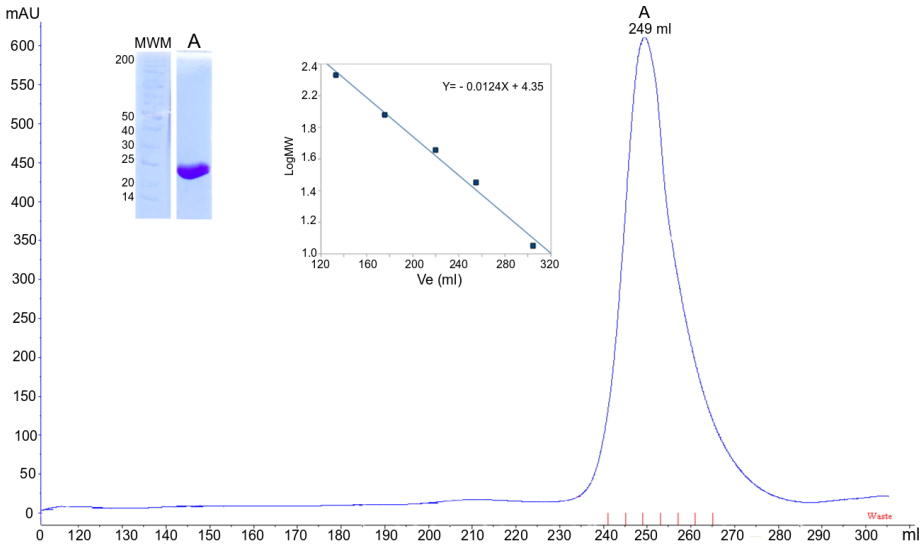

Figure B.3: Elution profile and purification of PfPdx2^{H196N} by SEC. Elution profile of PfPdx2^{H196N} from a Superdex S200 26/60 column shows a fraction peak of 249 ml with molecular mass of 18.2 KDa calculated using the calibration curve (middle). The calibration of the column was performed as described in § 2.2. Theoretical value of the molar mass of PfPdx2^{H196N} is 24.563 KDa (accession code Q8IIK4 `http://www.uniprot.org/`). Evaluation of the fraction peak by SDS-PAGE is shown (left).

Appendix C

Glossary

AEC	Anion exchange chromatography
A	Alanine
Å	Angström
APAD	3-acetylpyrimidine adenine dinucleotide
At	*Arabidopsis thaliana*
AUC	Analytical ultracentrifugation
Bs	*Bacillus subtilis*
C-terminal	Carboxy terminal
D	Aspartate
E. coli	*Escherichia coli*
EDTA	Ethylenediaminetetraacetic acid
e.g.	exempli gratia
ESRF	European Synchrotron Radiation Facility
EM	Electron Microscopy
GATases	Glutamine amidotransferases
G. stereaothermophilus	*Geobacillus stereaothermophilus*
GF	Gel filtration (Size exclusion chromatography)
L-Gln	L-Glutamine
Glu	Glutamate
G3P	DL-glyceraldehyde 3-phosphate
G	Glycine
i.e.	id est
HEPES	4-(2-hydroxyethyl)-1-piperazineethanesulfonic acid
HIV	Human immunodeficiency virus
H	Histidine
K	Lysine
KCl	Potassium Chloride
kDa	Kilo Dalton
Leu	Leucine
Lys	Lysine
M	Methionine
MTG	1-Thioglycerol

NaCl	Sodium Chloride
NaH_2PO_4	Sodium monobasic Phosphate
NH_4Cl	Ammonium chloride
$(NH_4)_2SO_4$	Ammonium sulphate
N-terminal	amino terminal
NCS	Non crystallographic symmetry
NMR	Nuclear magnetic resonance
Pb	*Plasmodium berghei*
Pf	*Plasmodium falciparum*
OXH	Oxyanion hole
P	Proline
PCR	Polymerase Chain Reaction
PDB	Protein data bank
PEG	Polyethylene glycol
Phe	Phenylalanine
PLP	Pyridoxal 5'-phosphate
Pro	Proline
R	Arginine
R5P	D-Ribose 5-phosphate
rmsd	Root mean square deviation
S	Serine
SEC	Size exclusion chromatography
Tm	*Thermotoga maritima*
Tt	*Thermus thermophilus*
Tris	Hydroxymethyl aminomethane
Tyr	Tyrosine
wt	Wild type

Appendix D

Alignments

The alignments were made using TEXshade [69]

Figure D.1: Alignment of amino acid sequences of selected Pdx1 proteins. The sequences are tinted with the purpose to highlight: putative residues of the ammonia tunnel (dark blue); residues of the α2' helix (red); and residues involved in substrate binding and/or catalysis in P1 (light green) and P2 (dark green). Enumeration is based on *P. berghei* Pdx1, excepting R129 is for *T. thermophilus* Pdx1. Residues in light blue correspond to the βN region of the *B. subtilis* and *T. maritima* Pdx1 proteins that interact with Pdx2 in the Pdx1/2 complexes. Arrows on top of the alignment mark the position where deletion of the C-terminus were made in *Derrer et al 2010*. Sequence shading and labeling were done using TEXshade package.

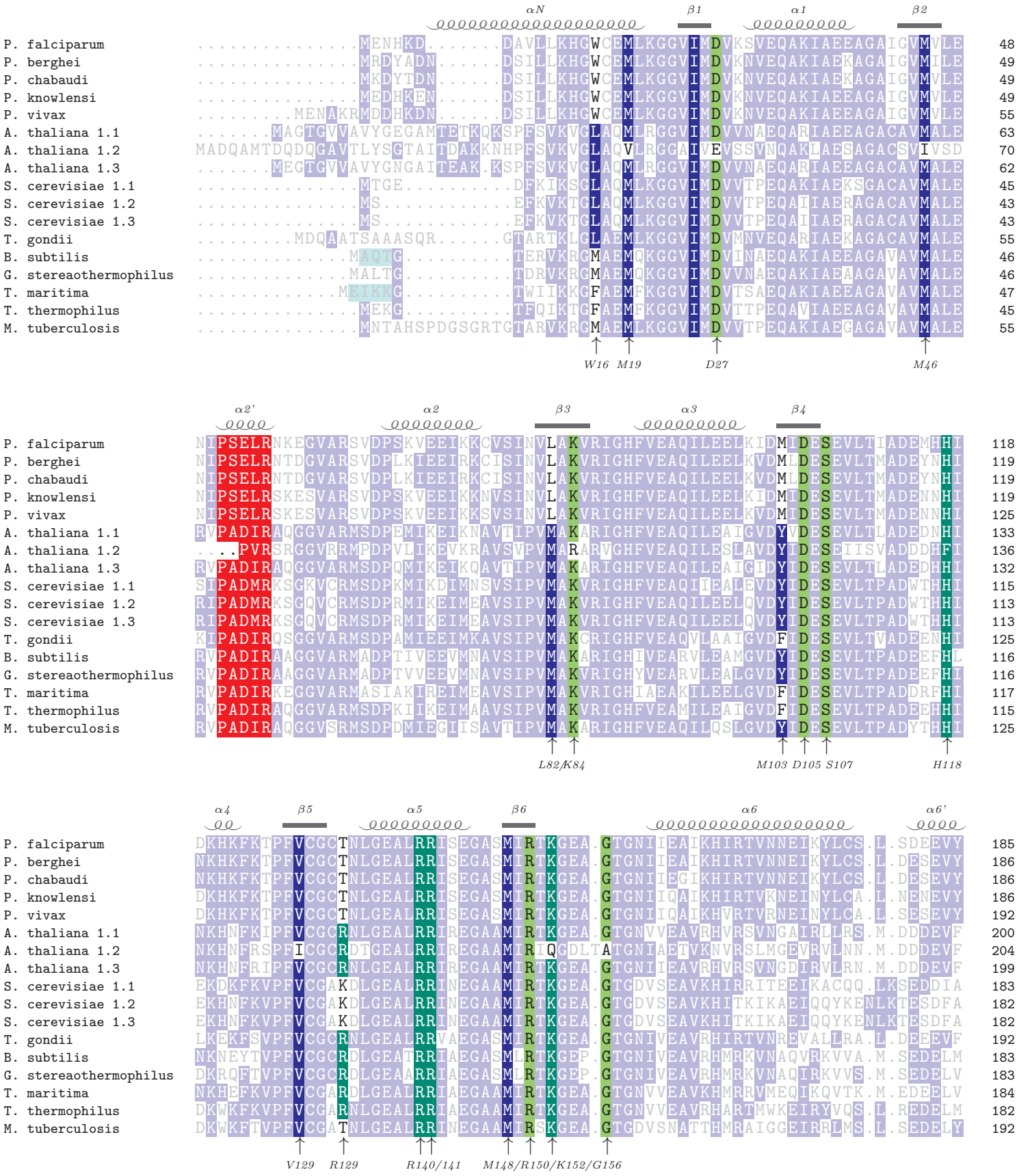

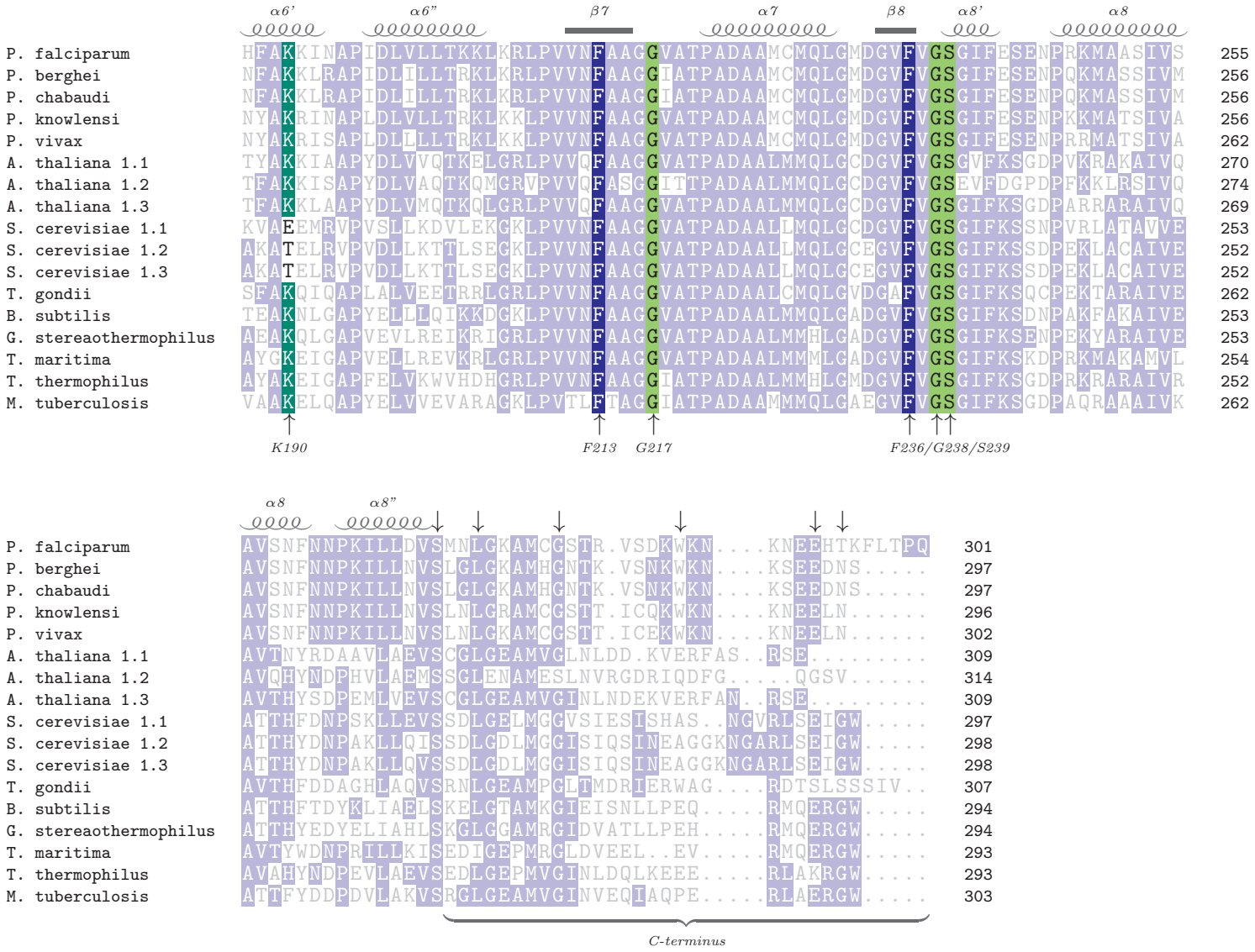
α6'
α6"
β7
α7
β8
α8'
α8
P. falciparum 255
P. berghei 256
P. chabaudi 256
P. knowlensi 256
P. vivax 262
A. thaliana 1.1 270
A. thaliana 1.2 274
A. thaliana 1.3 269
S. cerevisiae 1.1 253
S. cerevisiae 1.2 252
S. cerevisiae 1.3 252
T. gondii 262
B. subtilis 253
G. stereaothermophilus 253
T. maritima 254
T. thermophilus 252
M. tuberculosis 262
K190
F213
G217
F236/G238/S239
α8
α8"
P. falciparum 301
P. berghei 297
P. chabaudi 297
P. knowlensi 296
P. vivax 302
A. thaliana 1.1 309
A. thaliana 1.2 314
A. thaliana 1.3 309
S. cerevisiae 1.1 297
S. cerevisiae 1.2 298
S. cerevisiae 1.3 298
T. gondii 307
B. subtilis 294
G. stereaothermophilus 294
T. maritima 293
T. thermophilus 293
M. tuberculosis 303
C-terminus

Figure D.2: Alignment of amino acid sequences of selected Pdx2 proteins. Residues in dark blue correspond to the residues at the interface with Pdx1 in the Pdx1/2 complexes from *B. subtilis*, *T. maritima* and chimera *P. berghei* Pdx1/ *P. falciparum* Pdx2. Residues involved in catalysis: triad catalytic (C87, H196 and E198), Q12, R121, R154, E53 and oxyanion hole peptide (P50, G51 and G52) are enumerated in the alignment based on *P. falciparum* Pdx2 protein.

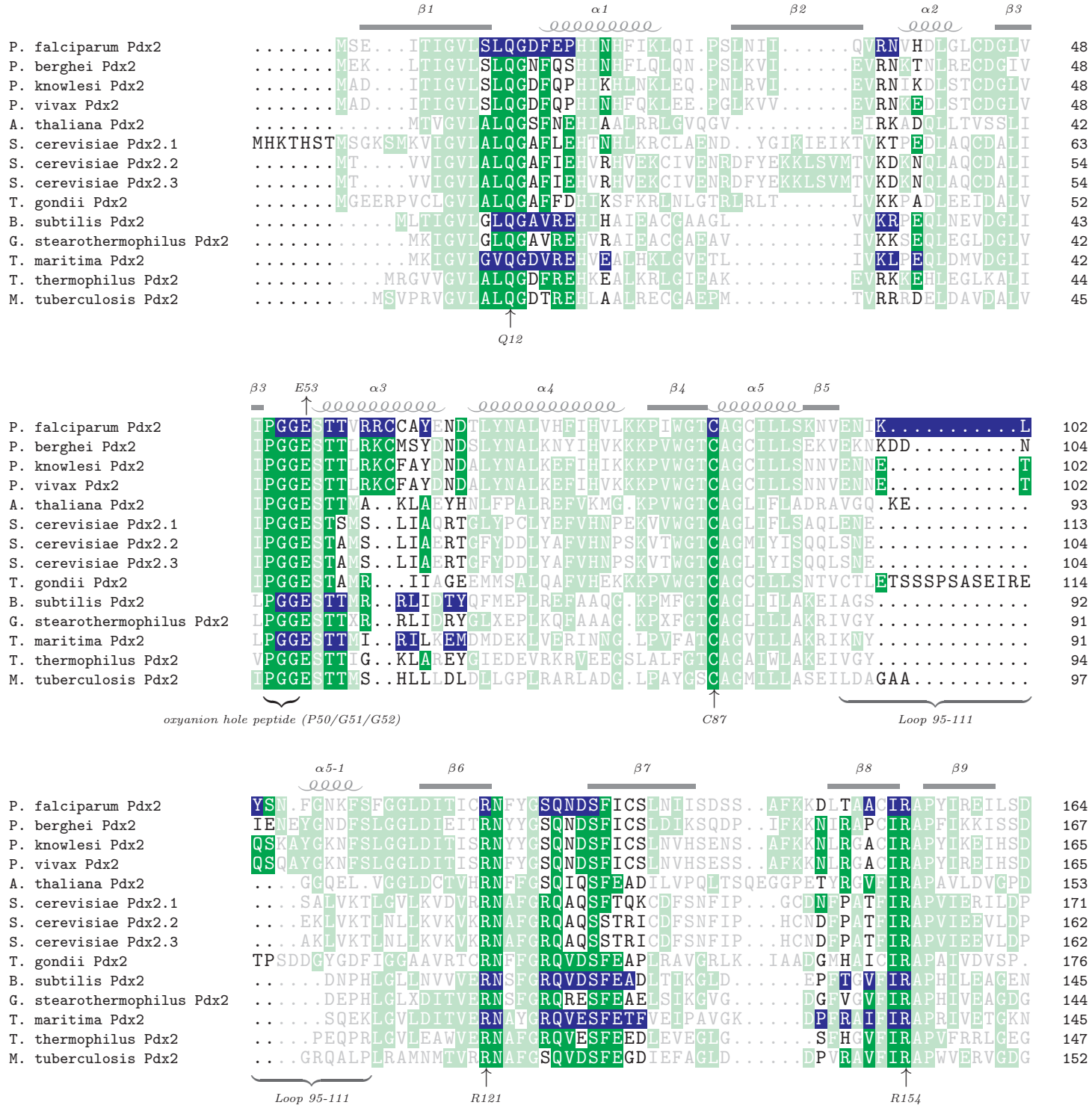

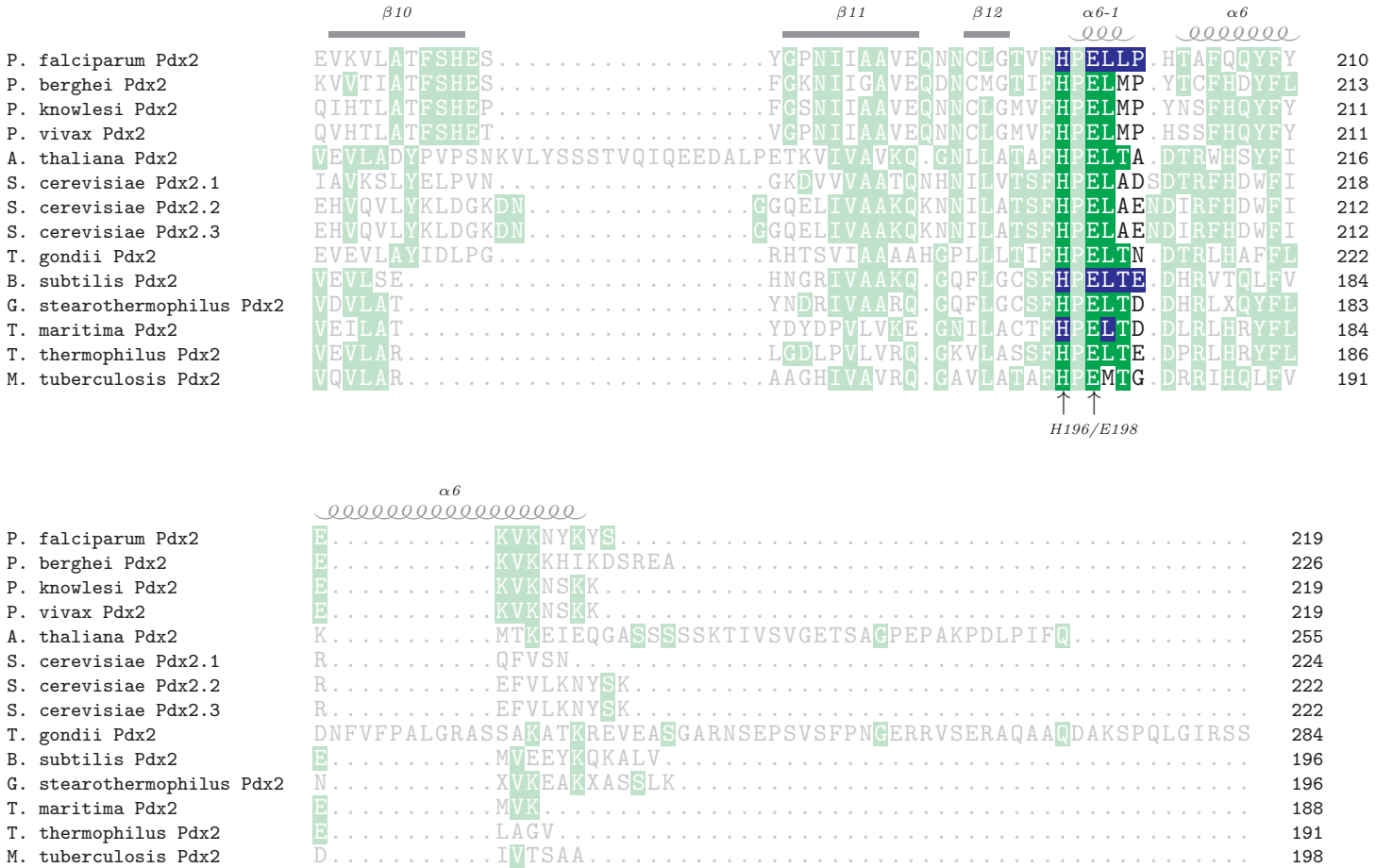
β10
β11
β12
α6-1
α6
P. falciparum Pdx2
P. berghei Pdx2
P. knowlesi Pdx2
P. vivax Pdx2
A. thaliana Pdx2
S. cerevisiae Pdx2.1
S. cerevisiae Pdx2.2
S. cerevisiae Pdx2.3
T. gondii Pdx2
B. subtilis Pdx2
G. stearothermophilus Pdx2
T. maritima Pdx2
T. thermophilus Pdx2
M. tuberculosis Pdx2
H196/E198
α6
P. falciparum Pdx2
P. berghei Pdx2
P. knowlesi Pdx2
P. vivax Pdx2
A. thaliana Pdx2
S. cerevisiae Pdx2.1
S. cerevisiae Pdx2.2
S. cerevisiae Pdx2.3
T. gondii Pdx2
B. subtilis Pdx2
G. stearothermophilus Pdx2
T. maritima Pdx2
T. thermophilus Pdx2
M. tuberculosis Pdx2

Bibliography

[1] R. Percudani and A. Peracchi, "A genomic overview of pyridoxal-phosphate-dependent enzymes," *EMBO rep.*, vol. 4, pp. 850–854, 2003.

[2] S. Mooney and H. Hellmann, "Vitamin B6: Killing two birds with one stone?," *Phytochem.*, vol. 71, pp. 495–501, 2010.

[3] T. Fitzpatrick, N. Amrheim, B. Kappes, P. Macheroux, I. Tews, and T. Raschle, "Two independent routes of *de novo* vitamin B_6 biosynthesis: not that different after all," *Biochem. J.*, vol. 407, pp. 1–13, 2007.

[4] M. Garrido-Franco, "Pyridoxine 5'-phosphate synthase: de novo synthesis of vitamin B_6 and beyond ," *Biochim. at Biophysica Acta*, vol. 1647, pp. 92–97, 2003.

[5] M. Ehrenshaft, P. Bilski, M. Li, C. Chignell, and M. Daub, "A highly conserved sequence is a novel gene involved in *de novo* vitamin B6 biosynthesis," *PNAS*, vol. 96, pp. 9374–9378, 1999.

[6] M. Ehrenshaft and M. Daub, "Isolation of *PDX2*, a second novel gene in the pyridoxine biosynthesis pathway of eukaryotic, archeabacteria, and a subset of eubacteria," *J. Bacteriol.*, vol. 183, no. 11, pp. 3383–3390, 2001.

[7] K. Tazuka, Y. Adachi, K. Mazuda, K. Yamada, and K. Kumaoka, "Origin of the nitrogen atom of pyridoxine in *Saccharomyces cerevisiae*," *Biochim. Biophys. Acta*, vol. 1244, pp. 113–116, 1995.

[8] K. Tanaka, K. Tazuka, K. Yamada, and H. Kumaoka, "Biosynthesis of pyridoxine in microorganisms," *J. Ntr. Sci. Vitaminol.*, vol. 46, pp. 55–57, 2000.

[9] S. Mouilleron and B. Golinelli-Pimpaneau, "Conformational changes in ammonia-channeling glutamine amidotransferases," *Curr. Opi. Struc. Biol.*, vol. 17, pp. 653–664, 2007.

[10] A. Douangamath, M. Walker, S. Beissmann-Driemeyer, M. Vega-Fernandez, R. Sterner, and M. Wilmanns, "Structural Evidence for Ammonia Tunneling across the α/β Barrel of the Imidazole Glycerol Phosphate Synthase Bienzyme Complex," *Structure*, vol. 10, pp. 185–193, 2002.

[11] J. Bauer, E. Bennett, T. Begley, and S. Ealick, "Three-dimensional structure of YaaE from *Bacillus subtilis*, a glutaminase implicated in the pyridoxal-5'-phosphate biosynthesis," *J. Biol. Chem.*, vol. 279, no. 4, pp. 2704–2711, 2004.

[12] T. Raschle, N. Amrhein, and T. Fitzpatrick, "On the two components of pyridoxal 5'-phosphate synthase from *Bacillus subtilis*," *J. Biol. Chem.*, vol. 280, pp. 32291–32300, 2005.

[13] F. Zein, Y. Zhang, Y. Kang, K. Burns, T. Begley, and S. Ealick, "Structural insights into the mechanism of the PLP synthase holoenzyme from *Thermotoga maritima*," *Biochem.*, vol. 45, pp. 14609–14620, 2006.

[14] M. Strohmeier, T. Raschle, J. Mazurkiewicz, K. Rippe, I. Sinning, and T. Fitzpatrick, "Structure of a bacterial pyridoxal 5'-phosphate synthase complex," *PNAS*, vol. 103, no. 51, pp. 19284–19289, 2006.

[15] K. Flicker, M. Neuwirth, M. Strohmeier, B. Kappes, I. Tews, and P. Macheroux, "Structural and thermodynamic insights into the assembly of the heteromeric pyridoxal phosphate synthase from *Plasmodium falciparum*," *J. Mol. Biol.*, vol. 374, pp. 732–748, 2007.

[16] S. Wallner, M. Neuwirth, K. Flicker, I. Tews, and P. Macheroux, " Dissection of contributions from invariant amino acids to complex formation and catalysis in the heteromeric pyridoxal 5-phosphate synthase complex from *Bacillus subtilis*," *Biochem.*, vol. 48, pp. 1928–1935, 2009.

[17] J. Zhu, J. Burgner, E. Harms, B. Belitsky, and J. Smith, "A new arrangement of $(\beta/\alpha)_8$ barrels in the synthase subunit of PLP synthase," *J. Biol. Chem.*, vol. 280, no. 30, pp. 27914–27923, 2005.

[18] M. Neuwirth, M. Strohmeier, V. Windeisen, S. Wallner, S. Deller, K. Rippe, I. Sinning, P. Macheroux, and Tews, "X-ray crystal structure of *Saccharomyces cerevisiae* Pdx1 provides insights into the oligomeric nature of PLP synthases," *FEBS letters*, vol. 583, no. 13, pp. 2179–2186, 2009.

[19] A. Lesk, C. Brändén, and C. Chothia, "Structural Principles of α/β Barrel Proteins: The Packing of the Interior pf the Sheet ," *Proteins: Structure, Function, and Genetics*, vol. 5, pp. 139–148, 1989.

[20] G. Farber and G. Petsko, "The evolution of α/β barrel enzymes," *TIBS*, pp. 228–234, 1990.

[21] J. Hanes, I. Keresztes, and T. Begley, "13C NMR snapshots of the complex reaction coordinate of pyridoxal phosphate synthase," *Nat. Chem. Biol.*, vol. 4, pp. 425–430, 2008.

[22] T. Raschle, D. Arigoni, R. Brunisholz, H. Rechsteiner, N. Amrheim, and T. Fitzpatrick, " Reaction Mechanism of Pyridoxal 5'-Phosphate Synthase. Detection of an enzyme-bound chromophoric intermediate," *J. Biol. Chem.*, vol. 282, no. 9, pp. 6098–6105, 2007.

[23] T. Raschle, D. Speziga, W. Kress, C. Moccand, P. Gehrig, N. Amrhein, E. Weber-Ban, and T. Fitzpatrick, "Intersubunit Cross-talk in Pyridoxal 5'-Phosphate Synthase, Coordinated by the C Terminus of the Synthase Subunit," *J. Biol. Chem.*, vol. 284, pp. 7706–7718, 2009.

[24] M. Gengenbacher, T. Fitzpatrick, T. Raschle, K. Flicker, I. Sinning, S. Muller, P. Macheroux, I. Tews, and B. Kappes, "Vitamin B6 biosynthesis by the malaria parasite *Plasmodium falciparum*: biochemical and structural insights," *J. Biol. Chem.*, vol. 281, pp. 3633–3641, 2006.

[25] W. H. Organization, "Malaria," vol. Fact Sheet #94, 2010.

[26] P. Loria, S. Miller, M. Foley, and L. Tilley, "Inhibition of the peroxidative degradation of haem as the basis of action of chloroquine and other quinoline antimalarials," *Biochem. J.*, vol. 339, pp. 363–370, 1999.

[27] S. Francis, D. Sullivan, and D. Goldberg, "Hemoglobin metabolism in the malaria parasite *Plasmodium falciparum*," *Annu. Rev. Microbiol.*, vol. 51, pp. 97–123, 1997.

[28] M. Fonda and C. Harker, "Metabolism of pyridoxine and protein binding of the metabolites in human erythrocytes.," *Am. J. Clin. Nutr.*, vol. 35, pp. 1391–1399, 1982.

[29] C. Wrenger, M. Eschbach, I. Mueller, D. Warnecke, and R. Walter, "Analysis of the vitamin B6 biosynthesis pathway in the human malaria parasite *Plasmodium falciparum*," *J. Biol. Chem.*, vol. 280, pp. 5242–5248, 2005.

[30] C. Moccand, M. Kaufmann, and T. Fitzpatrick, "It takes two to Tango: Defining an essential second active site in Pyridoxal 5'-Phosphate Synthase," *Plos One*, vol. 6, no. 1, p. e16042, 2011.

[31] B. Derrer, V. Windeisen, G. Guédez Rodríguez, G. Seidler, M. Gengenbacher, W. Lehmann, K. Rippe, I. Sinning, I. Tews, and B. Kappes, "Defining the structural requirements of ribose 5-phosphate-binding and intersubunit cross-talk of the malarial pyridoxal 5-phosphate synthase," *FEBS Letters*, vol. 584, pp. 4169–4174, 2010.

[32] M. Pierce, C. Raman, and B. Nall, "Isothermal Titration Calorimetry of Protein-Protein Interactions," *Methods*, vol. 19, pp. 213–221, 1999.

[33] M. Neuwirth, K. Flicker, M. Strohmeier, I. Tews, and P. Macheroux, "Thermodynamic characterization of the protein-protein interaction in the heteromeric *Bacillus subtilis* Pyridoxal phosphate synthase," *Biochem.*, vol. 46, pp. 5131–5139, 2007.

[34] M. LLC, *ITC Data Analysis in Origin®. Tutorial Guide Version 7.0.* 2004.

[35] J. Dam and P. Schuck, "Calculating sedimentation coefficient distribution by direct modeling of sedimentation velocity concentration profiles," *Meth. Enzymol.*, vol. 384, pp. 185–212, 2004.

[36] P. Schuck, "Size-distribution analysis of macromolecules by sedimentation velocity ultracentrifugation and lamm equation modeling," *Biophys. J.*, vol. 78, pp. 1606–1619, 2000.

[37] Blow D., *Outline of Crystallography for Biologists* . Great Britain: Oxford University Press, 2002.

[38] A. Leslie, H. Powell, G. Winter, O. Svensson, D. Spruce, S. McSweeney, D. Love, S. Kinder, E. Duke, and C. Nave, "Automation of the collection and processing of X-ray diffraction data - a generic approach," *Acta Cryst.*, vol. D58, pp. 1924–1928, 2002.

[39] Z. Otwinowski and W. Minor, "Processing of x-ray diffraction data collected in oscillation mode ," *In Macromol. Cryst. Pt A. Methods in Enzymology*, pp. 307–326, 1997.

[40] P. Evans, "Scala," *Joint CCP4 and ESF-EACBM Newsl.*, vol. 33, no. 22-24, 1994.

[41] Collaborative Computational Project, Number 4, "The CCP4 Suite: Programs for Protein Crystallography," *Acta Cryst.*, vol. D50, pp. 760–763, 1994.

[42] P. Emsley and K. Cowtan, "Coot: model-building tools for molecular graphics," *Acta Crystallogr. D Biol. Crystallogr.*, vol. 60, pp. 2126–2132, 2004.

[43] G. Murshudov, A. Vagin, and E. Dodson, " Refinement of macromolecular structures by the maximum-likelihood method," *Acta Crystallogr. D Biol. Crystallogr.*, vol. 53, pp. 240–255, 1997.

[44] A. McCoy, R. Grosse-Kunstleve, P. Adams, M. Winn, L. Storoni, and R. Read, "Phaser Crystallographic Software," *J. Appl. Cryst.*, vol. 40, pp. 658–674, 2007.

[45] Rupp B., *Biomolecular Crystallography. Principles, Practice and Application to Structural Biology* . Garland Science, Taylor & Francis Group, LLC, 2010.

[46] A. Wallace, R. Laskowski, and J. Thornton, "LIGPLOT: a program to generate shematic diagrams of protein-ligand interactions ," *Prot. Eng.*, vol. 8, pp. 127–134, 1995.

[47] M. Diepholz, D. Venzke, S. Prinz, C. Batisse, B. Florchinger, D. Rossle, M. Svergun, B. B., and J. Fethiere, "A different conformation for EGC stator subcomplex in solution and in the assembled yeast V-ATPase: possible implications for regulatory disassembly ," *Structure*, vol. 16, pp. 1789–1798, 2008.

[48] S. Ludtke, P. Baldwin, and W. Chiu, "EMAN: semiautomated software for high-resolution single-particle reconstructions," *J. Struct. Biol.*, vol. 128, pp. 82–97, 1999.

[49] M. Van Heel, G. Harauz, E. Orlova, R. Schmidt, and M. Schatz, "A new generation of the IMAGIC image processing system ," *J. Struct. Biol.*, vol. 116, pp. 17–24, 1996.

[50] M. Tambasco-Studart, I. Tews, N. Amrhein, and T. Fitzpatrick, "Functional Analysis of PDX2 from Arabidopsis, a Glutaminase Involved in Vitamin B6 Biosynthesis," *Plant Physiol.*, vol. 144, pp. 915–925, 2007.

[51] P. Adams, R. Grosse-Kunstleve, L. Hung, T. Ioerger, A. McCoy, N. Moriarty, R. Read, J. Sacchettini, N. Sauter, and T. Terwilliger, " PHENIX: building new software for automated crystallographic structure determination ," *Acta Cryst.*, vol. D58, pp. 1948–1954, 2002.

[52] J. Hanes, S. Ealick, T. Begley, and I. Tews, *Pyridoxal Phosphate Biosynthesis, in Comprehensive Natural Products II.* Lew, M., and Hung-Wen, L., Eds. pp. 259-272, Elsevier, Oxford, 2010.

[53] N. Ohtani, M. Tomita, and M. Itaya, "An Extreme Thermophile, *Thermus thermophilus*, is a polyploid bacterium," *J. Bacteriol.*, vol. 192, no. 20, pp. 5499–5505, 2010.

[54] I. Mueller, J. Knoeckel, M. Groves, R. Jordanova, S. Ealick, R. Walter, and C. Wrenger, "The assembly of the plasmodial PLP synthase complex follows a defined course," *Plos One*, vol. 3, p. e1819, 2008.

[55] X. Zhang, Y. Teng, J. Liu, Y. He, K. Zhou, Y. Chen, and C. Zhou, "Structural insights into the catalytic mechanism of the yeast pyridoxal 5-phosphate synthase Snz1," *Biochem. J.*, vol. 432, no. 3, pp. 445–450, 2010.

[56] S. Weber, "Funktionelle und strukturelle Untersuchungen zur Vitamin-B6-Produktion PLP-Synthase-basierend auf der PLP-Synthase-Untereinheit von Arabidopsis thaliana," Diploma Thesis. Ruprecht-Karls-Universität Heidelberg, Germany, 2008.

[57] M. Strohmeier, *It is all about Vitamin B_6. Structural insights into pyridoxal 5-phosphate de novo biosynthesis.* PhD thesis, University of Heidelberg, Germany, 2007.

[58] A. Morollo and M. Eck, "Structure of the cooperative allosteric anthranilate synthase from *Salmonella typhimurium*," *Nat. Struct. Biol.*, vol. 8, no. 3, pp. 243–247, 2001.

[59] J. Nakamura, K. Straub, J. Wu, and L. Lou, "The Glutamine Hydrolysis Function of Human GMP Synthetase," *J. Bio. Chem.*, vol. 270, no. 40, pp. 23450–23455, 1995.

[60] R. Myers, J. Jensen, I. Deras, J. Smith, and V. Davisson, "Substrate-Induced Changes in the Ammonia Channel for Imidazole Glycerol Phosphate Synthase," *Biochemistry*, vol. 42, pp. 7013–7022, 2003.

[61] A. Horovitz and K. Willison, "Allosteric regulation of chaperonins," *Curr. Opin. Struc. Biol.*, vol. 15, pp. 646–651, 2005.

[62] K. Willison, "Structural changes underlying allostery in group II chaperonins," *Structure Previews*, vol. 19, pp. 754–755, 2011.

[63] H. Morgan, I. McNae, M. Nowicki, V. Hannaert, P. Michels, L. Fothergill-Gilmore, and M. Walkinshaw, "Allosteric Mechanism of Pyruvate Kinase from *Leishmania mexicana* uses a Rock and Lock Model," *J. Bio. Chem.*, vol. 285, no. 17, pp. 1289–12898, 2010.

[64] J. Knoeckel, I. Mueller, B. Bergmann, R. Walter, and C. Wrenger, " The apicomplexan parasite *Toxoplasma gondii* generates pyridoxal phosphate de novo ," *Mol. Biochem. Parasitol.*, vol. 152, pp. 108–111, 2007.

[65] S. Cole, R. Brosch, J. Parkhill, T. Garnier, C. Churcher, D. Harris, S. Gordon, K. Eiglmeier, S. Gas, C. Barry, F. Tekaia, K. Badcock, D. Basham, D. Browm, T. Chillingworth, R. Connor, R. Davies, K. Devlin, T. Feltwell, S. Gentles, N. Hamlin, S. Holroyd, T. Hornsby, K. Jagels, A. Krogh, J. McLean, S. Moule, L. Murphy, S. Oliver, J. Osborne, M. Quail, M. Rajandream, J. Rogers, S. Rutter, K. Seeger, S. Skelton, S. Squares, R. Squares, J. Sulston, K. Taylor, S. Whitehead, and B. BG., "Deciphering the biology of Mycobacterium tuberculosis from the complete genome sequence," *Nature*, vol. 393, pp. 537–544, 1998.

[66] T. Dick, U. Manjunatha, B. Kappes, and M. Gengenbacher, " Vitamin B6 biosynthesis is essential for survival and virulence of Mycobacterium tuberculosis ," *Mol. Microbiol.*, vol. 78, no. 4, pp. 980–988, 2010.

[67] D. Nelson and M. Cox, *Lehninger. Principle of Biochemistry.* New York: W.H. Freeman and Company. 4th edition., 2005.

[68] S. Sia, P. Carr, A. Cochran, V. Malashkevich, and P. Kim, "Short constrained peptides that inhibit HIV-1 entry," *PNAS*, vol. 99, no. 23, pp. 14664–14669, 2002.

[69] E. Beitz, "TEXshade: shading and labeling multiple sequence alignments using LATEX 2_ε," *Bioinformatics*, vol. 16, pp. 135–139, 2000.